**Technical Report Documentation Page**

| 1. Report No. | 2. Government Accession No. | 3. Recipient's Catalog No. |
|---|---|---|
| FHWA/TX-85/74+345-1 | | |

| 4. Title and Subtitle | 5. Report Date |
|---|---|
| Establishing Material Properties for Thin Asphalt Concrete Surfaces on Granular Bases | November, 1985 |
| | 6. Performing Organization Code |
| | 8. Performing Organization Report No. |
| 7. Author(s) | |
| Freddy L. Roberts and Barry T. Rosson | 345-1 |
| 9. Performing Organization Name and Address | 10. Work Unit No. (TRAIS) |
| Texas Transportation Institute<br>Texas A&M University<br>College Station, TX 77843 | 11. Contract or Grant No.<br>HPR 2-8-83-345 |
| | 13. Type of Report and Period Covered |
| 12. Sponsoring Agency Name and Address | Interim - September 1982<br>November 1985 |
| Texas State Department of Highways and Public Transportation; Transportation Planning Division<br>P. O. Box 5051<br>Austin, Texas 78763 | 14. Sponsoring Agency Code |

15. Supplementary Notes

Research performed in cooperation with DOT,FHWA.
Research Study Title: Performance Considerations and Specifications of Hot-Mix Asphaltic Concrete

16. Abstract

This report includes the results of an analytical study of thin asphalt pavements over flexible bases to define the engneering properties required for adequate performance. Since truck tire pressures have dramatically increased in recent years, included are the effects of the increased tire pressures on surface tensile strains, base shear stresses, and subgrade compressive strains.

A finite element computer program developed for the FHWA was used to calculate vertical and horizontal surface shear pressure distribution for a bias ply truck tire inflated to both 75 and 125 psi.

A series of ILLIPAVE computer runs was made to determine the horizontal tensile strains, lateral shear stresses, and vertical compressive strains for asphalt concrete surfaces 1, 1.5, 2, and 4 inches thick over 8- and 14-inch granular bases having three different moduli and a subgrade soil that is stress-sensitive with an initial modulus of 10 ksi. These results showed that some thin pavement structures cannot provide adequate service, and that design procedures must be upgraded to include materials more resistant to higher strains. To provide adequate service, these surfaces should be either flexible and thin on a stiff, thick base, or be stiff and thick.

| 17. Key Words | 18. Distribution Statement |
|---|---|
| Increased tire pressure, thin pavements, low volume, fatigue cracking, tensile strain, ILLIPAVE, horizontal surface shear | No restrictions. This document is available to the public through the National Technical Information Service<br>5285 Port Royal Road<br>Springfield, Virginia 22161 |

| 19. Security Classif. (of this report) | 20. Security Classif. (of this page) | 21. No. of Pages | 22. Price |
|---|---|---|---|
| Unclassified | Unclassified | 157 | |

Form DOT F 1700.7 (8-72) Reproduction of completed page authorized

# ESTABLISHING MATERIAL PROPERTIES FOR THIN ASPHALT CONCRETE SURFACES ON GRANULAR BASES

by

Freddy L. Roberts

and

Barry T. Rosson

Research Report 345-1

Conducted for

State Department of Highways and Public Transportation

in cooperation with the

U.S. Department of Transportation

Federal Highway Administration

by the

Texas Transportation Institute

Texas A&M University

College Station, Texas

November, 1985

The contents of this report reflect the views of the authors, who are responsible for the facts and the accuracy of the data presented herein. The contents do not necessarily reflect the official views or policies of the Federal Highway Administration. This report does not constitute a standard, specification, or regulation.

# PREFACE

This is the first in a series of reports describing the conditions of use, construction, and specifications of hot mixed asphalt concrete materials used in thin, flexible pavements. This report includes not only study results from Study 345 but also Study 372 entitled "Effects of Truck Tire Pressures on Flexible Pavements", which provided the truck tire contact pressure distributions. This first report has concentrated on an evaluation of strain in thin asphalt concrete pavements and in determining the material properties sufficient for adequate performance. Subsequent reports will include evaluation of permanent deformation in these pavements as well as specification and construction requirements for adequate service from thin flexible pavements.

This report was completed with the assistance of many people. Special appreciation is extended to Drs. Robert L. Lytton and Thomas Tielking for their help with the computer modeling and to Messrs. James L. Brown and Robert L. Mikulin of the Texas State Department of Highways and Public Transportation for their encouragement and constructive criticism. Appreciation is also extended to the secretarial staff of the Materials, Pavements, and Construction Division of TTI who prepared the manuscript materials. The support of the Federal Highway Administration, Department of Transportation, is gratefully acknowledged.

Freddy L. Roberts
Barry T. Rosson

## SUMMARY

This report summarizes the results from an analytical study to determine the material properties and thicknesses of asphalt surface layers needed to provide adequate resistance to fatigue cracking for thin flexible pavements. The analytical study includes the effects of an important parameter not generally considered in these studies: the tire contact pressure distribution.

Results indicate that the effects of tire inflation pressure on strain are so important that surface materials which served adequately at 75 or 80 psi inflation pressure fail very prematurely when the same load is applied at 125 psi inflation pressure. The contact pressure distributions used in the study were developed from a finite element computer program that models the tire using its constitutent elements. The contact pressure distributions were for a typical bias ply truck tire that carried a legal load of 4500 pounds per tire and was inflated to 75 to 125 psi. These contact pressure distributions were then used to evaluate the effect of surface and base properties and thicknesses. The results indicate that (1) thick and stiff granular bases provide the best protection for the subgrade soil, (2) that current asphalt materials can serve adequately at the lower tire inflation pressures and (3) that at 125 psi inflation pressure only the thin, very flexible surfaces or the thick, very stiff surfaces can provide reasonable fatigue life.

## IMPLEMENTATION STATEMENT

Based on the findings from this study it is apparent that thin layers of conventional asphalt concrete materials should be used with caution. For relatively thin flexible pavements with unbound bases conventional hot mixed surfacing materials should probably not be used at all. The reason for this suggestion is that the significant increase in truck tire inflation pressures since the early 1970's has raised the strain at the bottom of conventional asphalt concrete surfaces to levels that lead to very premature fatigue cracking.

Evaluations of the results from this study show that for flexible pavements over unbound, granular bases the surface thickness and stiffness combinations affect the tensile strains significantly and that bituminous surfaces of

(1) 1-inch or less should be very flexible and placed on very stiff bases, and probably be seal coat construction,

(2) 4 to 8-inches should be stiff and strong and placed on stiff bases, and

(3) 1 to 3 inches should probably not be placed since the strains are very high and early cracking is expected.

The primary reason for recommending caution in the use of 1 to 3-inch bituminous surfaces is that the higher tire pressures produced the greatest increase in tensile strains for surface moduli ranging from 200 to 600 ksi, which is the range of moduli of these materials during most of the Spring through Fall of each year. Therefore, the results of this study indicate that intermediate surface thicknesses should be used only after a careful analysis of each pavement structure to ensure that overstressing of the surface does not occur.

## DISCLAIMER

The contents of this report reflect the views of the authors who are responsible for the facts and the accuracy of the data presented herein. The contents do not necessarily reflect the official views or policies of the Federal Highway Administration. This report does not constitute a standard, specification or regulation.

# METRIC CONVERSION FACTORS

## Approximate Conversions to Metric Measures

| Symbol | When You Know | Multiply by | To Find | Symbol |
|---|---|---|---|---|
| | | **LENGTH** | | |
| in | inches | *2.5 | centimeters | cm |
| ft | feet | 30 | centimeters | cm |
| yd | yards | 0.9 | meters | m |
| mi | miles | 1.6 | kilometers | km |
| | | **AREA** | | |
| $in^2$ | square inches | 6.5 | square centimeters | $cm^2$ |
| $ft^2$ | square feet | 0.09 | square meters | $m^2$ |
| $yd^2$ | square yards | 0.8 | square meters | $m^2$ |
| $mi^2$ | square miles | 2.6 | square kilometers | $km^2$ |
| | acres | 0.4 | hectares | ha |
| | | **MASS (weight)** | | |
| oz | ounces | 28 | grams | g |
| lb | pounds | 0.45 | kilograms | kg |
| | short tons (2000 lb) | 0.9 | tonnes | t |
| | | **VOLUME** | | |
| tsp | teaspoons | 5 | milliliters | ml |
| Tbsp | tablespoons | 15 | milliliters | ml |
| fl oz | fluid ounces | 30 | milliliters | ml |
| c | cups | 0.24 | liters | l |
| pt | pints | 0.47 | liters | l |
| qt | quarts | 0.95 | liters | l |
| gal | gallons | 3.8 | liters | l |
| $ft^3$ | cubic feet | 0.03 | cubic meters | $m^3$ |
| $yd^3$ | cubic yards | 0.76 | cubic meters | $m^3$ |
| | | **TEMPERATURE (exact)** | | |
| °F | Fahrenheit temperature | 5/9 (after subtracting 32) | Celsius temperature | °C |

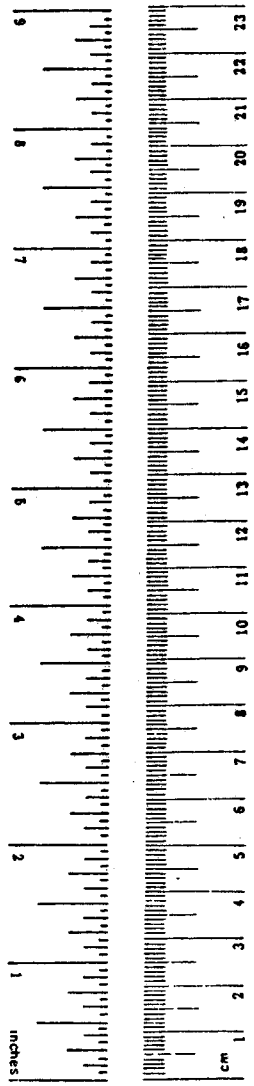


## Approximate Conversions from Metric Measures

| Symbol | When You Know | Multiply by | To Find | Symbol |
|---|---|---|---|---|
| | | **LENGTH** | | |
| mm | millimeters | 0.04 | inches | in |
| cm | centimeters | 0.4 | inches | in |
| m | meters | 3.3 | feet | ft |
| m | meters | 1.1 | yards | yd |
| km | kilometers | 0.6 | miles | mi |
| | | **AREA** | | |
| $cm^2$ | square centimeters | 0.16 | square inches | $in^2$ |
| $m^2$ | square meters | 1.2 | square yards | $yd^2$ |
| $km^2$ | square kilometers | 0.4 | square miles | $mi^2$ |
| ha | hectares (10,000 $m^2$) | 2.5 | acres | |
| | | **MASS (weight)** | | |
| g | grams | 0.035 | ounces | oz |
| kg | kilograms | 2.2 | pounds | lb |
| t | tonnes (1000 kg) | 1.1 | short tons | |
| | | **VOLUME** | | |
| ml | milliliters | 0.03 | fluid ounces | fl oz |
| l | liters | 2.1 | pints | pt |
| l | liters | 1.06 | quarts | qt |
| l | liters | 0.26 | gallons | gal |
| $m^3$ | cubic meters | 35 | cubic feet | $ft^3$ |
| $m^3$ | cubic meters | 1.3 | cubic yards | $yd^3$ |
| | | **TEMPERATURE (exact)** | | |
| °C | Celsius temperature | 9/5 (then add 32) | Fahrenheit temperature | °F |

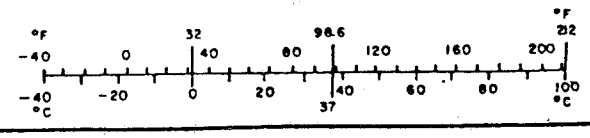

TABLE OF CONTENTS


| | | PAGE |
|---|---|---|
| PREFACE | | iv |
| SUMMARY | | v |
| IMPLEMENTATION STATEMENT | | vi |
| DISCLAIMER | | vii |
| METRIC CONVERSION CHART | | viii |
| TABLE OF CONTENTS | | ix |
| LIST OF TABLES | | xi |
| LIST OF FIGURES | | xii |
| CHAPTER | | |
| I | INTRODUCTION | 1 |
| II | PAVEMENT MODELS | 3 |
| | CRANLAY | 3 |
| | PLANE | 4 |
| | Modified ILLIPAVE | 7 |
| III | TIRE MODELS | 7 |
| | Tielking Tire Model | 11 |
| | Uniform Pressure Model | 12 |
| | Use of Tire Models | 13 |
| IV | STUDY PARAMETERS | 13 |
| | Pavements | 13 |
| | Truck Tire Loads | 14 |
| V | STUDY RESULTS | 21 |
| | Tire Pressure Efects | 21 |
| | Layer Modulus and Thickness Effects | 28 |
| | Fatigue Damage Effects | 52 |
| | Rutting Effects | 71 |
| | Combined Effects | 75 |
| VI | CONCLUSIONS | 79 |
| VII | RECOMMENDATIONS | 83 |

TABLE OF CONTENTS (continued)


| CHAPTER | | PAGE |
|---|---|---|
| REFERENCES | | 85 |
| APPENDIX A. | DERIVATION OF THE UZ AND UR NODAL FORCE VALUES | 87 |
| APPENDIX B. | EXPLANATION AND USE OF ADJRAD | 101 |
| APPENDIX C. | EXPLANATION AND USE OF PAVELD | 103 |
| APPENDIX D. | TENSILE STRAIN AND ESAL DATA AT THE TOP AND BOTTOM OF THE ASPHALT CONCRETE SURFACE | 105 |
| APPENDIX E. | SHEAR STRESS DATA AT THE TOP OF THE BASE | 123 |
| APPENDIX F. | COMPRESSIVE STRAIN AND ESAL DATA AT THE TOP OF THE SUBGRADE | 133 |

LIST OF TABLES


| TABLE | | PAGE |
|---|---|---|
| 1 | Tensile strains at the bottom of A.C. surface and ESAL produced by a uniform pressure distribution. . . . . | 29 |
| 2 | The 27 AASHO sections used for the fatigue curve development from ELSYM5 and ILLIPAVE. . . . . | 54 |
| 3 | Compressive strains at the top of the subgrade for a range of numbers of equivalent standard 18-kip axle loads using $W_{18} = 6.15 \times 10^{17}(\frac{1}{\varepsilon_c})^{4.0}$ . . . . . | 74 |
| 4 | ESAL applications based on different limiting criteria. . . . . | 77 |

LIST OF FIGURES


| FIGURE | | PAGE |
|---|---|---|
| 1 | Finite elements positioned on the G78-14 tire carcass mid-surface. . . . . | 9 |
| 2 | Deflected shape and tire contact pressure distribution results from finite element tire model for a G78-14 tire . | 10 |
| 3 | Base Resilient Modulus - Bulk Stress Relationships for three base moduli defined by $8787\,\theta^{0.365}$, $7000\,\theta^{0.325}$ and $4886\,\theta^{0.239}$. . . . . | 15 |
| 4 | Resilient Modulus-Deviator Stress Relationship for subgrade soil. . . . . | 16 |
| 5 | Non-linear vertical tire pressure distribution with lateral surface shear forces as developed using finite element model by Tielking for an inflation pressure of 75 psi and tire load of 4,500 lbs. . . . . | 18 |
| 6 | Non-linear vertical tire pressure distribution with lateral surface shear forces as developed using finite element model by Tielking for an inflation pressure of 125 psi and tire load of 4,500 lbs . . . . . | 18 |
| 7 | Effects of increased tire pressure on tensile strain at the bottom of the surface for a surface modulus of 400 ksi and base thickness of 8 inches . . . . . | 22 |
| 8 | Effects of increased tire pressure on tensile strain at the bottom of the surface for a surface modulus of 50 ksi and base thickness of 8 inches . . . . . | 23 |
| 9 | Effects of increased tire pressure on tensile strain at the top of the surface for a surface modulus of 400 ksi and base thickness of 8 inches . . . . . | 25 |

LIST OF FIGURES (continued)


| FIGURE | | PAGE |
|---|---|---|
| 10 | Effects of increased tire pressure on compressive strain at the top of the subgrade for a surface modulus of 400 ksi and base thickness of 8 inches . . . . . | 27 |
| 11 | Differences in the tensile strains produced from using the Tielking tire model and the uniform pressure model . . . | 30 |
| 12 | Tensile micro-strain contours at the bottom of the surface for $8787\theta^{0.365}$ base modulus and 8-inch base . . . . | 33 |
| 13 | Tensile micro-strain contours at the bottom of the surface for $7000\theta^{0.325}$ base modulus and 8-inch base . . . . | 34 |
| 14 | Tensile micro-strain contours at the bottom of the surface for $4886\theta^{0.239}$ base modulus and 8-inch base . . . . | 35 |
| 15 | Tensile micro-strain contours at the bottom of the surface for $8787\theta^{0.365}$ base modulus and 14-inch base . . . | 36 |
| 16 | Tensile micro-strain contours at the bottom of the surface for $7000\theta^{0.325}$ base modulus at 14-inch base . . . . | 37 |
| 17 | Tensile micro-strain contours at the bottom of the surface for $4886\theta^{0.239}$ base modulus and 14-inch base . . . | 38 |
| 18 | Tensile micro-strain contours at the top of the surface for $8787\theta^{0.365}$ base modulus and 8-inch base . . . . | 39 |
| 19 | Tensile micro-strain contours at the top of the surface for $7000\theta^{0.325}$ base modulus and 8-inch base . . . . | 40 |
| 20 | Tensile micro-strain contours at the top of the surface for $4886\theta^{0.325}$ base modulus and 8-inch base . . . . | 41 |
| 21 | Tensile micro-strain contours at the top of the surface for $8787\theta^{0.365}$ base modulus and 14-inch base . . . . . | 42 |
| 22 | Tensile micro-strain contours at the top of the surface for $7000\theta^{0.325}$ base modulus and 14-inch base . . . | 43 |

LIST OF FIGURES (continued)


| FIGURE | | PAGE |
|---|---|---|
| 23 | Tensile micro-strain contours at the top of the surface for $4886\theta^{0.239}$ base modulus and 14-inch base. . . | 44 |
| 24 | Compressive micro-strain contours at the top of the subgrade for $8787\theta^{0.365}$ base modulus and 8-inch base. . . | 46 |
| 25 | Compressive micro-strain contours at the top of the subgrade for $7000\theta^{0.325}$ base modulus and 8-inch base. . . | 47 |
| 26 | Compressive micro-strain contours at the top of the subgrade for $4886\theta^{0.239}$ base modulus at 8-inch base . . . | 48 |
| 27 | Compressive micro-strain contours at the top of the subgrade for $8787\theta^{0.365}$ base modulus and 14-inch base . . | 49 |
| 28 | Compressive micro-strain contours at the top of the subgrade for $7000\theta^{0.325}$ base modulus and 14-inch base . . | 50 |
| 29 | Compressive micro-strain contours at the top of the subgrade for $4886\theta^{0.239}$ base modulus and 14-inch base . . | 51 |
| 30 | Asphalt concrete fatigue curves developed from AASHO Road Test sections using ELSYM5 and ILLIPAVE . . . . . | 56 |
| 31 | ESAL contours as a function of the tensile strain at the bottom of the surface for a $8787\theta^{0.365}$ base modulus and 8-inch base. . . . . | 58 |
| 32 | ESAL contours as a function of the tensile strain at the bottom of the surface for a $7000\theta^{0.325}$ base modulus and 8-inch base. . . . . | 59 |
| 33 | ESAL contours as a function of the tensile strain at the bottom of the surface for a $4886\theta^{0.239}$ base modulus and 8-inch base. . . . . | 60 |

LIST OF FIGURES (continued)


| FIGURE | | PAGE |
|---|---|---|
| 34 | ESAL contours as a function of the tensile strain at the bottom of the surface for a $8787\,\theta^{0.365}$ base modulus and 14-inch base | 61 |
| 35 | ESAL contours as a function of the tensile strain at the bottom of the surface for a $7000\,\theta^{0.325}$ base modulus and 14-inch base | 62 |
| 36 | ESAL contours as a function of the tensile strain at the bottom of the surface for a $4886\,\theta^{0.239}$ base modulus and 14-inch base | 63 |
| 37 | ESAL contours as a function of the tensile strain at the top of the surface for a $8787\,\theta^{0.365}$ base modulus and 8-inch base | 65 |
| 38 | EASL contours as a function of the tensile strain at the top of the surface for a $7000\,\theta^{0.325}$ base modulus and 8-inch base | 66 |
| 39 | ESAL contours as a function of the tensile strain at the top of the surface for a $4886\,\theta^{0.239}$ base modulus and 8-inch base | 67 |
| 40 | ESAL contours as a function of the tensile strain at the top of the surface for a $8787\,\theta^{0.365}$ base modulus and 14-inch base | 68 |
| 41 | ESAL contours as a function of the tensile strain at the top of the surface for a $7000\,\theta^{0.325}$ base modulus and 14-inch base | 69 |

LIST OF FIGURES (continued)


| FIGURE | | PAGE |
|---|---|---|
| 42 | ESAL contours as a function of the tensile strain at the top of the surface for a $4886\,\theta^{0.239}$ base modulus and 14-inch base. . . . . | 70 |
| 43 | Vertical Compressive Strain versus the number of weighted 18-kip axle load applications for three different rutting equations . . . . . | 73 |

# CHAPTER I

## INTRODUCTION

In the past, methods of structural design for flexible pavements have almost exclusively been developed for pavements with surface thicknesses greater than two inches. However, there are many miles of thin, less than 2-inch, asphalt concrete surfaces already in service that have been designed assuming that thinner pavements behave structurally in much the same way as thicker pavements. Unfortunately, this is not the case; there are certain pavement distresses that occur in thin pavements that cannot be explained by using current analysis methods. Recent study of the pavements may help to explain these discrepancies. One primary reason for these differences may lie in the assumptions made about the tire load.

In previous analyses, the tire load was represented as a uniform pressure over a circular area with no lateral shear stresses produced by the tire rolling on the surface. Work in the tire industry has shown that the contact pressure is not uniform but rather has a unique shape, depending on the type of tire. The result is that the actual tire contact pressure distribution produces pavement stresses much larger than those calculated using a uniform tire contact pressure distribution.

Another reason for the discrepancies may lie in the fact that highway engineers have largely ignored in their analyses another factor of great importance: increased tire inflation pressures. With the increased cost of fuel, the trucking industry has attempted to reduce rolling resistance and increase fuel economy. Tire manufacturers have responded by designing and marketing both bias and radial tires that operate at higher inflation pressures. To determine the current levels of tire pressures and their effects on Texas highways the State Department of Highways and Public Transportation (SDHPT) has contracted with the Texas Transportation Institute (TTI) to perform two research projects. The first project is to determine typical tires, the inflation pressures, the contact pressure distributions, and their effects on highway pavements. The second

project includes the evaluation and design of thin asphalt concrete pavements including the evaluation of suitable materials with which to build these thin pavements. This report includes results from both these studies, with a major emphasis on the latter.

# CHAPTER II

## PAVEMENT MODELS

For selecting a pavement computer model, two requirements were of primary interest: (1) actual tire contact pressure distributions had to be accepted as input, and (2) the modulus of non-stabilized pavement layers had to be modelled as stress sensitive materials.

The technical literature shows that tire contact pressure distributions have non-linear vertical and horizontal components. Therefore, to adequately model these pressure distributions, the pavement computer program must accept such input. Because the commonly used pavement computer programs such as ELSYM5 accept only uniform vertical contact pressure, other computer programs were considered for this research. The CRANLAY and PLANE (1) computer models were considered because their input capabilities included lateral and uniform vertical pressures. The finite element program ILLIPAVE (2) had the capability to model the non-stabilized materials as stress sensitive but was set up to accept only a uniform vertical tire contact pressure. Each of these candidate programs is discussed briefly in the sections below.

### CRANLAY

The computer program CRANLAY was written by Harrison, Wardle, and Gerrard in Australia in 1972 (1). It is an elastic layer theory program that can accept up to five horizontal layers with material properties being defined as either cross-anisotropic or isotropic. The tire load is input as a circular load of specified radius and magnitude. CRANLAY accepts only two load cases which must be run separately: uniform vertical pressure and linear radial shear stress. The stresses, strains, and displacements of the coordinates in the layer or layers are tabulated as output.

This pavement model was not chosen because it did not meet either of the two requirements cited above. However, several CRANLAY runs were made

in order to compare the magnitude of its outputs with those from ILLIPAVE.

## PLANE

The pavement program PLANE was also written by Harrison, Wardle, and Gerrard in Australia in 1972 (1). It is an elastic layer theory program which only considers a single layer of infinite depth with material property inputs defined elastically in two directions as orthorhombic, cross-anisotropic or isotropic. The tire load is represented as a strip of specified width and magnitude but infinite in extent. There are, however, twelve different load cases which can occur in pairs: uniform and linear vertical stress; uniform and linear lateral shear stress; and displacement defined loads. The stresses, strains, and displacements of the coordinates in the layer are tabulated as output.

This program was rejected for the same reasons that CRANLAY was rejected. Even though the twelve different input load cases allow much flexibility, the unique vertical and horizontal tire contact pressures of a particular tire could not be input. In addition, the single elastic layer of infinite depth was considered inappropriate for this project.

## Modified ILLPIAVE

The computer program model ILLIPAVE is a version of a program written by Wilson (3, 4, and 5) that was modified and made user-friendly by the research staff of the Construction Engineering Laboratory at Champaign, Illinois, in 1982 (2). It is a finite element program that models a pavement three-dimensionally by using a two-dimensional half-space of a finite solid of revolution. This rectangular half-space is divided into a set of rectangular elements connected at their nodal points. The ILLIPAVE loading is of the "flexible plate" type, i.e., a uniform circular contact pressure. The modulus properties can be input as a function of the minor principal stress, the deviator stress, the first stress invariant, or simply as a constant.

ILLPAVE internally calculates the forces at each node. UZ represents the vertical force or displacement at a node, and UR represents the horizontal force of displacement at a node. For the uniform vertical pressure case, the UZ nodal forces are calculated internally. To allow the tire load to be input as a circular, non-uniform vertical load with lateral shear pressures, the computer program was modified to allow the UZ and UR nodal force values to be read directly into the program as input while the uniform contact pressure of the original ILLIPAVE was set to approximately zero. The original ILLIPAVE neglected the horizontal shear pressures by internally setting the UR nodal forces equal to zero. The UZ and UR values are calculated externally using a procedure defined in Appendix A. Any desired distribution of vertical and horizontal pressure can be input. The UZ and UR nodal forces for a typical truck tire have been generated in Appendix A.

To verify that the modified ILLIPAVE produces the same output as the original ILLIPAVE, a uniform presure of 80 psi was run using both programs. A comparison of the displacement indicated that the changes made to ILLIPAVE were valid because the displacements were identical to three significant digits.

# CHAPTER III

# TIRE MODELS

Historically, initial analyses of the states of stress in solid bodies involved the use of a point load applied to a uniform elastic material of semi-infinite extent; later analysis techniques included strip loads of finite width and infinite length. As analysis of pavement systems became more sophisticated, Love (6) and Burmister (7) extended the analysis to include more than one layer and also began to model their tire as a circle of uniform vertical pressure with no surface shear forces. This tire model continued to be used in the highway design community until the last few years. More recently, highway engineers have begun to use finite element models developed for tire carcass analysis to define the stress conditions that occur at the tire-pavement interface.

## Tielking Tire Model

The finite element tire model used in this study was originally developed for the Federal Highway Administration as part of an analytical and experimental investigation of tire-pavement interaction (8). The program was developed to provide the capability for calculating the distributions of sliding velocity and normal pressure at the tire-pavement contact interface. Tielking (9,10) chose a relatively general, non-linear, finite element shell of revolution computer program to be the foundation for the finite element tire model. A Fourier transform procedure for solving the shell contact problems of the foundation program was developed (11) and incorporated into the finite element program, giving this tire model the unique capability of calculating the contact boundary and interface pressure distribution for a specified tire deflection.

The shell elements used in the tire model are orthotropic. A material property subroutine was developed to generate orthotropic moduli

from cord and rubber property data and geoemtric data describing the ply structure in the tire carcass. Although the shell elements are homogeneous orthotropic, they are sensitive to details of the carcass design including tire materials and geometry.

The tire is modeled by an assemblage of axisymmetric curved shell elements. The elements are connected to form a meridian of arbitrary curvature and are located at the carcass midsurface. Figure 1 shows the assembly of 21 elements along the midsurface of a G78-14 tire. A cylindrical coordinate system is used with r, $\omega$, and z indicating the radial, circumferential, and axial directions, respectively. Each element forms a complete ring which is initally axisymmetric with respect to z. The elements are connected at nodal circles (numbered in Figure 1, hereafter referred to as nodes).

The finite elements are homogeneous orthotropic with a set of moduli specified for each individual element. The orthotropic moduli for each element are determined by the ply structure surrounding the element.

The finite element model is clamped at the edges (node 22 in Figure 1), pressurized, and rotated to induce centrifugal force loading. It is then brought into contact with a rigid, frictionless surface perpendicular to the plane of symmetry (the r-$\omega$ plane). The contact surface (the pavement) is at the specified loaded radius, $R_\ell$, measured from the z-axis. The internal pressure, the angular velocity and the loaded radius are the only operating variables specified prior to calculating contact deformation and pressure in the contact region. Reference 11 describes the mathematical procedures used to calculate the contact pressure distribution and deformation of the tire deflected against the pavement.

The deflected shape of a nylon tire meridian passing through the center of the contact region is plotted in Figure 2 for a tire deflection of 0.9 inches. Figure 2 also shows both the inflated, undeflected meridian, and the calculated contact pressure distribution along the meridian. The calculated tire load is 850 lb for a deflection of 0.9 inches.

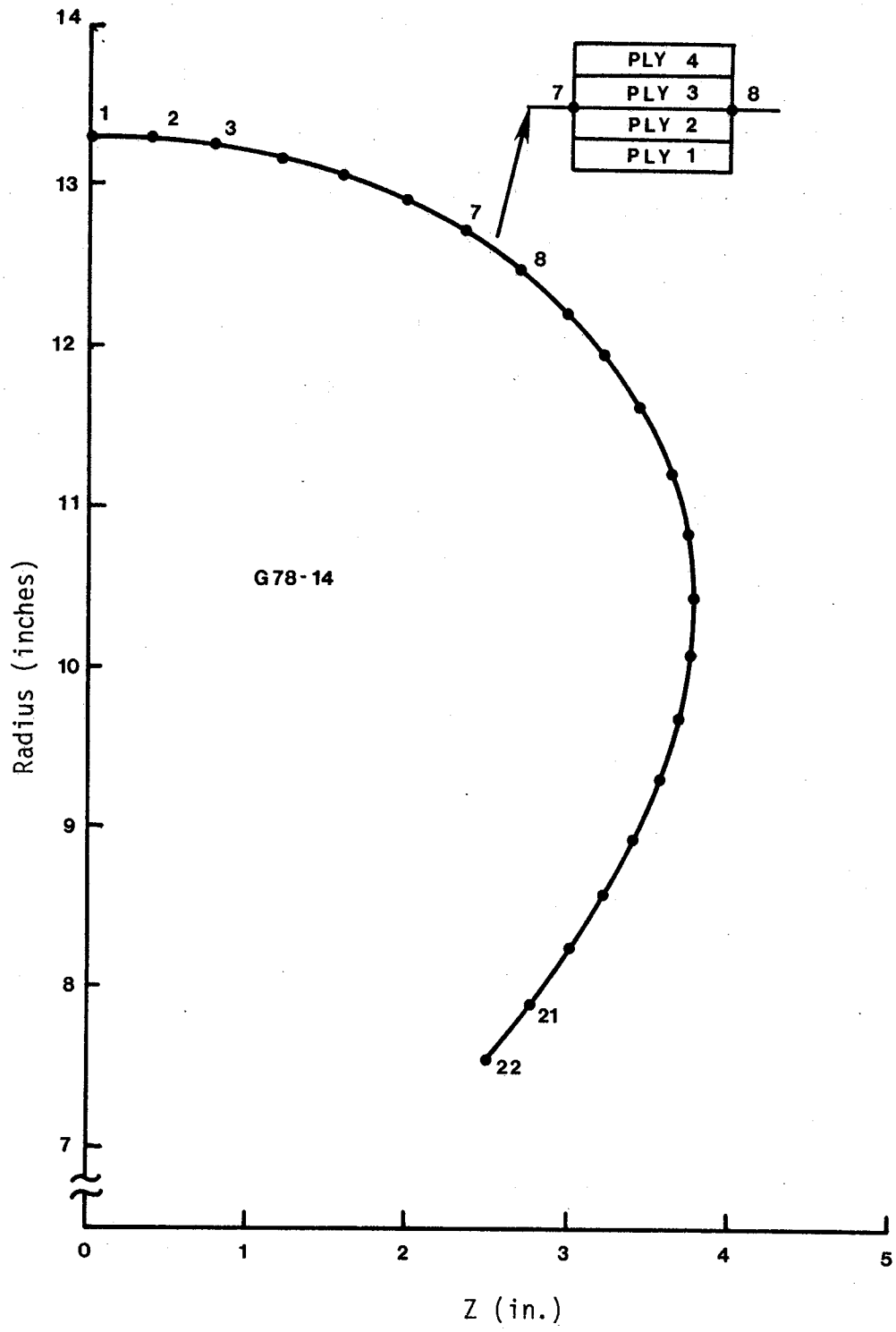


Figure 1. Finite elements positioned on the G78-14 tire carcass mid-surface.

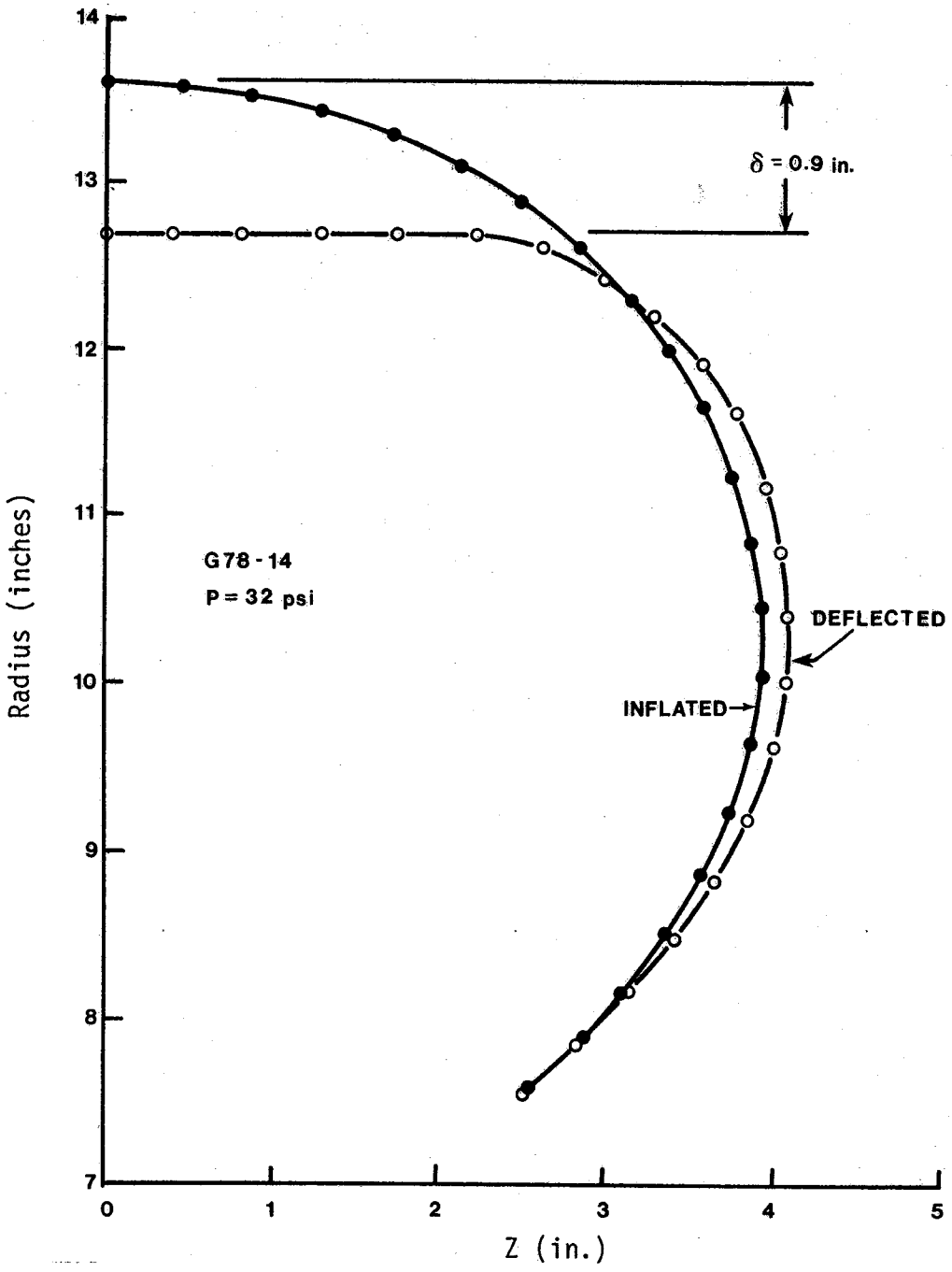


Figure 2. Deflected shape and tire contact pressure distribution results from finite element tire model for a G78-14 tire.

This finite element tire model is believed to be the first to have the capability of calculating the contact pressure distribution in the footprint of a deflected tire. Such a capability is important because contact pressure has a profound influence on all aspects of tire performance. The finite element tire model permits analytical investigations of the effects of tire design variables on contact pressure distribution.

The rolling tire results are calculated by superimposing the angular velocity of the rolling tire on the solution for static contact against a frictionless surface. The sliding velocities of points in the contact region are calculated as outlined in Reference 12. The sliding velocity and the normal contact pressure determine the friction coefficient at each point in the footprint. The resulting braking, driving, and steering shear forces respond to tire operating variables such as inflation pressure, tire load, and slip angle through the influence of these operating variables on the distributions of sliding velocity in the footprint. Tire slide force is similarly obtained by summing the lateral shear forces in the contact region.

## Uniform Pressure Model

Love (6) and Burmister (7) first modeled the tire load as a circular uniform vertical pressure. The type of tire and lateral shear forces were not included in the analysis; only the inflation pressure and total tire load were considered important. Until recently, this same method of modeling the tire load was used extensively.

The radius of the circular uniform load is calculated based on the tire inflation pressure and the total tire load. The tire inflation pressure was considered to be constant and the radius of the circular tire print can be calculated by the following equation:

$$R = \sqrt{\frac{P}{\pi \quad p}}$$

where:

R = radius of the circular uniform contact pressure, inches;

P = total tire load, pounds; and

p = inflation pressure, psi.

## Use of Tire Models

In analytical studies, the tire model is used to determine the intensity of the pressure or the area of the surface over which the load is spread. Since the Tielking tire model more accurately reflects the tire carcass itself, this study was conducted using the Tielking tire model. However, to indicate the magnitude of the differences between results from these two models, a few comparative analyses were made.

# CHAPTER IV

## STUDY PARAMETERS

The basic objective of this research is to analyze thin asphalt concrete surfaces on granular bases with material combinations and layer thicknesses that frequently occur on the Texas farm to market systems. This analysis must also include careful consideration of the type of truck tire loads these pavements are experiencing. Therefore, after studying the Texas Transportation Institute's data base of flexible pavements in Texas, and after determining from a concurrent TTI project the types of truck tires commonly in use on Texas highways, the following set of study parameters was selected as representative of the thin flexible pavements in Texas.

### Pavements

To determine the typical cross-section of these pavements, all the thin pavements in the TTI flexible pavement data base were reviewed. From this data, a set of pavements with flexible bases were selected and thin surface and base thicknesses determined. The flexible base thicknesses generally fell into 2 categories: those with 8-inch bases and those with 14-inch bases. Surface thicknesses ranged from about 1 inch up to 16 inches when successive overlays occurred over a period of time. Taking into consideration the soil types, temperature ranges and moisture levels within the different regions of the state, a range of material properties was selected for typical surface, base, and subgrades. The following series of material combinations and layer thicknesses were included in the study:

Surface

Thicknesses: 1, 1.5, 2 and 4 inches
Elastic Moduli: 50, 100, 200, 400 and 800 ksi
Poisson's Ratio: 0.3
Density: 145 pcf

Base

Thicknesses: 8 and 14 inches
Elastic Moduli: As defined in Figure 3

| | |
|---|---|
| 4886 | 0.239 |
| 7000 | 0.325 |
| 8787 | 0.365 |

where = bulk stress
Poisson's Ratio = 0.4
Density = 135 pcf

Subgrade

Thickness: Infinite
Elastic Moduli: As defined in Figure 4
Poisson's Ratio: 0.45
Density: 120 pcf

The finite element mesh consisted of 18 columns and 19 rows. The element sizes were then smallest nearest to the load, in accordance with the ILLIPAVE User's Manual (2). Five iterations of each computer run were conducted in order to insure convergence.

Truck Tire Loads

A typical 10.00-20 bias-ply truck tire was selected for use in this study. This tire is representative of the type of bias-ply truck tires in use on Texas highways. Radial truck tires were considered and are

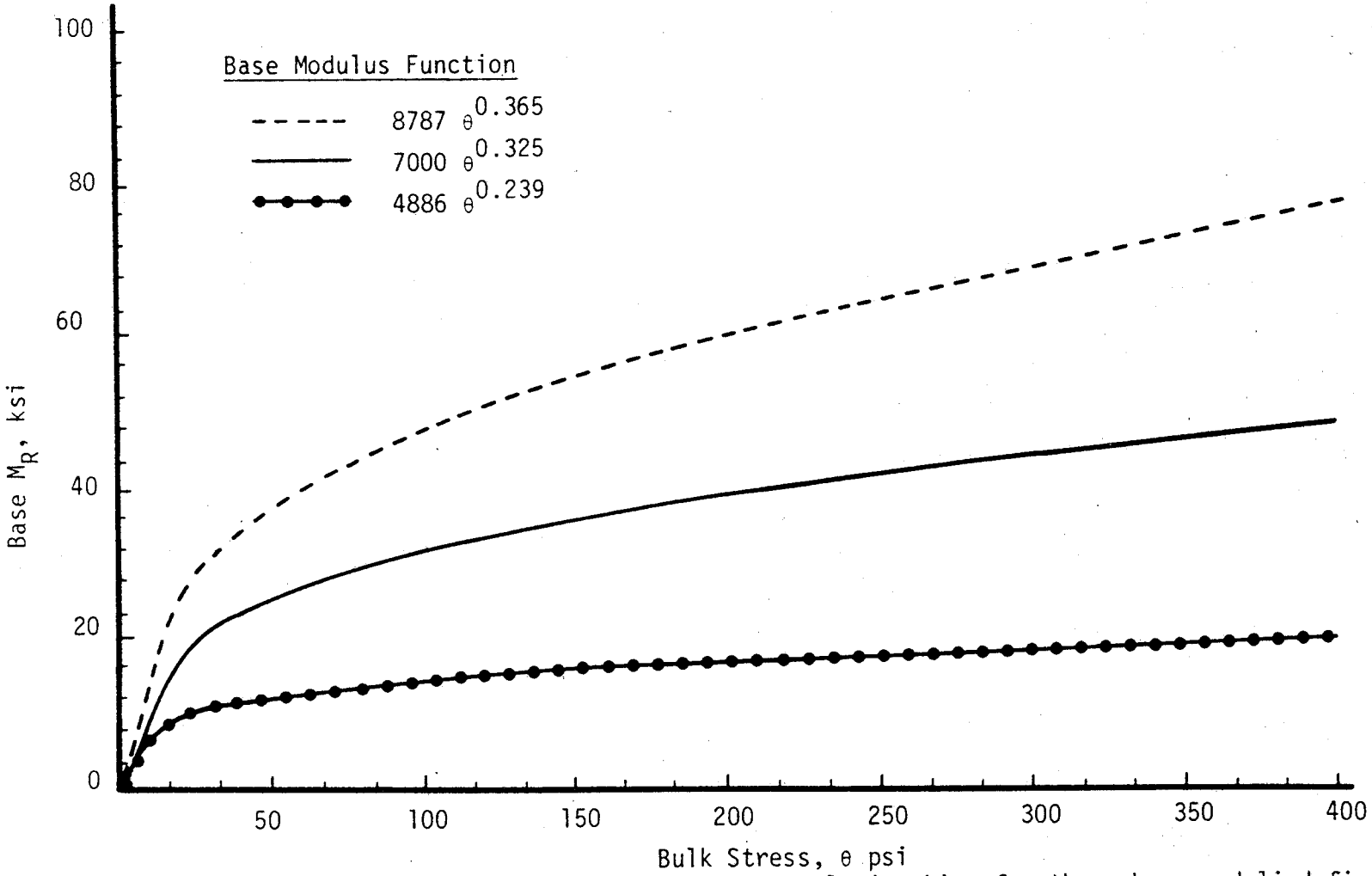


Figure 3. Base Resilient Modulus - Bulk Stress Relationships for three base moduli defined by $8787\ \theta^{0.365}$, $7000\ \theta^{0.325}$ and $4886\ \theta^{0.239}$.

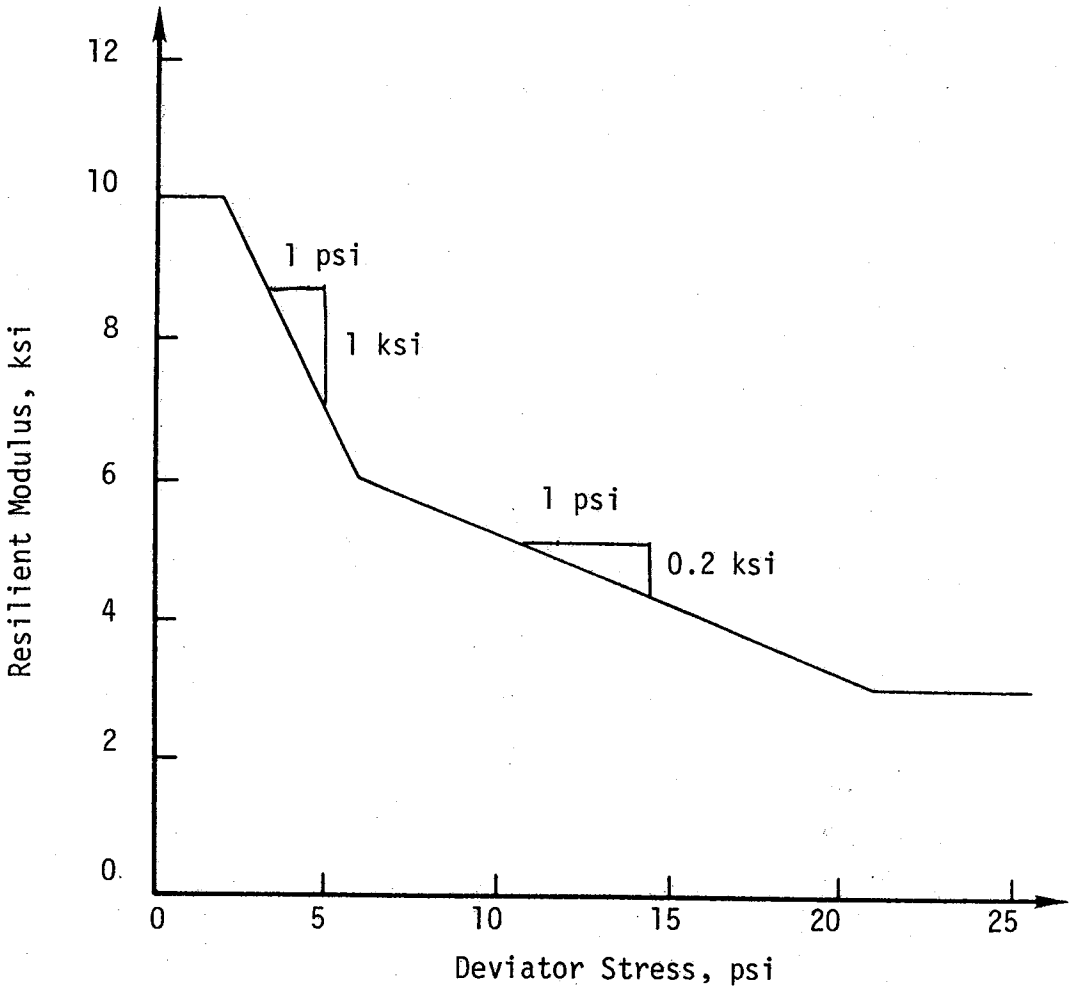


Figure 4. Resilient Modulus-Deviator Stress Relationship for subgrade soil.

begining to be more prevalent in the highway stream, especially on the interstates and primary system. However, because the bias tire has historically been the most prevalent type, it was selected for use in these inital analyses.

For this study, a thin cross-section of a Goodyear Hi-Miler 10.00-20 14-ply bias truck tire carcass was obtained; the input data for the Tielking tire model was developed by measuring cord locations, angles, and plies on a section of the tire; and the tire pressure distributions were calculated using output from the Tielking tire model.

Two tire pressures were selected for this analysis: 75 psi and 125 psi. Figures 5 and 6 show the vertical and horizontal contact pressure distributions developed from the Tielking tire model for this tire inflated to 75 psi and 125 psi, respectively. Appendix A shows in detail how these pressure distributions were resolved into forces for input into ILLIPAVE. The Tielking tire model gives as output pressures at designated points throughout the entire tireprint. Since ILLIPAVE can only accept one plane of pressure as input, the vertical plane with the axis parallel to the truck axles and at the centerline of the tire print was selected for the study.

The two inflation pressure values were selected because the first value represents a typical historical value used for the design and analysis of highway pavement structures while the second value represents the inflation pressure level of about the highest 20% of truck tires on Texas highways according to field study data collected by Texas Transportation Institute personnel during the spring and summer of 1984. While the 125 psi value may appear high to some readers, representatives from tire manufacturers indicate that within the next five years, inflation pressures will continue to rise to nearly 150 psi. The impetus for these higher values is reduced rolling resistance which produces reduced vehicle operating costs. The tire load selected was the maximum legal load for an 18-kip single axle and corresponds to 4500 pounds per tire.

The horizontal shear pressures were modeled as a funcion of a sine curve with a maximum lateral pressure of 50 psi. After consultation with

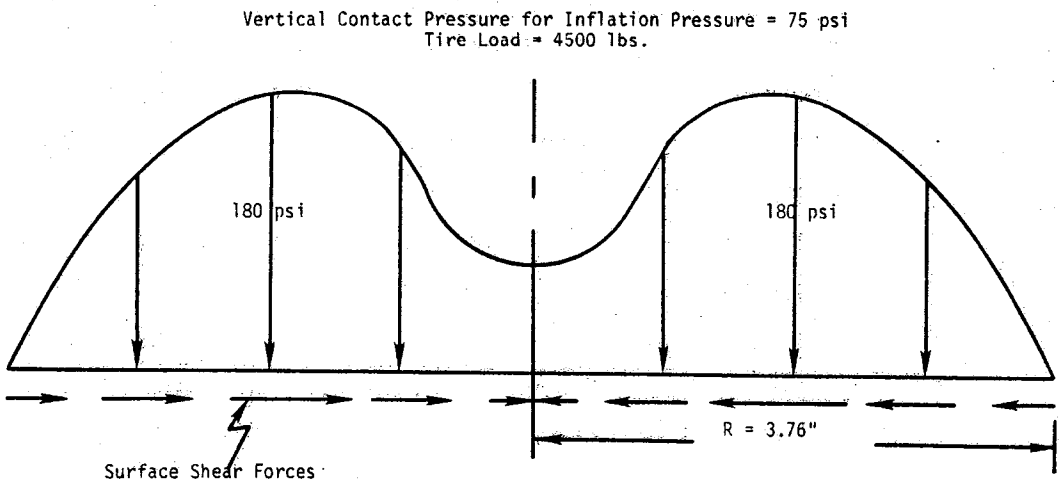


Figure 5. Non-linear vertical tire pressure distribution with lateral surface shear forces as developed using finite element model by Tielking for an inflation pressure of 75 psi and tire load of 4,500 lbs.

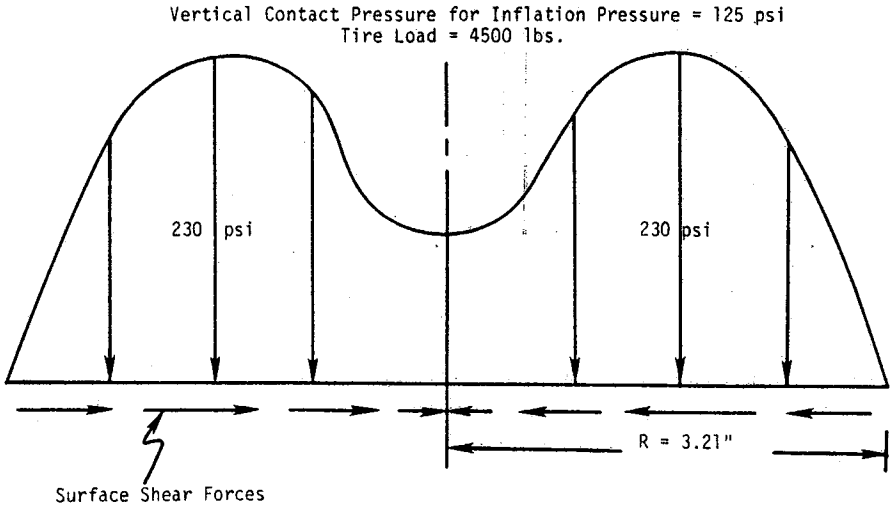


Figure 6. Non-linear vertical tire pressure distribution with lateral surface shear forces as developed using finite element model by Tielking for an inflation pressure of 125 psi and tire load of 4,500 lbs.

Dr. Tom Tielking, this distribution and maximum value of pressure were selected to be a reasonable representation of the lateral pressure distribution. The derivation of the nodal force values, along with a more detailed explanation of the distributions, is contained in Appendix A. The equation for the lateral pressure distribution is:

$$T = c \sin \frac{\pi y}{R}$$

where:

T = lateral shear pressure at a particular point, psi;
c = maximum lateral pressure (50 psi for this case), psi;
y = distance from centerline of tire at which the lateral pressure is desired, inches; and
R = adjusted radius of the tire print, inches.

Two different lateral pressure distributions were developed since the radius changes slightly as the tire inflation pressure increases from 75 psi to 125 psi.

# CHAPTER V

## STUDY RESULTS

Several types of comparisons have been made using results from the ILLIPAVE computer runs. These comparisons include plots to show the effects of tire pressure on horizontal tensile strains in the surface; the effects of layer modulus and thickness on strains in the pavement; and the effects of layer modulus and thickness on the shear stresses in the base. Additional analyses include the evaluation of the effects of the tensile strains on predicted fatigue damage and the evaluation of the effects of the compressive strains on the permanent deformation of the pavement. Each analysis is presented separately in the following sections.

### Tire Pressure Effects

The series of computer runs used in this analysis is the same set described in the tire models and study parameters sections of this report. The Tielking tire model, using inflation pressures of 75 and 125 psi, is used to determine the effects of increased tire pressures on the tensile strains in the surface. Comparisons are also made between the tensile strains produced by using the Tielking tire model and the uniform pressure model.

To describe the effects of truck tire pressure on tensile strains at the bottom of the surface, Figures 7 and 8 have been prepared. Figure 7 shows the change in tensile strain for a surface of varying thickness and with a modulus of 400 ksi on an eight-inch base with an increase in tire pressure from 75 psi to 125 psi. Figure 8 shows the same information for a surface with a modulus of 50 ksi.

The increase in tire pressure produces increases in the strain ranging from 20 to 30 percent for the 1-inch surface data in Figure 7 with the 30 percent increase occurring for the weakest base layer. Notice that the effect of increased tire pressure decreases with

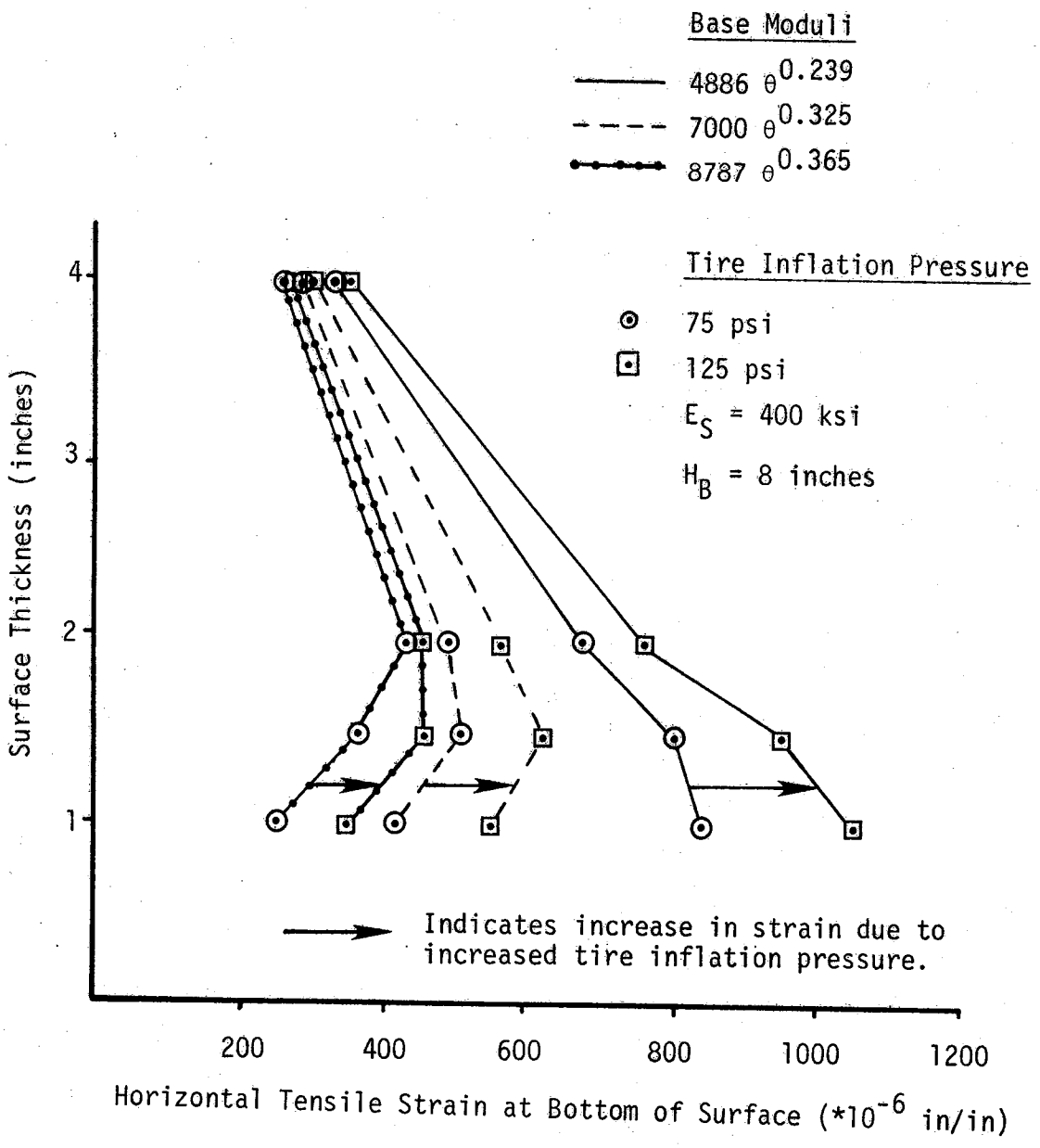


Figure 7. Effects of increased tire pressure on tensile strain at the bottom of the surface for a surface modulus of 400 ksi and base thickness of 8 inches.

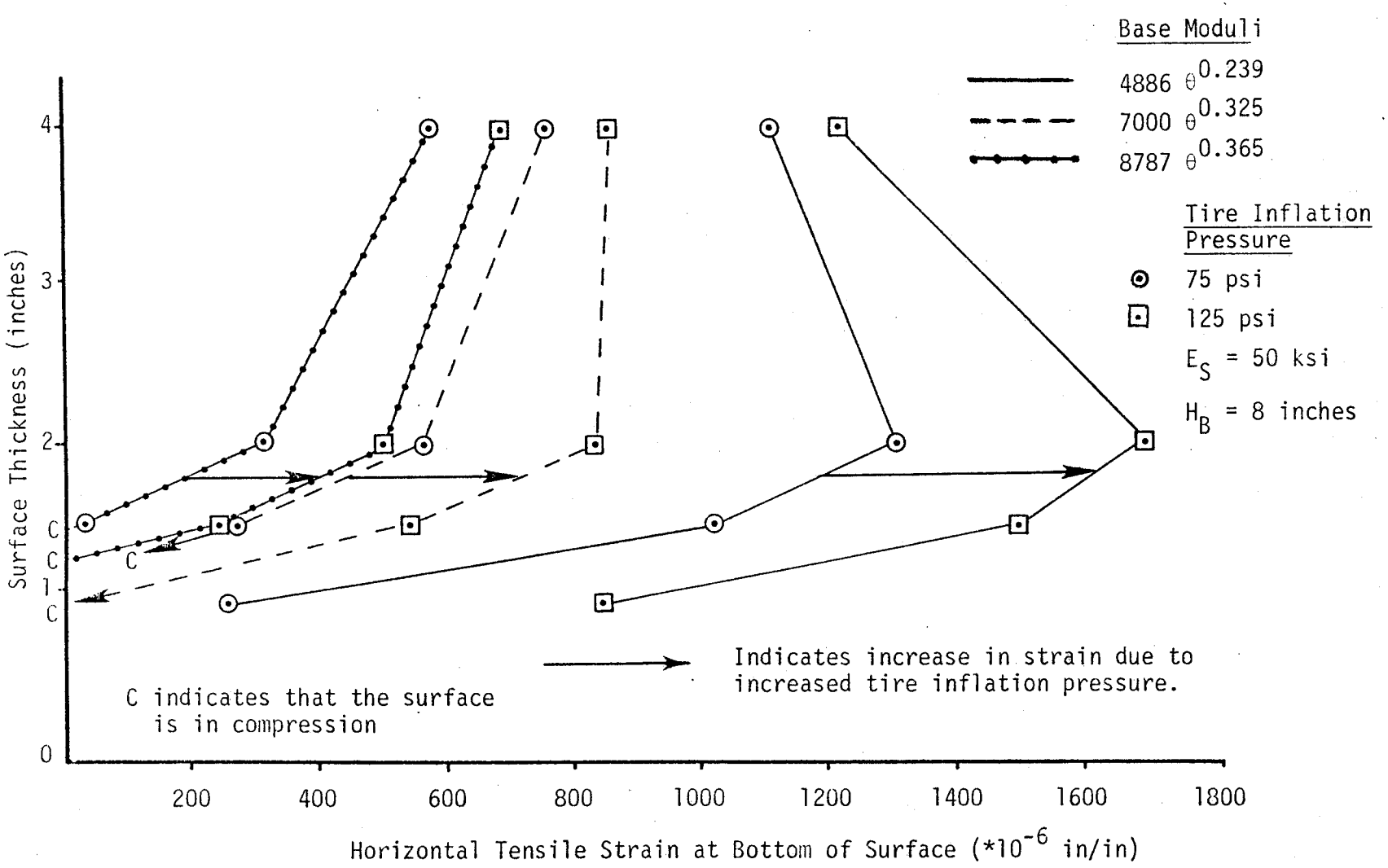


Figure 8. Effects of increased tire pressure on tensile strain at the bottom of the surface for a surface modulus of 50 ksi and base thickness of 8 inches.

increasing surface thickness and that the relative strain increase for a 4-inch surface is less than 10 percent.

Figure 8 shows that at 75 psi inflation pressure a surface 1-inch thick is in compression for the moderate and strong bases and that the tensile strain is low for the weak base. However, when the tire pressure increases to 125 psi, the 1-inch surface still remains in compression for the moderate and strong bases but the tensile strain increases 30 percent for the weak base layer. In fact, for the low modulus base all the thicknesses experience strains near or in excess of 0.001 in./in., which Monismith says is the upper limit of linear behavior of these materials "...for strains exceeding 0.001 in./in., asphalt concrete mixtures are non-linear, rate dependent materials with different properties in tension and compression" (14).

The increases in strain for the 1.5-inch surface range from about 30 to 55 percent for the strong to weak bases, indicating the significance of the effect of increasing tire pressures on surfaces having low moduli. Therefore, it is important to recognize that the advice often given, to make thin pavements flexible, must be conditioned by adding that the surface thickness should be limited to less than 1.5 inches and that the base should be moderate to strong. Also, very flexible asphalt concrete materials should not be used in combinations with weak granular bases because with increases in tire pressures these pavements will experience tensile strains well over 1000 micro-strain.

For the thick flexible surfaces the increase in tire pressure produces a smaller increase in tensile strain than for the thinner surface. But the increase in strain for the more flexible surfaces in Figure 8 is much larger than that experienced by the stiffer surfaces included in Figure 7. The 14-inch base will produce the same type of figures but with smaller magnitudes of tensile strain.

To describe the effects of the truck tire pressure on tensile strains at the top of the surface, Figure 9 has been prepared. It shows the change in tensile strain for a surface of varying thickness and with a modulus of 400 ksi on an 8-inch base with an increase in tire pressure from 75 psi to 125 psi.

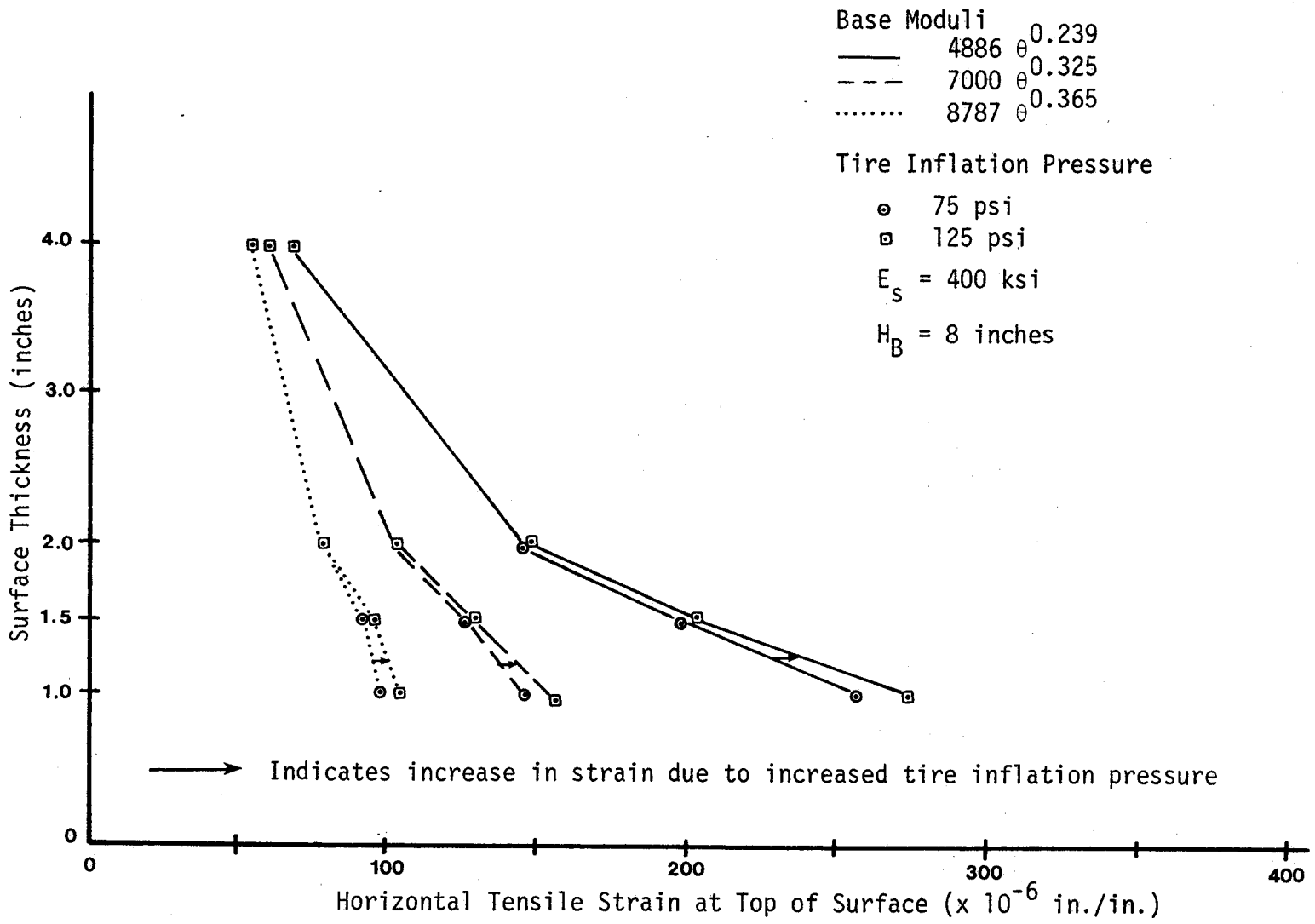


Figure 9 . Effects of increased tire pressure on tensile strain at the top of the surface for a surface modulus of 400 ksi and base thickness of 8 inches.

The increase in tire pressures produces a minimal amount of increase in the tensile strains at the top of the surface. The 1-inch surface has strains that have increased, due to the higher pressures, by about 5 percent for all three base moduli. The effects of increased tire pressures begin to decrease until there are no differences in strain for surfaces thicker than 2-inches.

The shape of the curves and the magnitudes of tensile strain change for different values of surface modulus and base thickness. However, the tensile strains at the top of the surface area, in general, are considerably lower and do not change with increased tire pressure as much as the strains at the bottom of the surface change. Therefore, tensile strains at the bottom of the surface will usually govern the design of pavements because of their larger tensile strains and higher sensitivity to increased tire pressures. The 14-inch base will produce the same type of figure with slightly larger magnitudes of tensile strain.

To describe the effects of the truck tire pressure on compressive strain at the top of the subgrade, Figure 10 has been prepared. It shows the change in compressive strain for a surface of varying thickness and with a modulus of 400 ksi on an 8-inch base with an increase in tire pressure from 75 psi to 125 psi.

The increase in tire pressures also produces a minimal amount of increase in the compressive strains at the top of the subgrade. The 1-inch to 1.5-inch surfaces have strains that have increased, due to the higher pressures, by less than 5 percent for all three base moduli. The effects of increased tire pressures also begin to decrease until there are no differences in compressive strain for surfaces thicker than 2-inches. There is a cross-over of lines in Figure 10 near the 4-inch surface; this cannot be readily explained, but the difference is only approximately 35 micro-strain and is within the range of inaccuracy of the computer model.

The shape of the curves and the magnitudes of compressive strain change for different values of surface modulus and base thickness. However, the compressive strains at the top of the subgrade do not significantly change as a result of increased truck tire pressures.

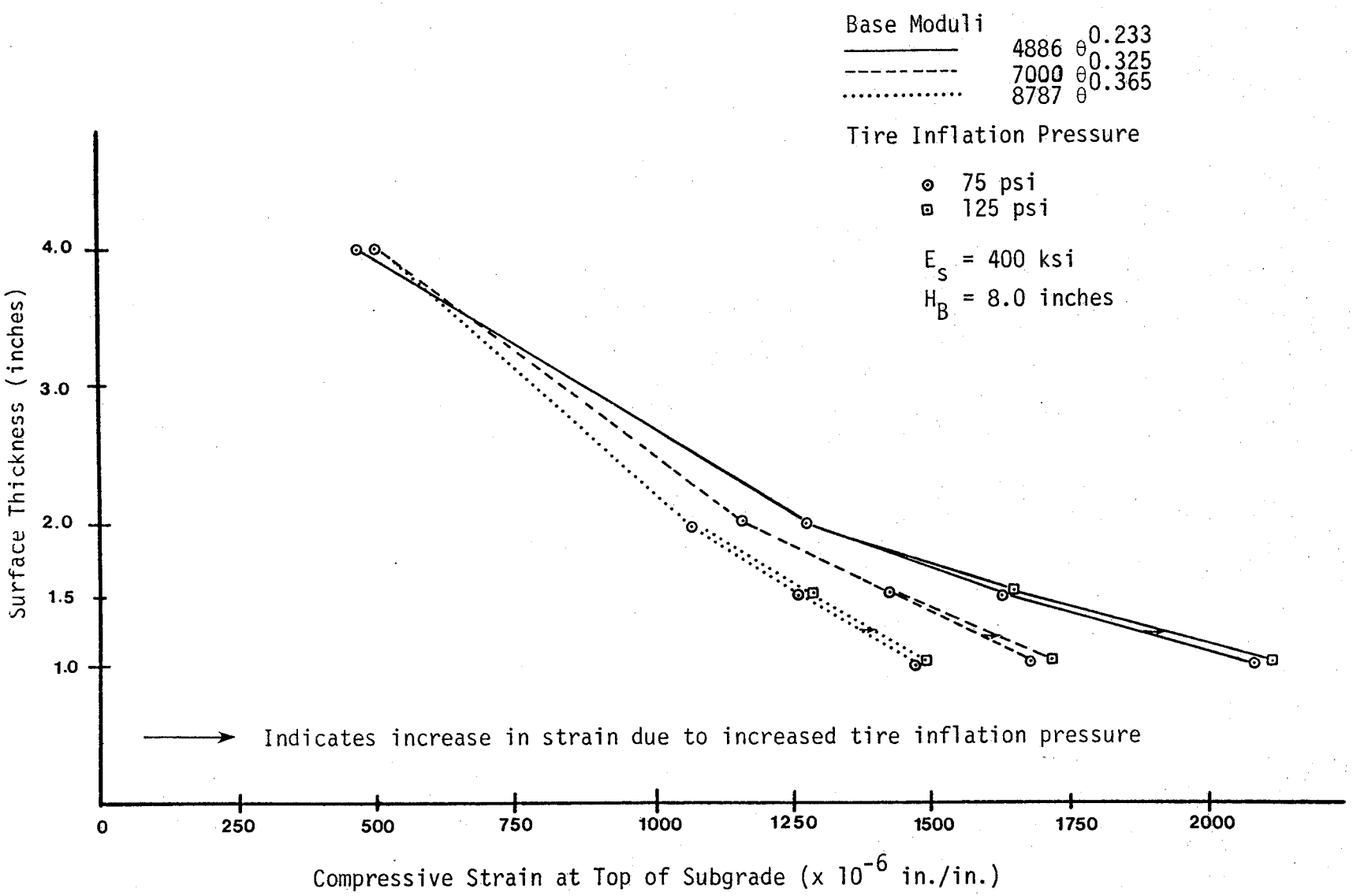


Figure 10 . Effects of increased tire pressure on compressive strain at the top of the subgrade for a surface modulus of 400 ksi and base thickness of 8 inches.

To describe the effects of using the Tielking tire model instead of the uniform pressure model, three computer runs using uniform pressure of 75 psi and three computer runs using a uniform pressure of 125 psi were made. Table 1 shows the tensile strain at the bottom of the surface and the corresponding ESAL produced by a uniform pressure distribution with no lateral pressures. The material properties that were used are shown at the bottom of Table 1.

To give an indication of the magnitude of the differences between using the Tielking tire model instead of the uniform pressure model, Figure 11 has been prepared. It shows that the tensile strains at the bottom of the surface are increased by almost 100 percent for surface thicknesses less than two inches and that for the 1-inch surface the Tielking tire model has the same effect on increasing the tensile strain as does changing the uniform pressure from 75 psi to 125 psi. For surface thicknesses greater than two inches, the effects begin to decrease but not to the point where the strains are anywhere close to being the same value. These large discrepancies in strain may help to explain why, within pavements, the surfaces begin to crack before they are expected to begin fatigue cracking.

Further discussion concerning the subject of tire inflation effects is given in the following sections. Numerous figures depicting the behavior of inflation pressures on strains in the pavement are present when discussions are made about the base modulus and thickness effects and the surface modulus and thickness effects.

## Layer Modulus and Thickness Effects

To show the effects of surface modulus and thickness on strains for different base moduli and thicknesses with inflation pressures of 75 psi and 125 psi, a series of figures has been prepared. This analysis has been divided into three categories to evaluate the effects of surface modulus and thickness on: (1) the tensile strains at the bottom of the surface, (2) the tensile strains at the top of the surface, (3) the

Table 1 . Tensile strains at the bottom of A.C. surface and ESAL produced by a uniform pressure distribution.

| Tire Pressure (psi) | Surface Thickness (inches) | $E_T$ Bottom ($x10^{-6}$ in/in) | $ESAL_{B.S.}$ |
|---|---|---|---|
| 75 | 1.0 | 140.1 | 447,800 |
| 75 | 2.0 | 259.9 | 25,202 |
| 75 | 4.0 | 195.7 | 94,447 |
| 125 | 1.0 | 245.5 | 32,863 |
| 125 | 2.0 | 355.9 | 5,831 |
| 125 | 4.0 | 237.2 | 38,571 |

With the material properties as follows:

Surface $E_S$ = 400 ksi

Base $E_B = 8787\ \theta^{0.365}$

$H_B$ = 8"

Subgrade $E_{SG}$ = As defined by Figure IV-2

where: $\theta$ = bulk stress, psi.

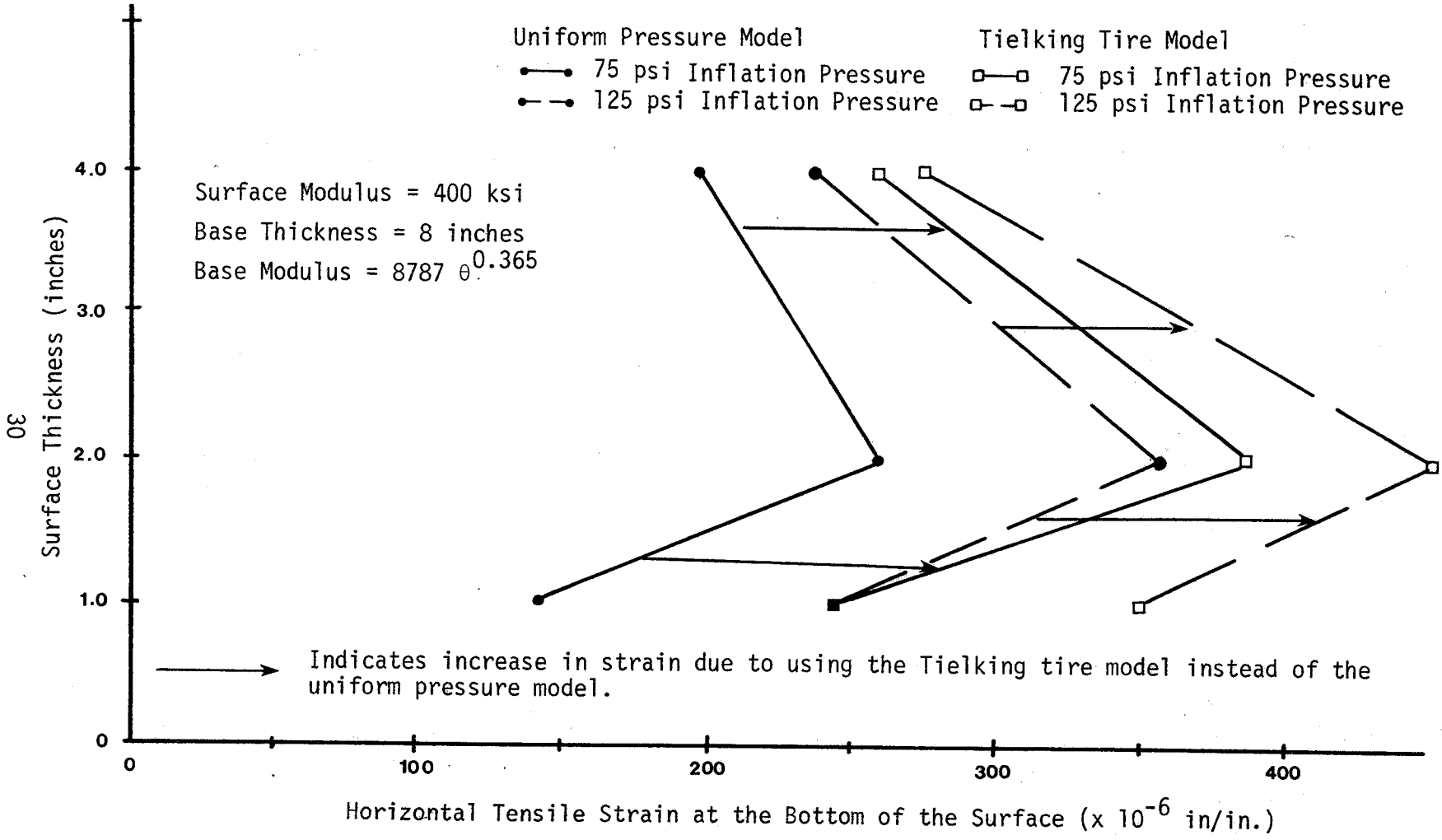


Figure 11 . Differences in the tensile strains produced from using the Tielking tire model and the uniform pressure model.

compressive strain at the top of the subgrade and (4) the shear stress at the top of the base.

The tensile strains at the bottom of the surface at a distance of 0.5 inches from the centerline of the tire print have been tabulated. At the center of each finite element the stresses are given as output. Between the two elements, the stresses are linearly interpolated to the 0.5 inch values and the resulting strain calculated. The tensile strains at the top of the surface have been tabulated at the point where the maximum tensile strain occurs. That distance did not vary with base modulus but varied substantially as the surface modulus and thickness changed. As the surface modulus and thickness increases, the distance to maximum tensile strain at the top also increases. Appendix D shows the tensile strains at the top and bottom of the surface and the distance to maximum tensile strain at the top of the surface.

The two primary distresses addressed in this analysis are fatigue and rutting. To evaluate the occurrence of these distresses, the tensile strain in the surface has been related to fatigue damage and the compressive strain at the top of the subgrade has been related to rutting. Permanent deformations that may occur in the surface layer itself will be evaluated in a subsequent report.

Using the computer outputs from this analysis, six figures have been prepared for each evaluation. The figures consist of two groups, each group of 3 figures has a different base thickness, 8 inches and 14 inches. Each group contains a figure for each of three different base moduli. The strain contours at the top of each figure are for a 75 psi tire inflation pressure and the bottom for a 125 psi tire inflation pressure.

Tensile Strain at Bottom of Surface. Tensile strains are the most critical in determining expected fatigue damage. For these thin pavements, the tensile strains at the bottom of the surface are generally much higher than those at the top of the surface.

To control the extent of fatigue damage, the tensile strains at the bottom of the surface must be kept fairly low, the exact level depending on the total traffic and the characteristics of the surface layer. Since

low strains are desirable, the first analysis of the tensile strain plots in Figure 12 through 17 involve identifying the low strain areas. For purposes of discussion, a strain level of 300 microinches/inch has been identified as a level below which reasonably adequate performance can be achieved for these thin pavement structures. Fatigue life is significantly reduced as strains exceed this level. The 300 microinches/inch strain level was determined by using a fatigue equation from the AASHO Road Test with typical traffic for these low volume roads to calculate the maximum strain that would be allowed to support this traffic.

For the 8-inch base, strain levels below 300 microinches/inch occur in both the upper right and the lower left corners in Figures 12 and 13, but only in the upper right corner in Figure 14. These corners correspond to either areas of low surface modulus and thickness or high surface modulus and thickness. Notice that increasing the tire inflation pressure from 75 to 125 psi causes higher strain contour levels to be edged between the areas of low strain level thereby compressing them into opposite corners. In fact, the increased tire pressure for the weakest base condition, Figure 14, produces no strain level below 300 microinches/inch for the low surface modulus combinations.

The tensile strain contours for the 14 inch base are shown in Figures 15 through 17. Increasing the thickness reduces the strain slightly. Strain levels below 300 microinches/inch cover a slightly larger range of surface modulus and thickness combinations than for the 8-inch base but the general trends are the same.

Tensile Strain at the Top of the Surface. Tensile strains at the top of the surface are generally lower than those at the bottom. However, when the surface modulus is less than 100 pksi and the surface thickness is less than 1.5 inches, the maximum tensile strains at the top of the surface area are often larger than those at the bottom. The first analysis of the tensile strain at the top of the surface invovled identifying the low strain areas in Figure 18 through 23.

For the 8-inch base (Figures 18 through 20), the strain levels exceed 300 microinches/inch only in the lower left corner of Figure 20. Notice

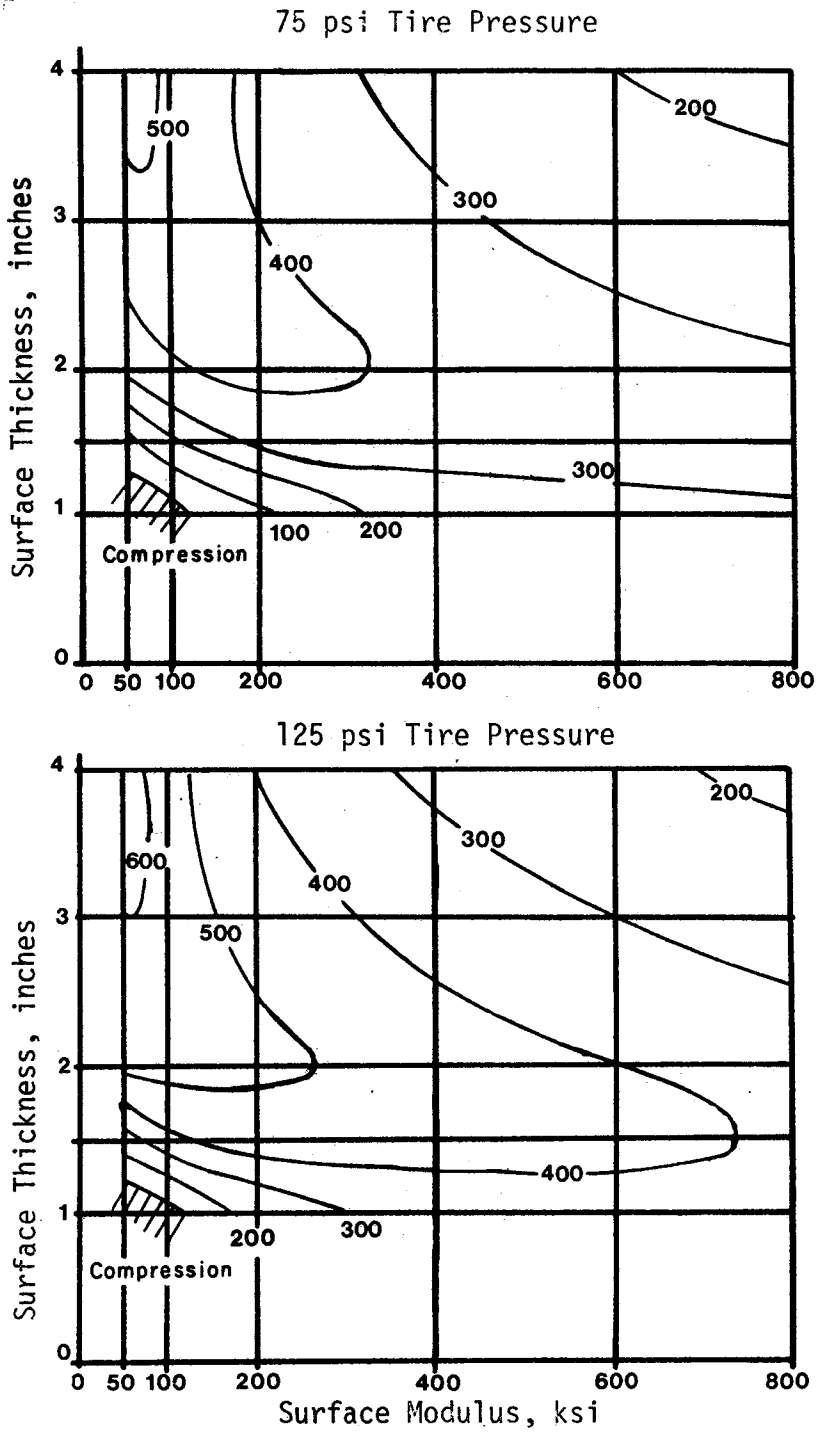


Figure 12. Tensile micro-strain contours at the bottom of the surface for $8787\theta^{0.365}$ base modulus and 8-inch base.

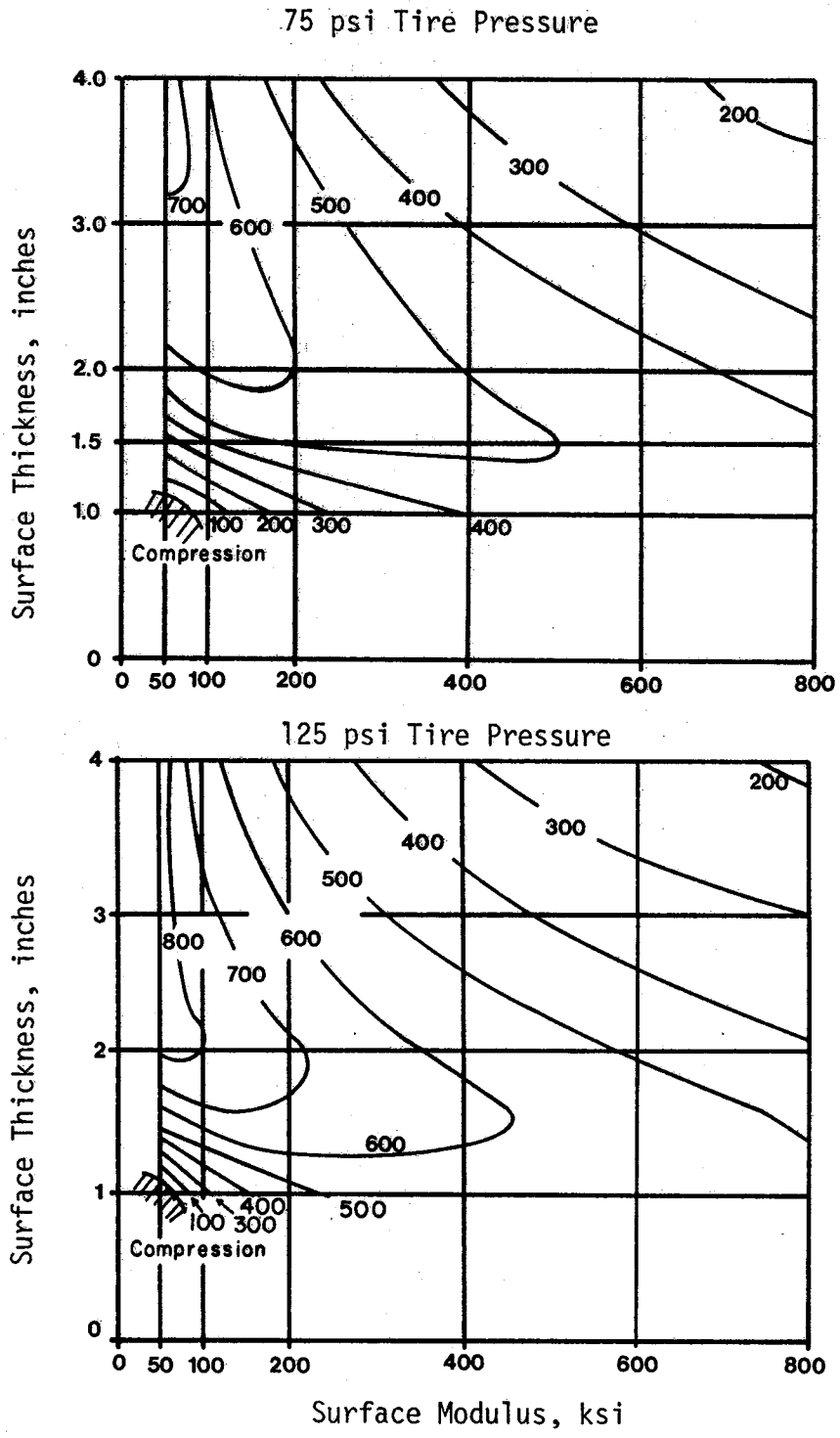


Figure 13. Tensile micro-strain contours at the bottom of the surface for $7000\,\theta^{0.325}$ base modulus and 8-inch base.

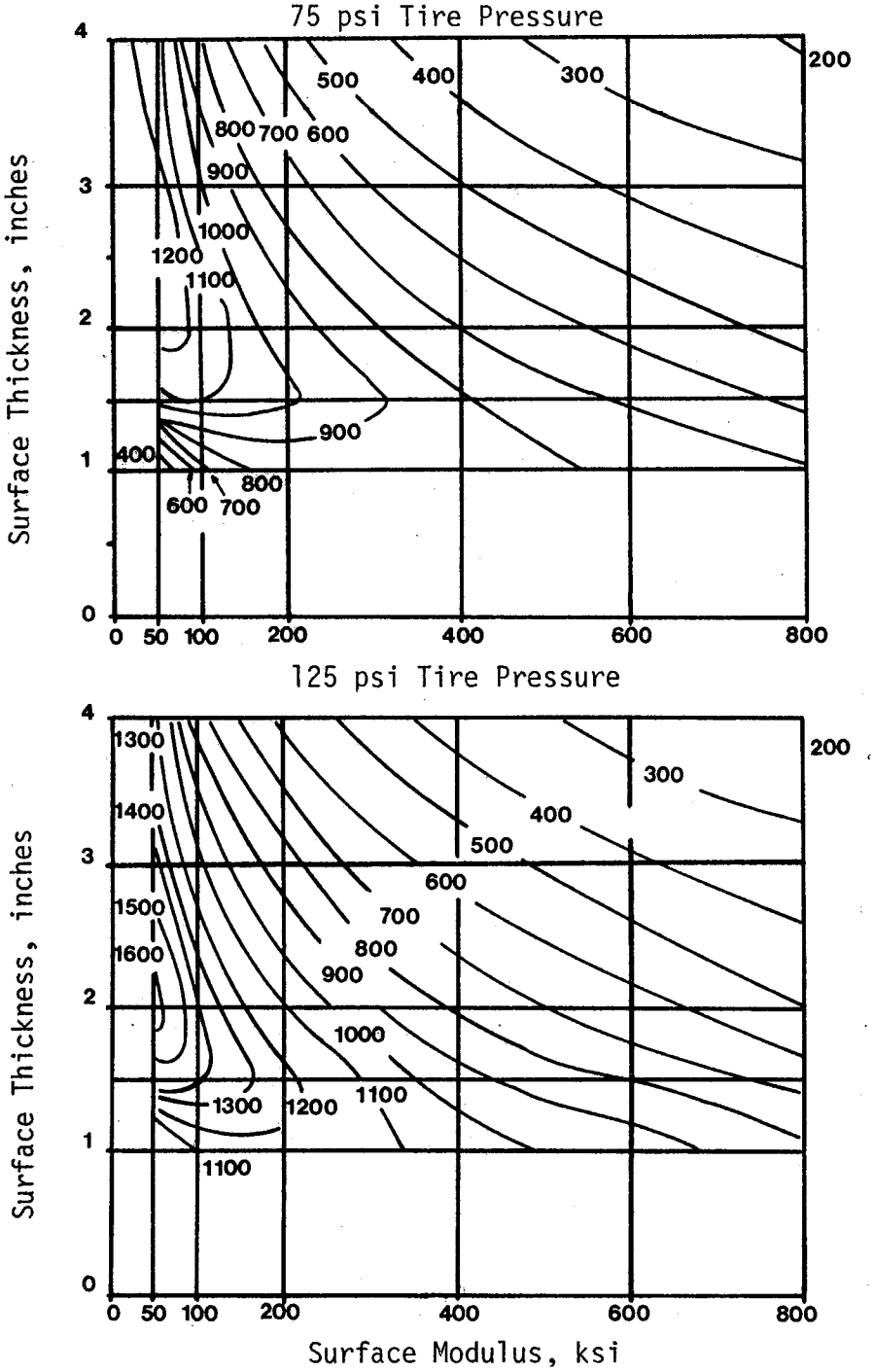


Figure 14. Tensile micro-strain contours at the bottom of the surface for $4886\theta^{0.239}$ base modulus and 8-inch base.

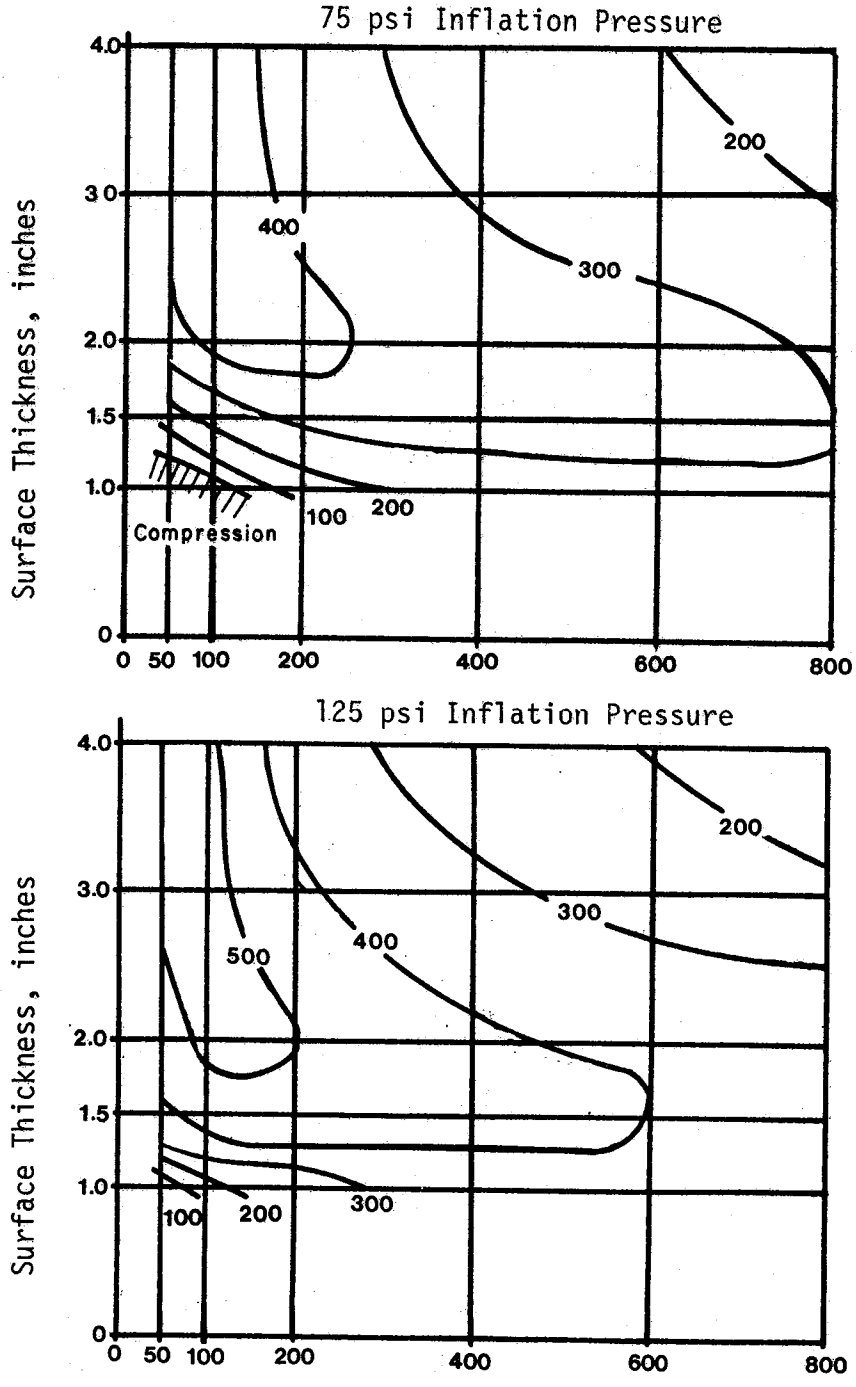


Figure 15. Tensile micro-strain contours at the bottom of the surface for $8787\theta^{0.365}$ base modulus and 14-inch base.

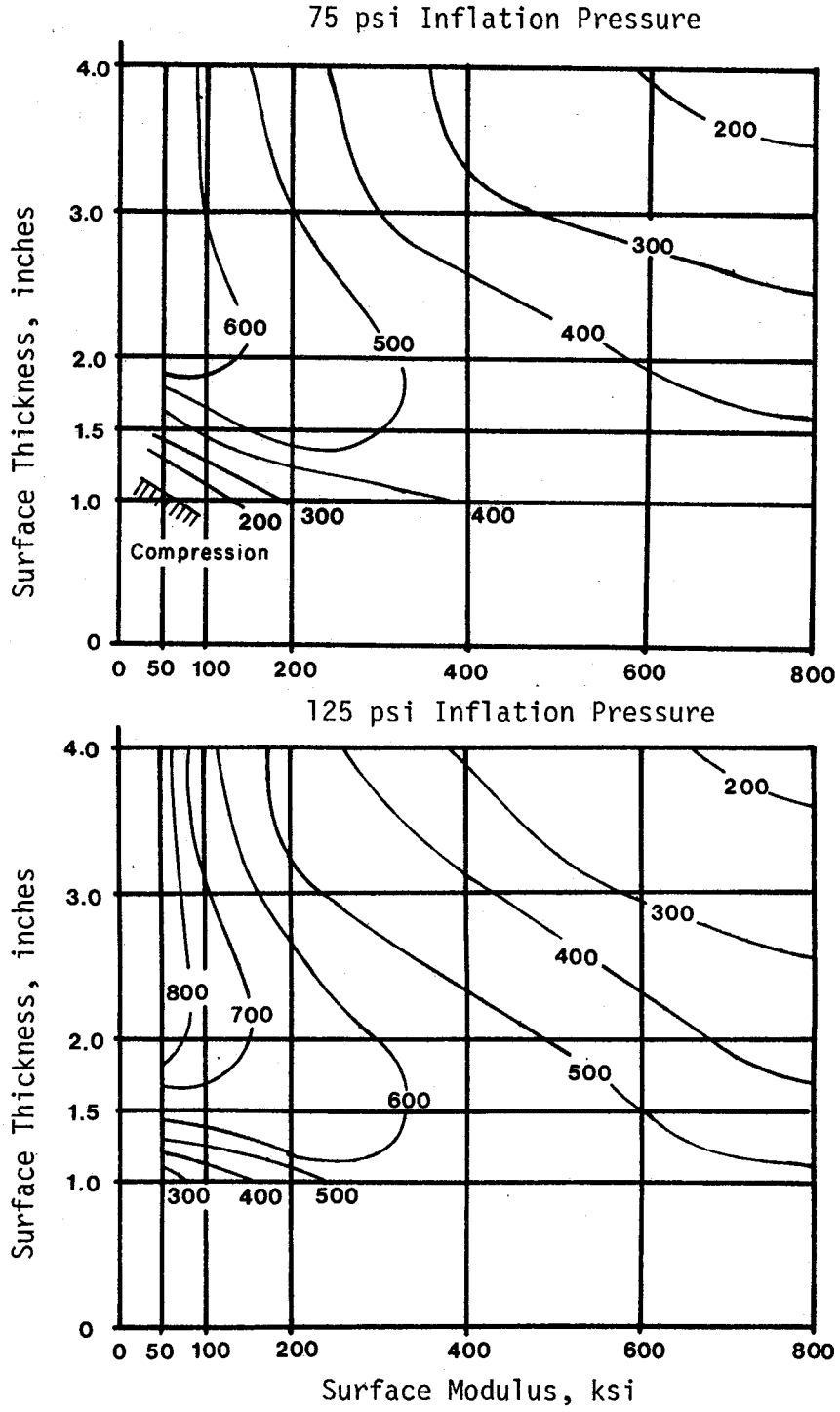


Figure 16. Tensile micro-strain contours at the bottom of the surface for $7000\theta^{0.325}$ base modulus and 14-inch base.

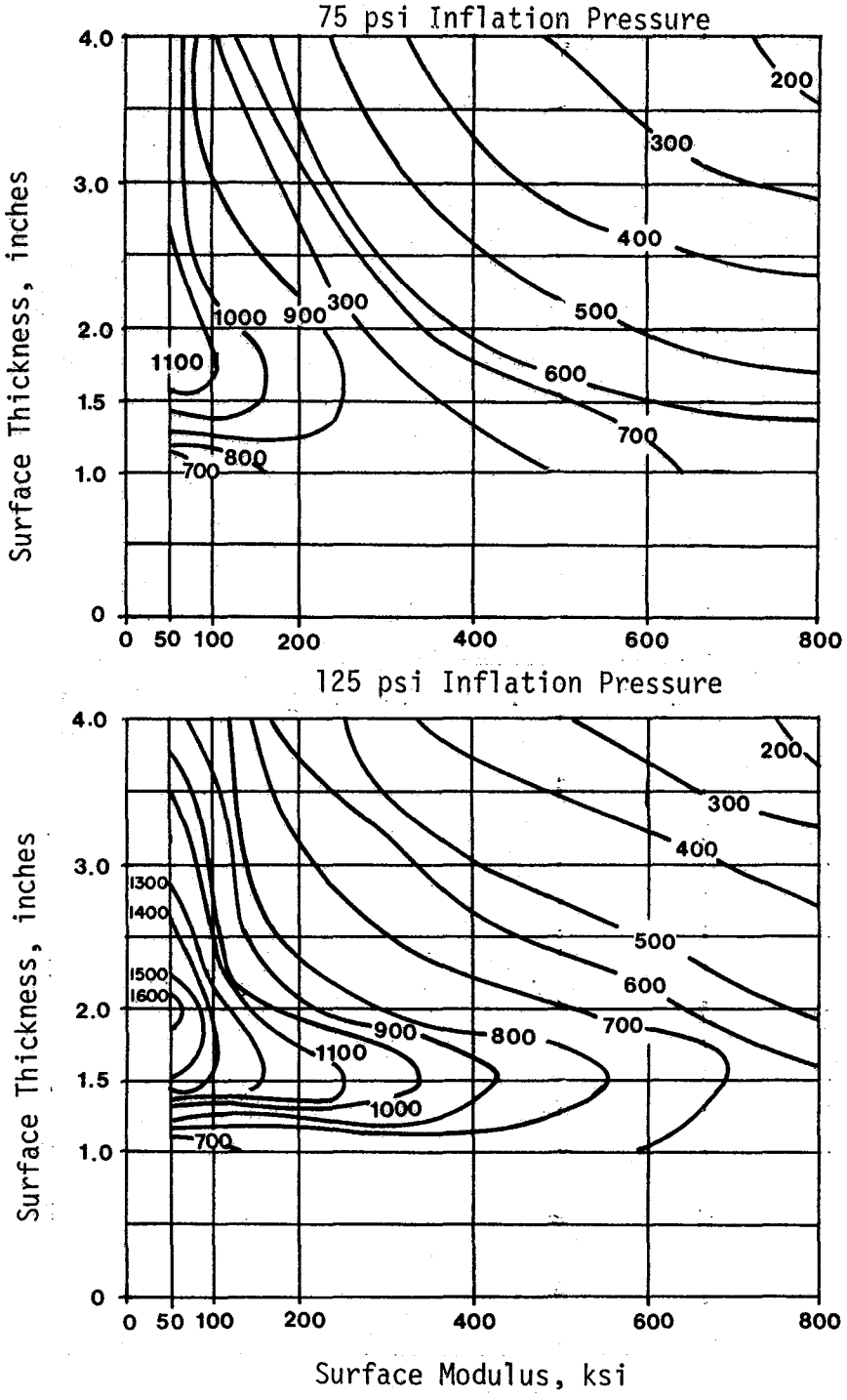


Figure 17. Tensile micro-strain contours at the bottom of the surface for $4886\theta^{0.239}$ base modulus and 14-inch base.

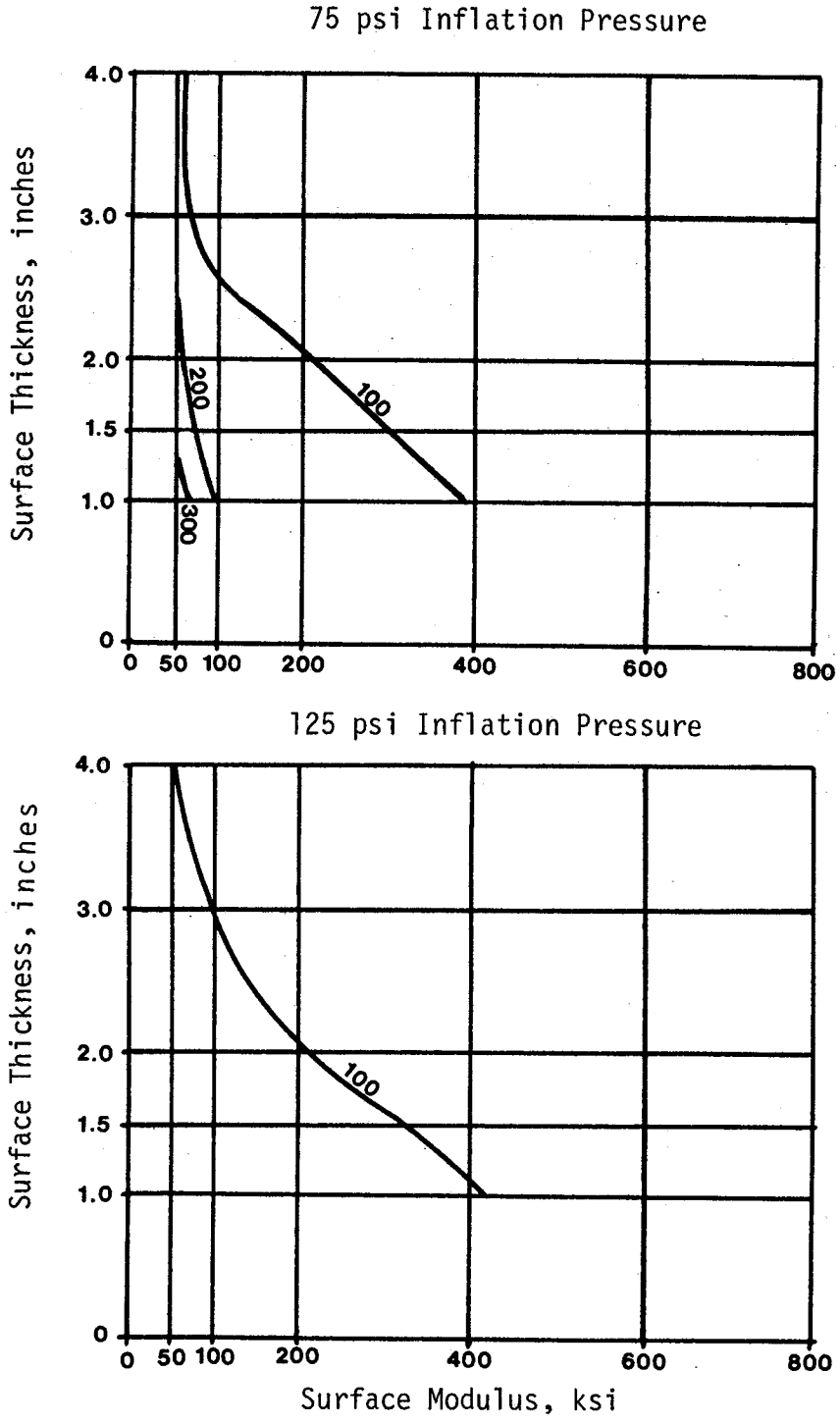


Figure 18. Tensile micro-strain contours at the top of the surface for 8787 $\theta^{0.365}$ base modulus and 8-inch base.

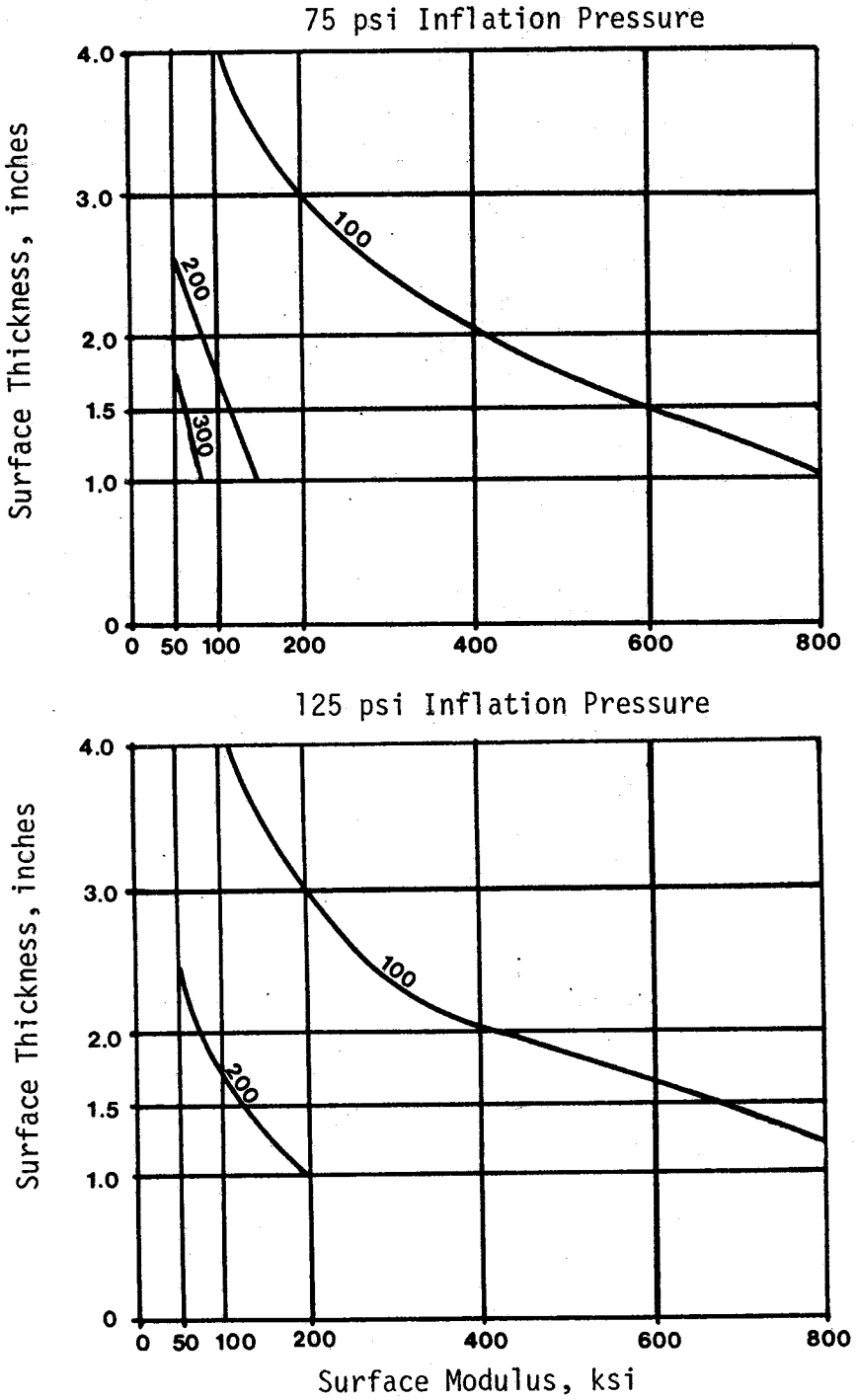


Figure 19. Tensile micro-strain contours at the top of the surface for 7000 $\theta^{0.325}$ base modulus and 8-inch base.

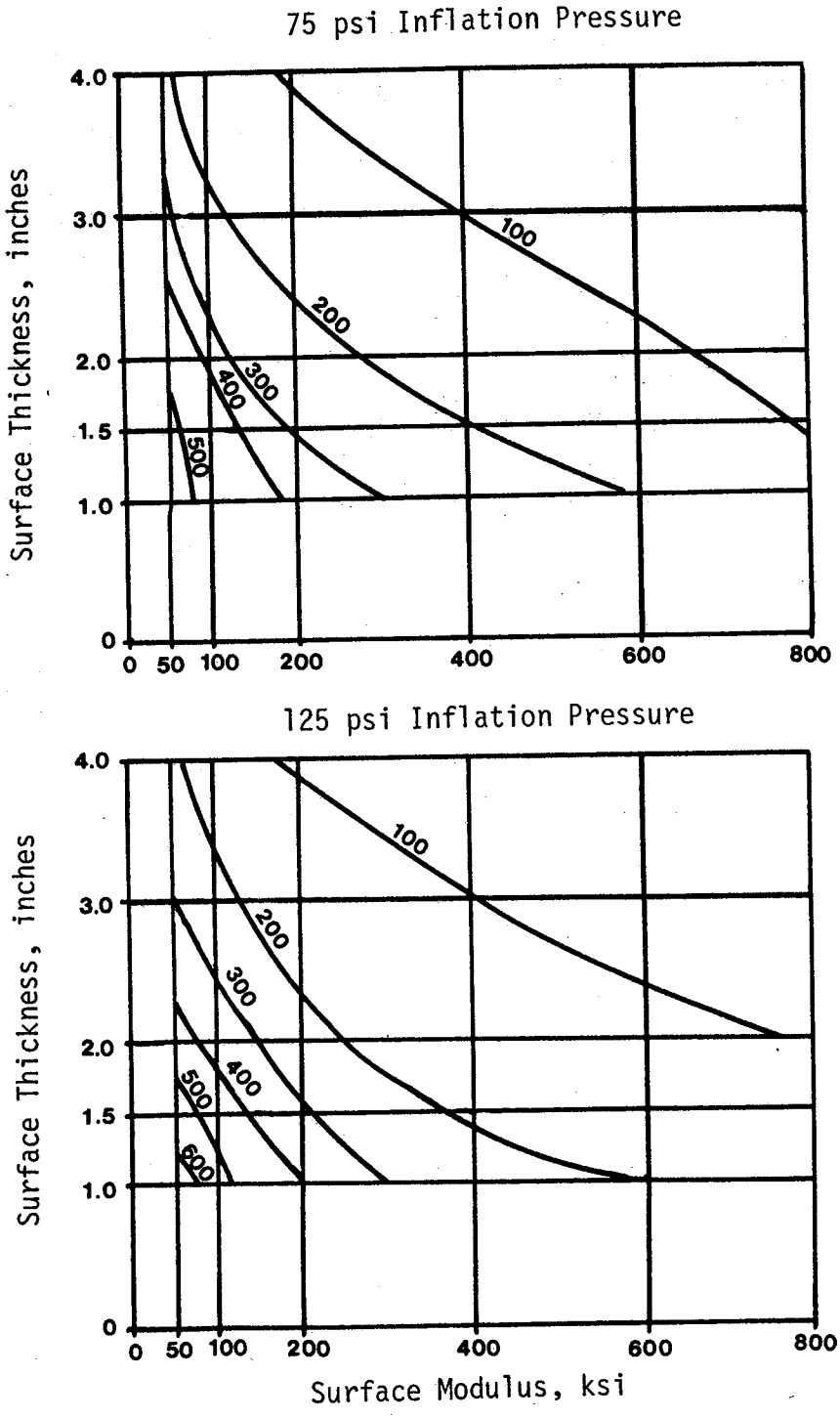


Figure 20. Tensile micro-strain contours at the top of the surface for 4886 $\theta^{0.325}$ base modulus and 8-inch base.

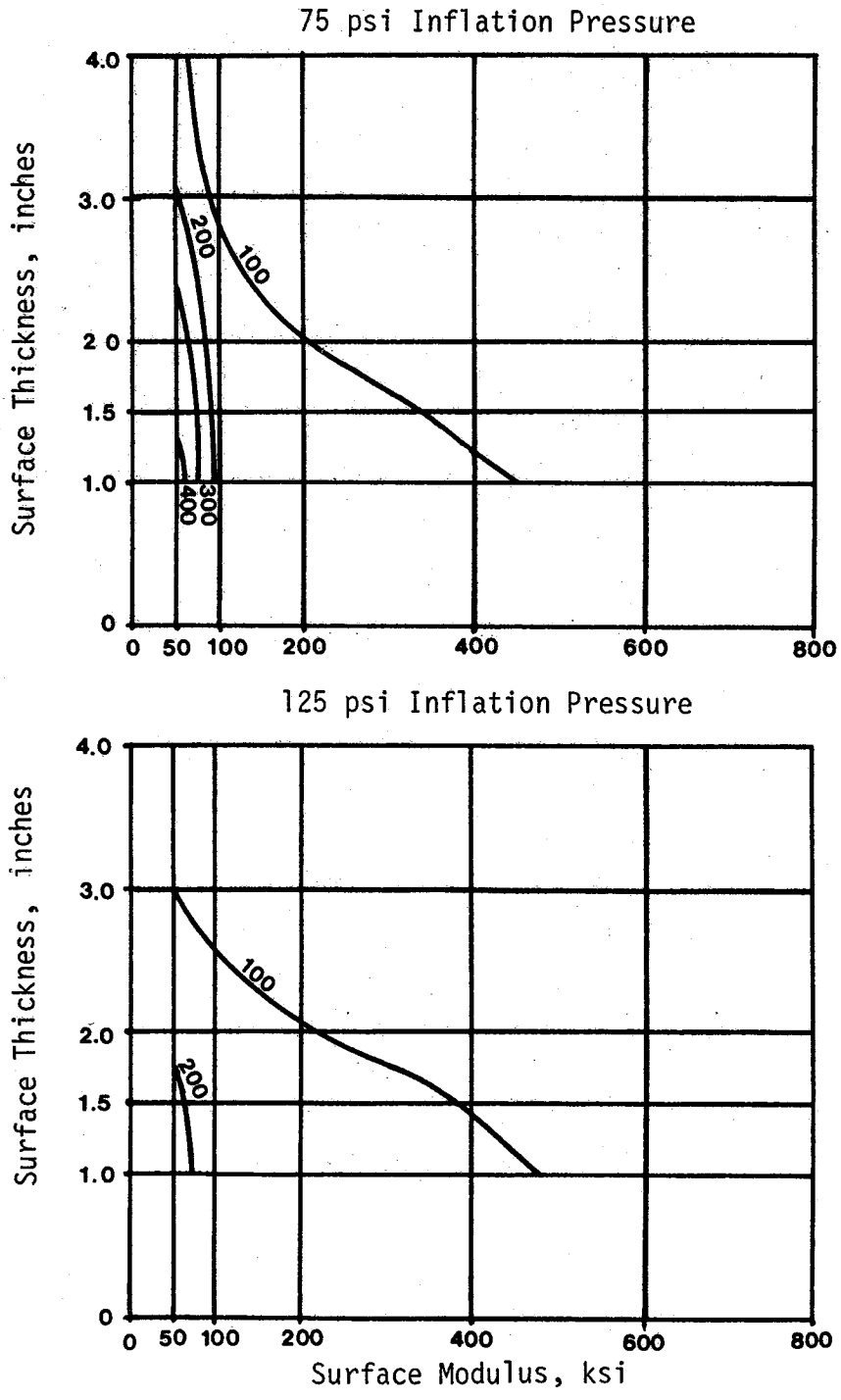


Figure 21 . Tensile micro-strain contours at the top of the surface for 8787 $\theta^{0.365}$ base modulus and 14-inch base.

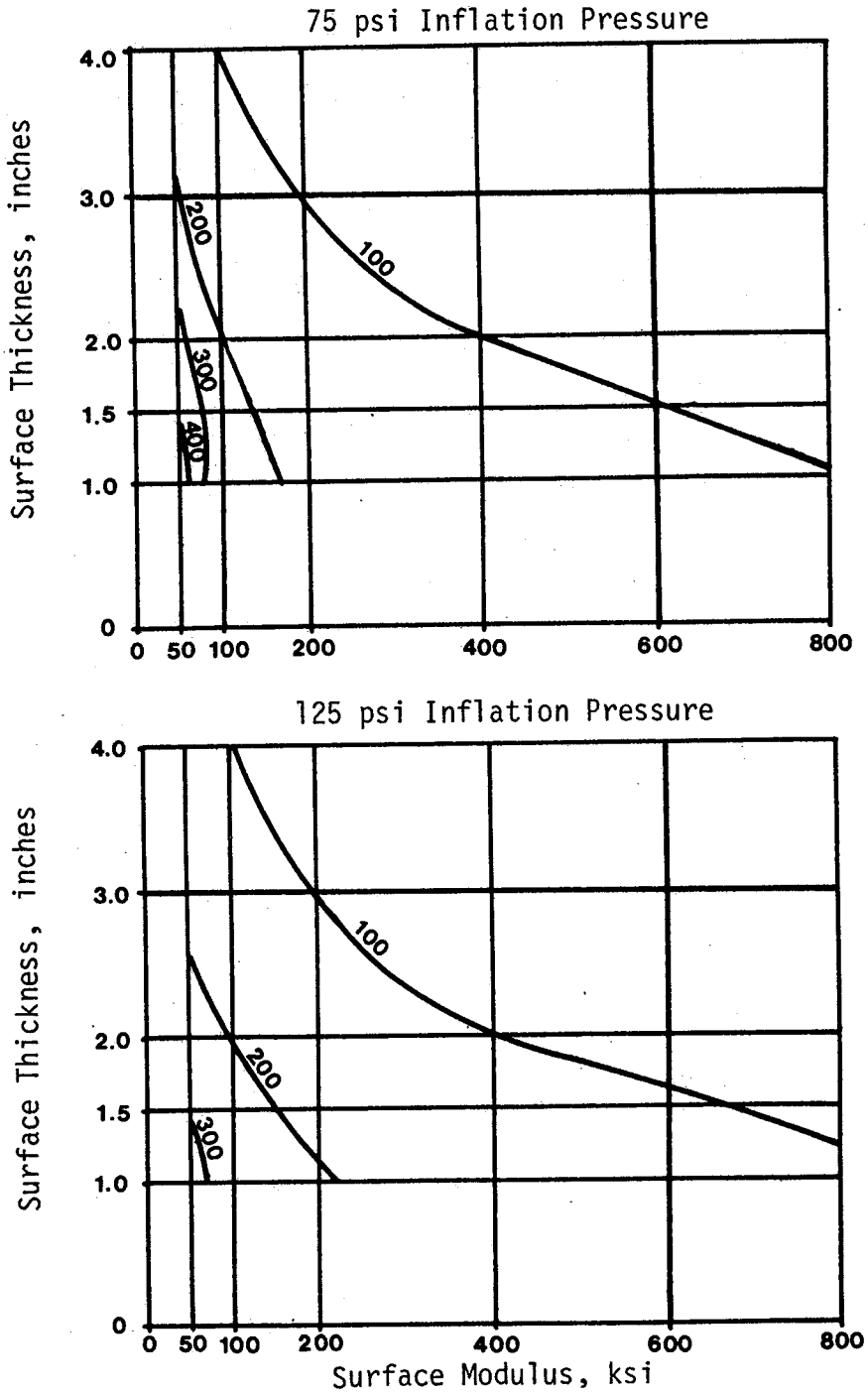


Figure 22. Tensile micro-strain contours at the top of the surface for 7000 $\theta^{0.325}$ base modulus and 14-inch base.

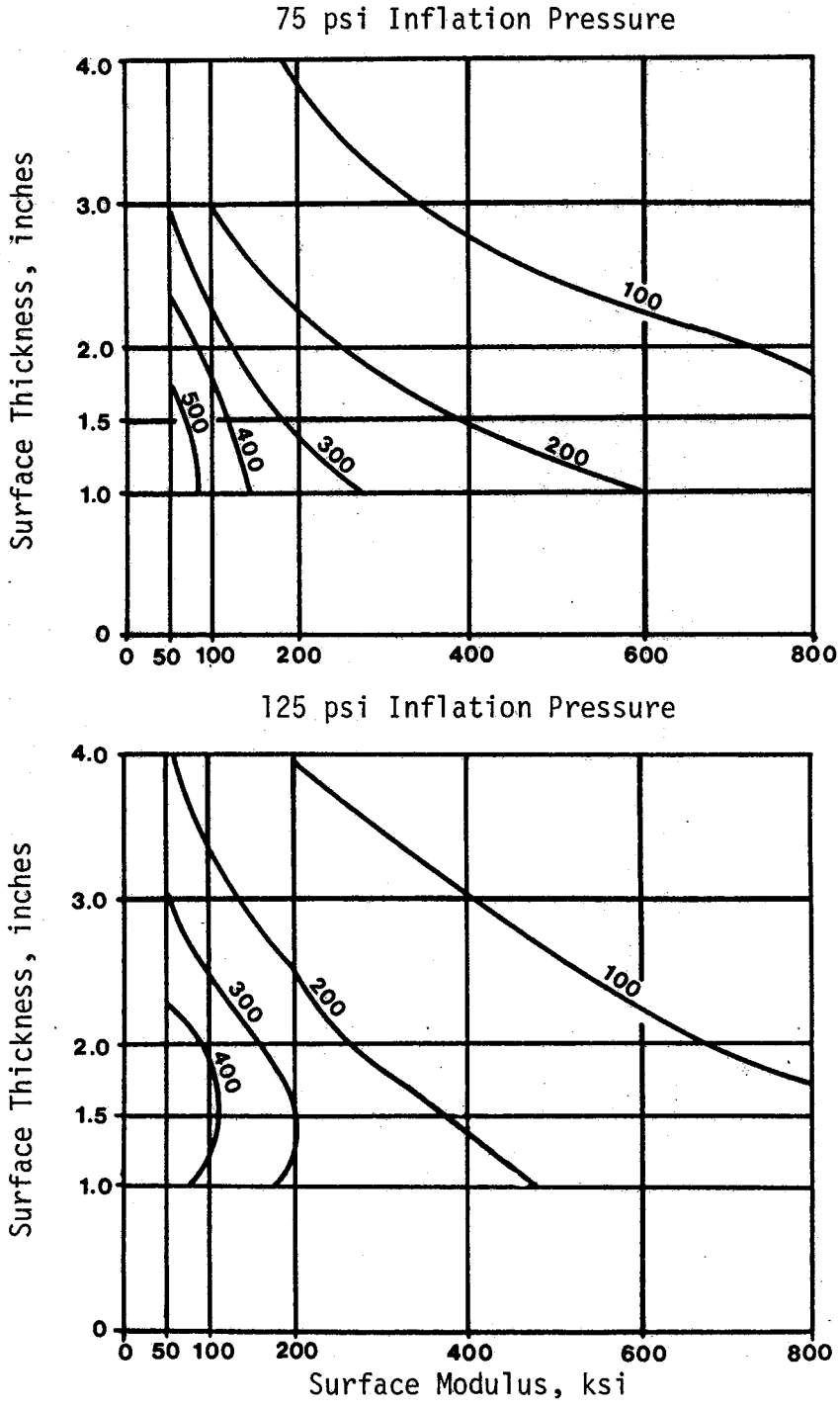


Figure 23 . Tensile micro-strain contours at the top of the surface for 4886 $\theta^{0.239}$ base modulus and 14-inch base.

that increasing the tire inflation pressure from 75 to 125 psi produces approximately the same strain at the top for all surface moduli equal to or greater than 100 ksi. Surface tensile strains for the 50 ksi surface modulus are higher for a 75 psi inflation pressure than for 125 psi.

The surface tensile strain contours for the 14-inch base are shown in Figure 21 through 23. For the strong and moderate base conditions, the maximum surface tensile strains increase as the thickness of the base increases from 8 inches to 14 inches because of the layered system effect. The thicker layer having higher stiffness produce a stiffer pavement system that exhibits lower strains at the bottom and higher strains at the top of the surface layer. There are small regions in the bottom left corner of the plots where the strain is above 300 microinches/inch. For the weak base condition, Figure 23, the strain decreases as the base thickness increases. However, for the weak base condition, the strain levels below 300 microinches/inch still cover a larger range of surface modulus and thickness combinations. Notice that increasing the tire inflation pressure from 75 to 125 psi produces a decrease in surface tensile strain for all base moduli in Figure 21 through 23.

Vertical Compressive Strain at Top of Subgrade. Vertical compressive strains have been used in pavement design to indicate whether the total pavement structure above the subgrades is sufficiently thick to protect the subgrade from excessive vertical permanent deformation. Strain levels in the pavements with 8-inch flexible bases are generally much higher than strains for pavements using stabilized bases. Compressive strains of well over 1000 microinches/inch have been calculated in the subgrade under the 8-inch base. Plots showing the effects of surface modulus and thickness in the compressive strain in the subgrade are found in Figures 24 through 29.

For the 8-inch base, Figure 24 through 26, the vertical subgrade compresive strains stay relatively constant for high surface moduli and thicknesses but begin to increased in the region of low surface moduli and thicknesses. Notice that the compressive strains change very little as a result of changing the tire inflation pressures from 75 to 125 psi.

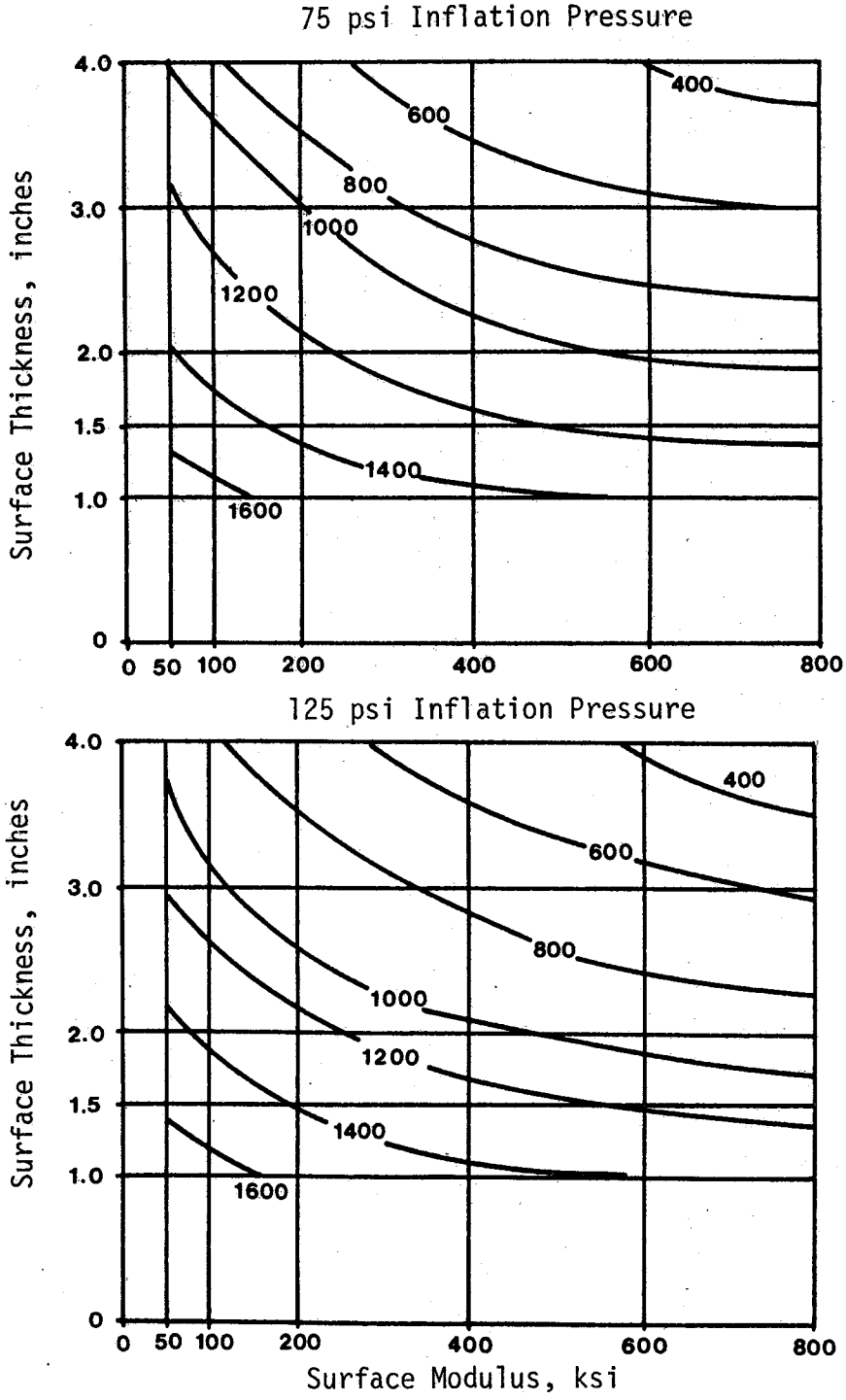


Figure 24. Compressive micro-strain contours at the top of the subgrade for 8787 $\theta^{0.365}$ base modulus and 8-inch base.

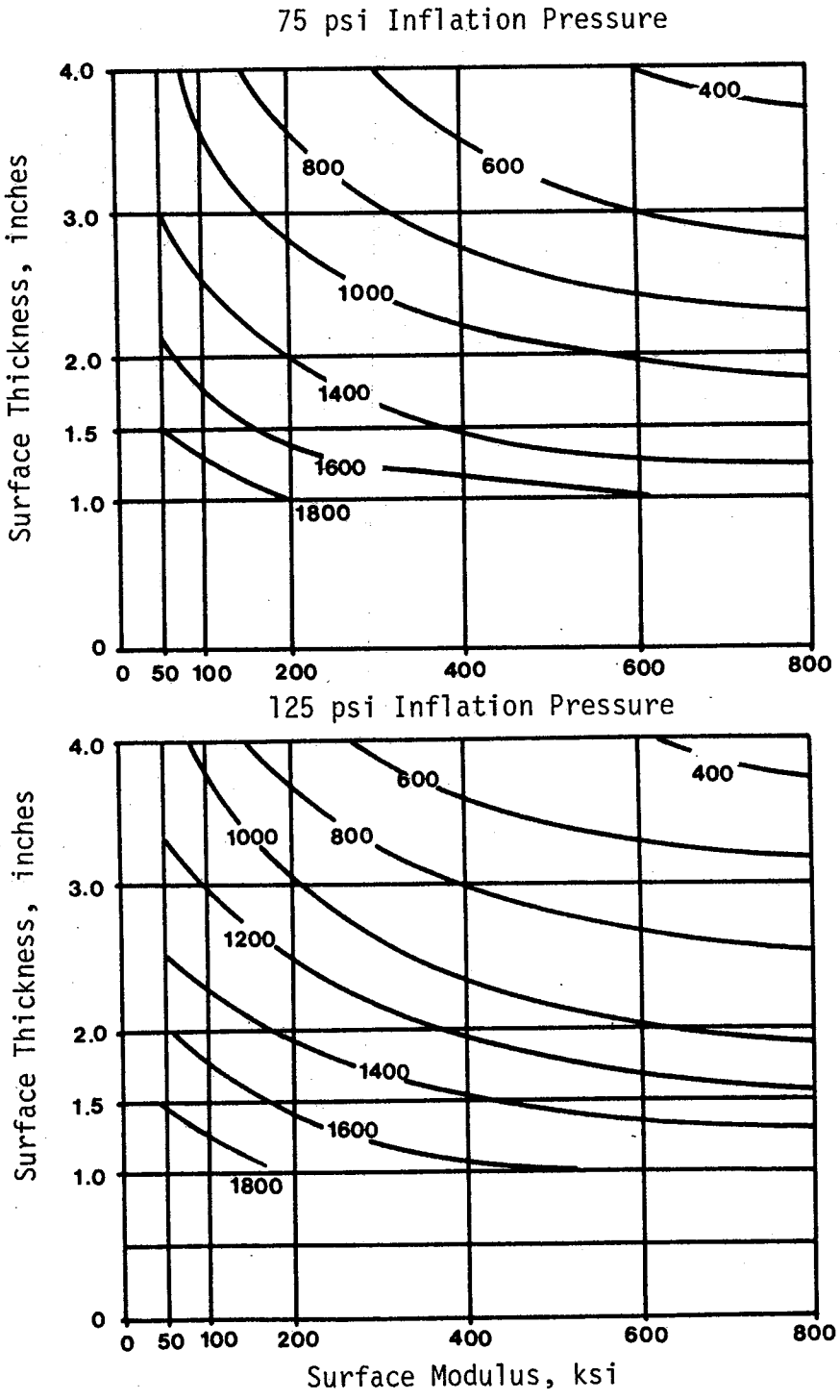


Figure 25 . Compressive micro-strain contours at the top of the sub-grade for 7000 $\theta^{0.325}$ base modulus and 8-inch base.

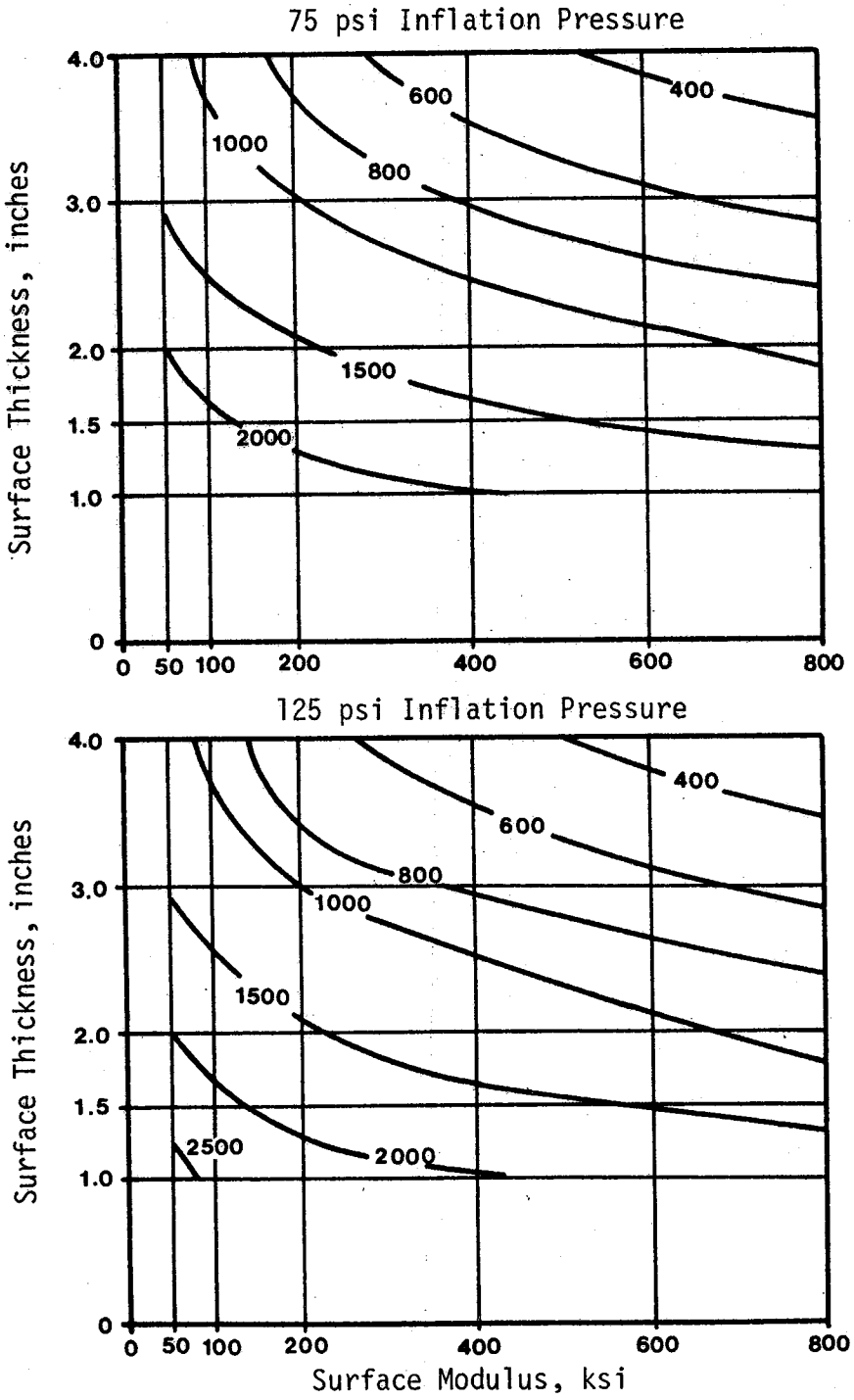


Figure 26. Compressive micro-strain contours at the top of the subgrade for 4886 $\theta^{0.239}$ base modulus and 8-inch base.

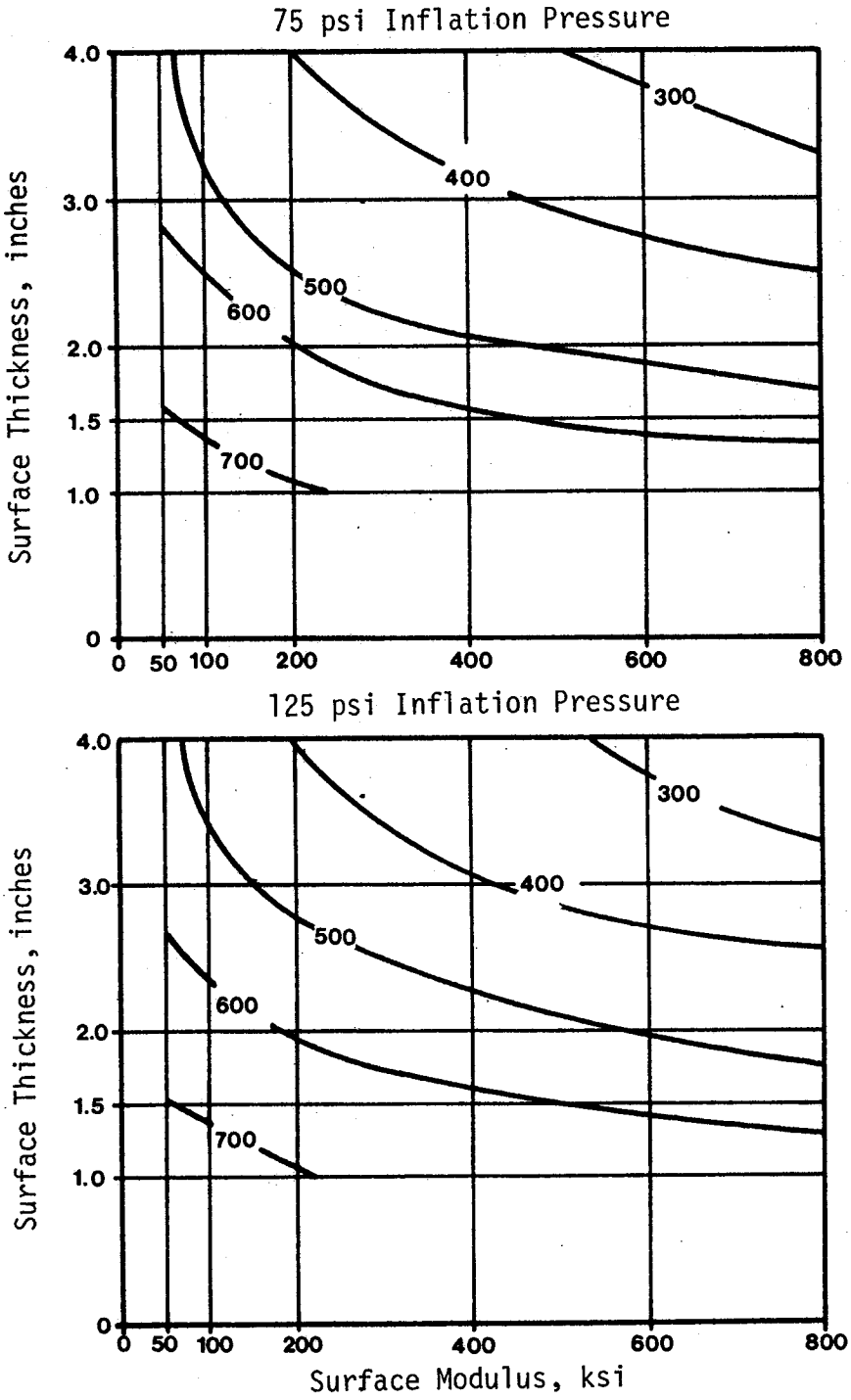


Figure 27 . Compressive micro-strain contours at the top of the subgrade for 8787 $\theta^{0.365}$ base modulus and 14-inch base.

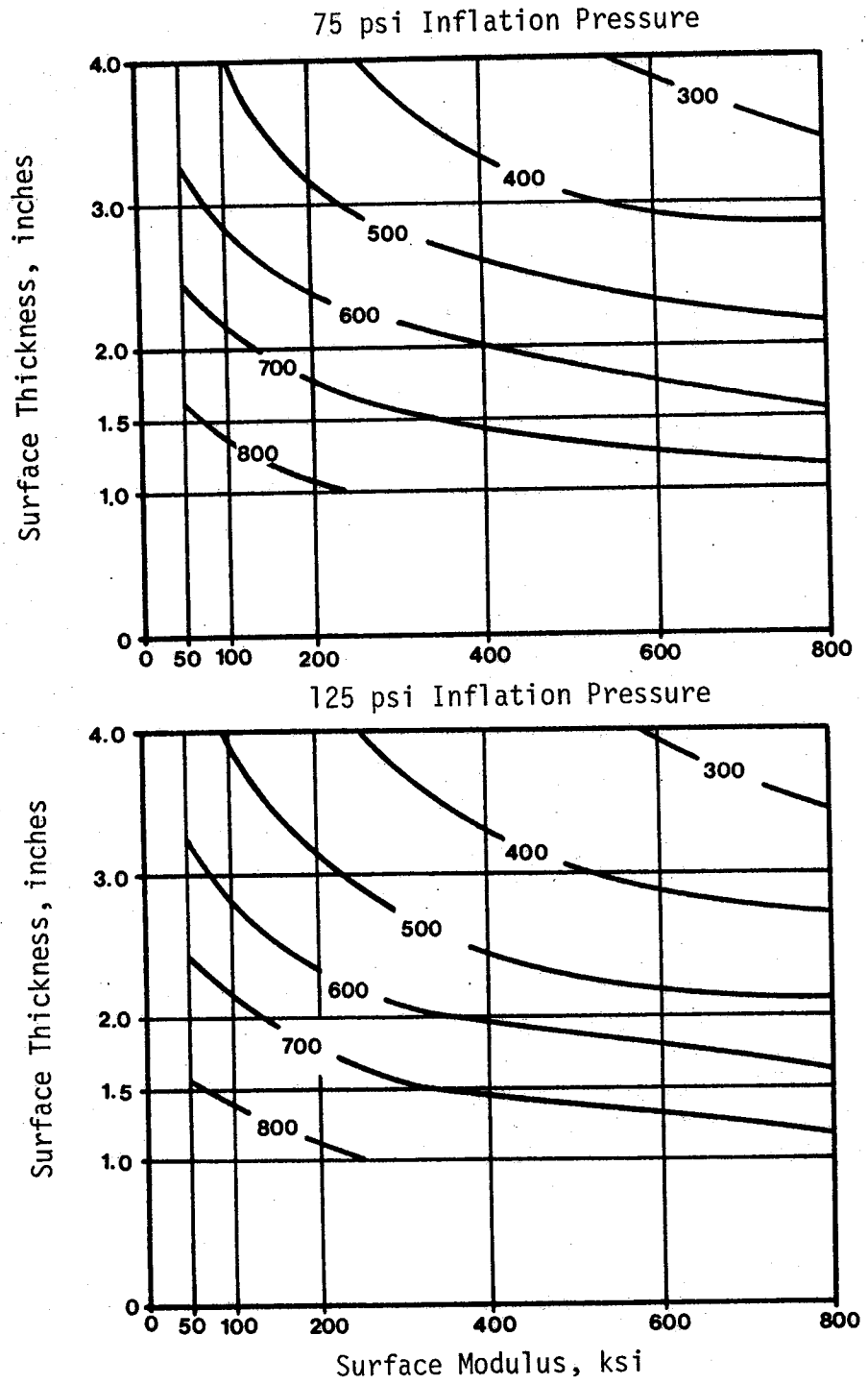


Figure 28. Compressive micro-strain contours at the top of the subgrade for 7000 $\theta^{0.325}$ base modulus and 14-inch base.

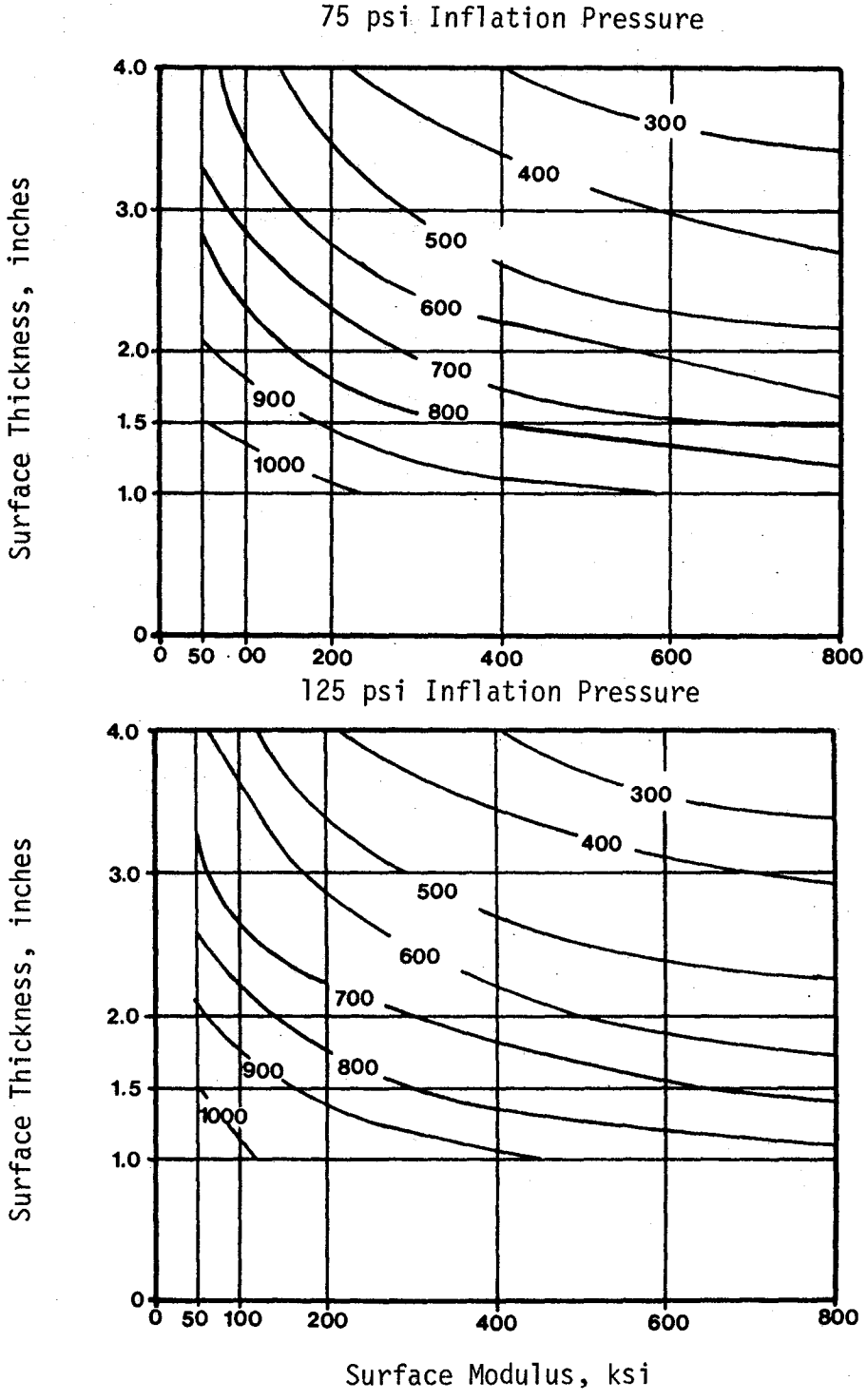


Figure 29. Compressive micro-strain contours at the top of the subgrade for 4886 $\theta^{0.239}$ base modulus and 14-inch base.

For the 14-inch base, Figures 27 through 29, the compressive strains are considerably lower than those for the 8-inch base. This reduction is expected; however, the magnitude of the decrease significantly varies from one-half to one-third the compressive strains for the 8-inch base. Again, the effect of change in inflation pressure on compressive strains is not significant.

Shear Stress at Top of Base. The maximum value of shear stress was obtained from the ILLIPAVE output. This stress, along the vertical compressive stress at the top of the base, was used to determine if the base layer has adequate shearing resistance based on the triaxial classification used by the SDHPT (15). This data, presented in Appendix E, was then plotted to determine whether the state of stress predicted for the computer runs exceeded the range of values used to classify flexible base materials based on triaxial compression tests.

The analysis showed that the magnitude of the shearing stress is not large when compared with the magnitude of the confining stresses; this combination of stresses were plotted on an extrapolated triaxial chart. The points plotted in the region for class 4 and class 6 materials. Materials in these classes are not used for base materials; therefore, it is concluded that the base materials in this study are adequate in providing shearing resistance since these base materials are much higher up in the triaxial chart.

These data show that the shear stress decreases with increasing base thickness but by only a small percentage. Also, the tire inflation pressure does not have a significant effect on the shear stress. As the tire inflation pressure increases the shear stress also increases; but the base material adequately resist those stresses.

## Fatigue Damage Effects

The transverse tensile strains that have been computed using ILLIPAVE at the top and bottom of the asphalt concrete surface are used to approximate the number of 18-kip axle load applications until Class 2 cracking occurs. Class 2 cracking is defined as cracking that has

progressed to the point where cracks have connected together to form a grid-type pattern (16). The pavement surface that has Class 2 cracking is assumed to have failed in fatigue. The cracks that exist still maintain some aggregate interlock and are so spaced that the surface layer is considered to retain some ability to support the load.

The development essential to measuring the fatigue damage effects is a fatigue curve based on actual field observations of strain and the number of strain applications to failure. Twenty- seven of the AASHO sections that displayed cracking are considered to provide a valid data base for a fatigue cracking model (17). These sections cover a wide range of pavement thicknesses and a number of weighted 18-kip axle load applications prior to Class 2 cracking. The FHWA report (17) used the computer program pavement model ELSYM5 to calculate the tensile strains for Class 2 cracking to occur in the 27 AASHO test sections; however, for comparison and validity purposes the tensile strain at all 27 AASHO test sections have been calculated again using ILLIPAVE. The strains calculated from ELSYM5 and ILLIPAVE for the 27 AASHO test sections that have been used to develop the fatigue curve are presented in Table 2. The modulus values that have been used for each layer are as follows: (17)

| Layer | Modulus, psi |
|---|---|
| Surface | 460,000 |
| Base | 40,000 |
| Subbase | 20,000 |
| Subgrade | 5,000 |

The input of ILLIPAVE consisted of these elastic moduli and a tire load as defined in Appendix A for a 10.00-20 bias ply truck tire inflated to 75 psi.

The traffic at first cracking at the top of the asphaltic surface is used in the development of the field fatigue curve and is calculated using equation 27 in the AASHO Report 5 (16) as follows:

Table 2. The 27 AASHO sections used for the fatigue curve development from ELSYM5 and ILLIPAVE.

| AASHO Section Number | Thickness of layers, inches Surface | Base | Subbase | Weighted 18-kip Axle Load Applications Prior to Class 2 Cracking * | Strain Calculated From ELSYM5 Micro-inches | Strain Calculated From ILLIPAVE Micro-inches |
|---|---|---|---|---|---|---|
| 710 | 2 | 3 | 4 | 11,967 | 273 | 319 |
| 717 | 1 | 3 | 4 | 3,837 | 367 | 251 |
| 727 | 1 | 0 | 4 | 1,138 | 542 | 577 |
| 755 | 1 | 6 | 0 | 3,560 | 366 | 218 |
| 758 | 2 | 6 | 0 | 11,224 | 249 | 298 |
| 111 | 2 | 6 | 8 | 68,856 | 235 | 285 |
| 140 | 4 | 6 | 8 | 306,055 | 163 | 176 |
| 145 | 4 | 3 | 0 | 32,896 | 241 | 217 |
| 161 | 4 | 6 | 0 | 72,386 | 193 | 187 |
| 575 | 4 | 3 | 12 | 318,786 | 175 | 185 |
| 583 | 4 | 0 | 4 | 34,767 | 268 | 245 |
| 619 | 4 | 0 | 8 | 79,918 | 233 | 226 |
| 625 | 4 | 6 | 13 | 664,098 | 157 | 174 |
| 427 | 5 | 9 | 12 | 1,710,544 | 125 | 131 |
| 439 | 5 | 3 | 4 | 164,943 | 174 | 149 |
| 445 | 5 | 6 | 12 | 1,036,698 | 134 | 135 |
| 473 | 4 | 6 | 4 | 154,246 | 174 | 179 |
| 477 | 4 | 9 | 12 | 984,141 | 148 | 107 |
| 261 | 5 | 3 | 12 | 605,460 | 148 | 143 |
| 297 | 6 | 3 | 8 | 616,817 | 135 | 113 |
| 319 | 5 | 3 | 8 | 325,321 | 158 | 145 |
| 333 | 6 | 9 | 16 | 4,555,401 | 104 | 103 |
| 336 | 6 | 3 | 12 | 1,091,658 | 127 | 111 |
| 719 | 1 | 6 | 4 | 10,867 | 371 | 223 |
| 156 | 3 | 6 | 8 | 150,816 | 193 | 228 |
| 325 | 6 | 6 | 8 | 1,054,747 | 120 | 107 |
| 260 | 5 | 6 | 8 | 585,288 | 139 | 136 |

* Calculated using the AASHO traffic equation.

$$\text{Log } W_c = 5.484 + 7.275 \text{ Log } (0.33D_1 + 0.10D_2 + 0.08D_3 + 1) + 2.947 \text{ Log } L_2 - 3.136 \text{ Log } (L_1 + L_2)$$

where:

$W_c$ = number of weighted axle applications sustained by the pavement before appearance of Class 2 cracking;

$D_1, D_2, D_3$ = thicknesses of surfacing, base and subbase, in inches

$L_1$ = nominal axle load (e.g., for an 18-kip single axle load $L_1$ = 18); and

$L_2$ = 1 for single axle configuration and

= 2 for tandem axle configuration.

Since with the 18-kip equivalent axle loads are used to develop the field fatigue curve, the above equation is reduced to

$$\text{Log } W_{18} = 1.474 + 7.275 \text{ Log } (0.33D_1 + 0.10D_2 + 0.080_3 + 1)$$

$W_{18}$ = number of weighted 18-kip axle load applications sustained by the pavement before the appearance of Class 2 cracking.

The number of 18-kip axle load applications prior to Class 2 cracking are also tabulated in Table 2. These values are used along with the computed tensile strains from ELSYM5 and ILLIPAVE to generate two field fatigue curves.

In generating the two field fatigue curves, the strains listed in Table 2 are plotted with the corresponding weighted 18-kip axle load applications. Regression equations are then used to achieve the best fit line for the 27 sections investigated. The dashed line drawn in Figure 30 represents the final field fatigue curve using the ELSYM5 generated strain values, and the solid line drawn in Figure 30 represents the final field fatigue curve using the strains calculated from ILLIPAVE. The regression equation generated using the ELSYM5 tensile strain is as follows: (17)

$$W_{18} = 9.7255 \times 10^{-15} \left(\frac{1}{\varepsilon_t}\right)^{5.16267}$$

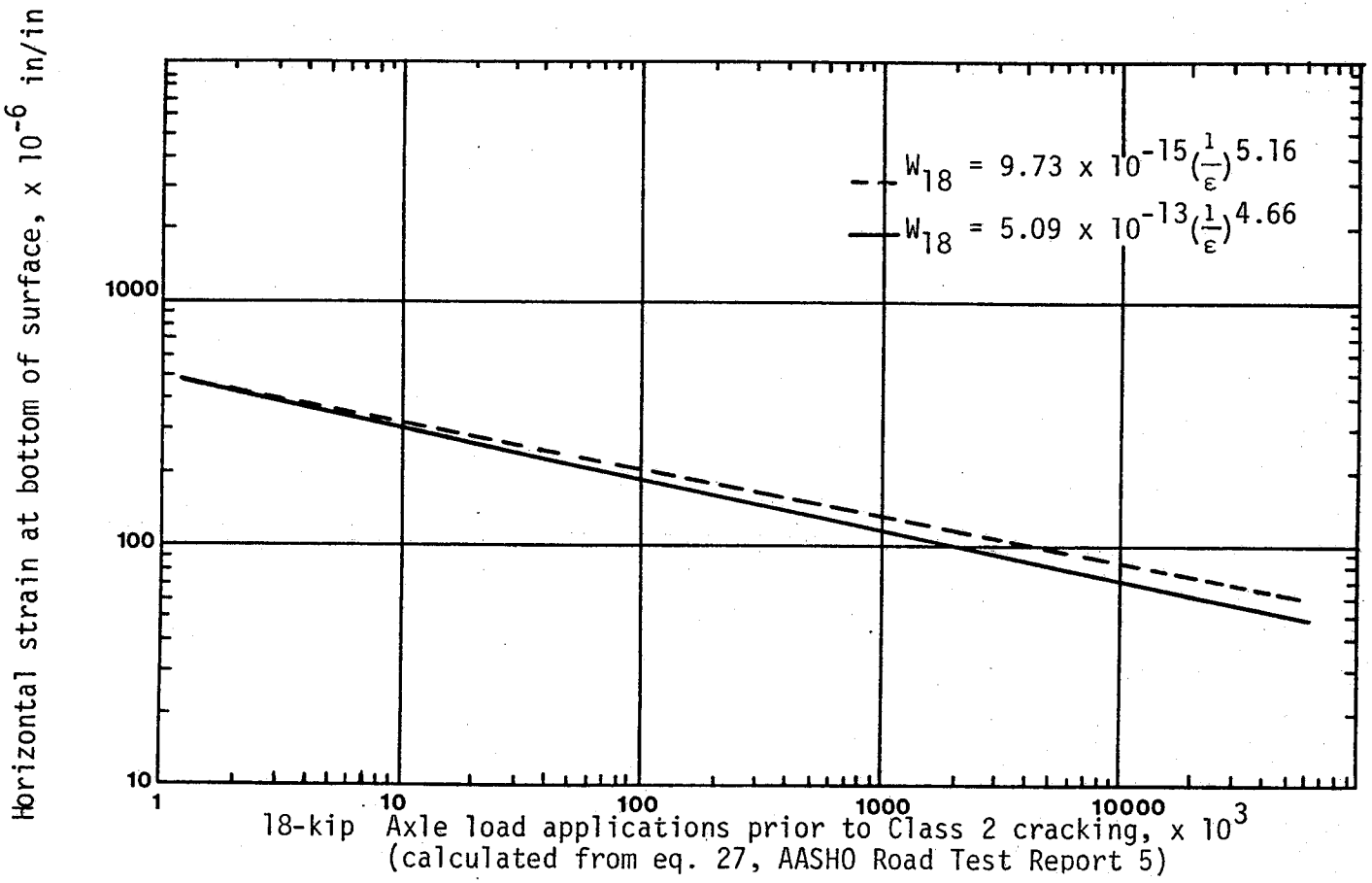


Figure 30. Asphalt concrete fatigue curves developed from AASHO Road Test sections using ELSYM5 and ILLIPAVE.

where:

$W_{18}$ = number of weighted 18-kip axle loads prior to Class 2 cracking; and

= transverse tensile strain.

The above regression equation has a standard error for residual of 0.298 and an $R^2$ term of 0.9294.

The regression equation that is used in this report to represent the number of equivalent 18-kip axle loads prior to Class 2 cracking is the one that was generated using the ILLIPAVE computed tensile strains. That equation is as follows:

$$W_{18} = 5.0957 \times 10^{-13} \left(\frac{1}{\varepsilon_t}\right)^{4.65644}$$

where:

$W_{18}$ = number of weighted 18-kip axle loads prior to Class 2 cracking; and

$\varepsilon_t$ = transverse tensile strain.

The above regression equation has a standard error of estimate of 0.495 and an $R^2$ term of 0.7796.

First to be discussed will be the fatigue effects due to the tensile strains at the bottom of the surface. As the base modulus becomes weaker, the fatigue effects become more pronounced; this is shown in Figures 31 through 33. Notice that for the weak base condition, Figure 33, the number of applications until Class 2 cracking for all surface thickness and modulus combinations is well below the values for a low volume road. A low volume road is defined in the literature as having approximately 500 ADT. This would correspond to a road that has normal traffic and a life of the pavement of 5 years, an ESAL of 20,000 load applications. This value or higher is shown only in the bottom left and upper right corners of the figures representing the ESAL for the strong and weak base condition.

Comparisons of Figure 23 through 33 with Figure 34 through 36, indicate that with increased base thickness the number of load

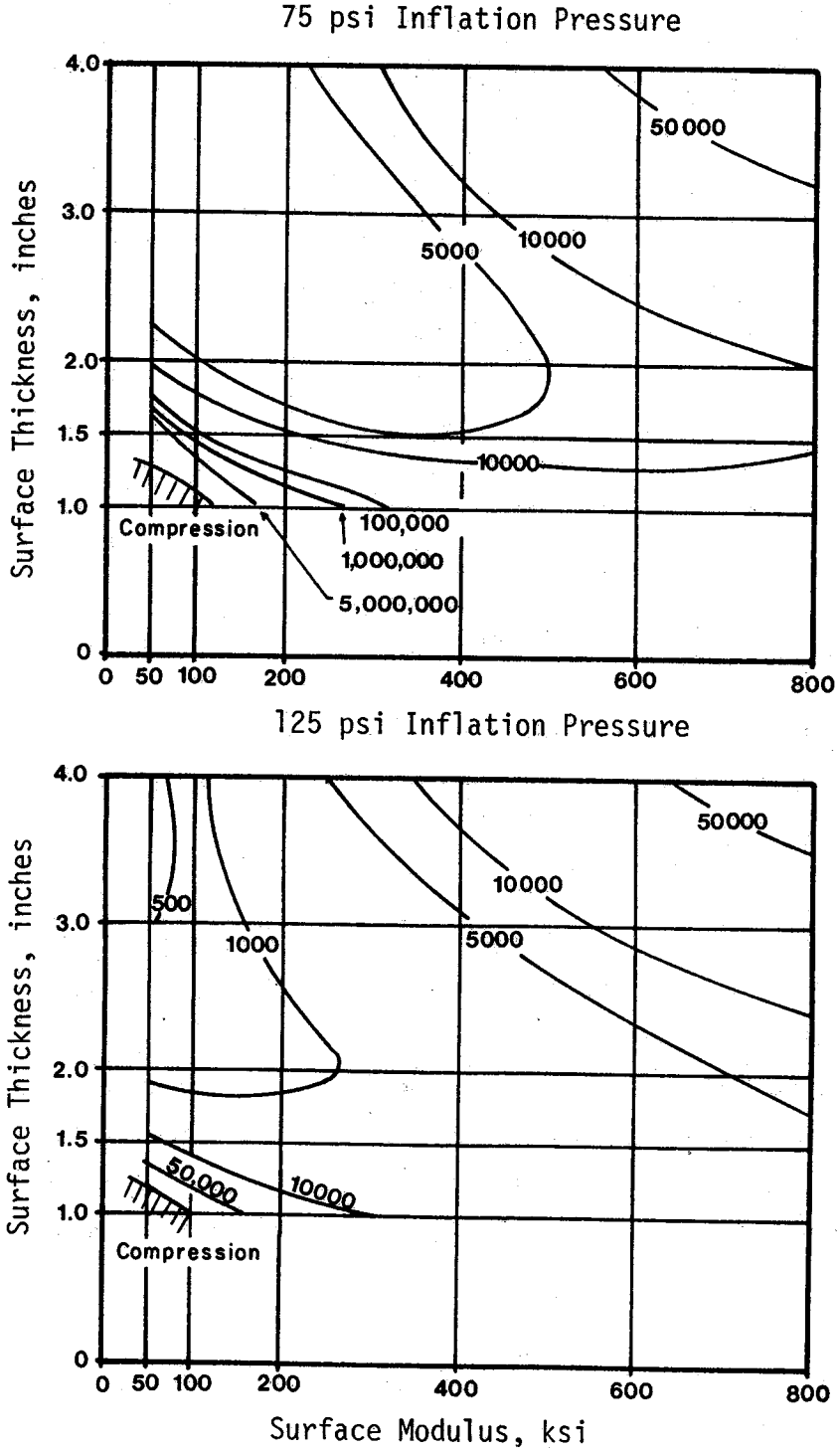


Figure 31. ESAL contours as a function of the tensile strain at the bottom of the surface for a $8787\theta^{0.365}$ base modulus and 8-inch base.

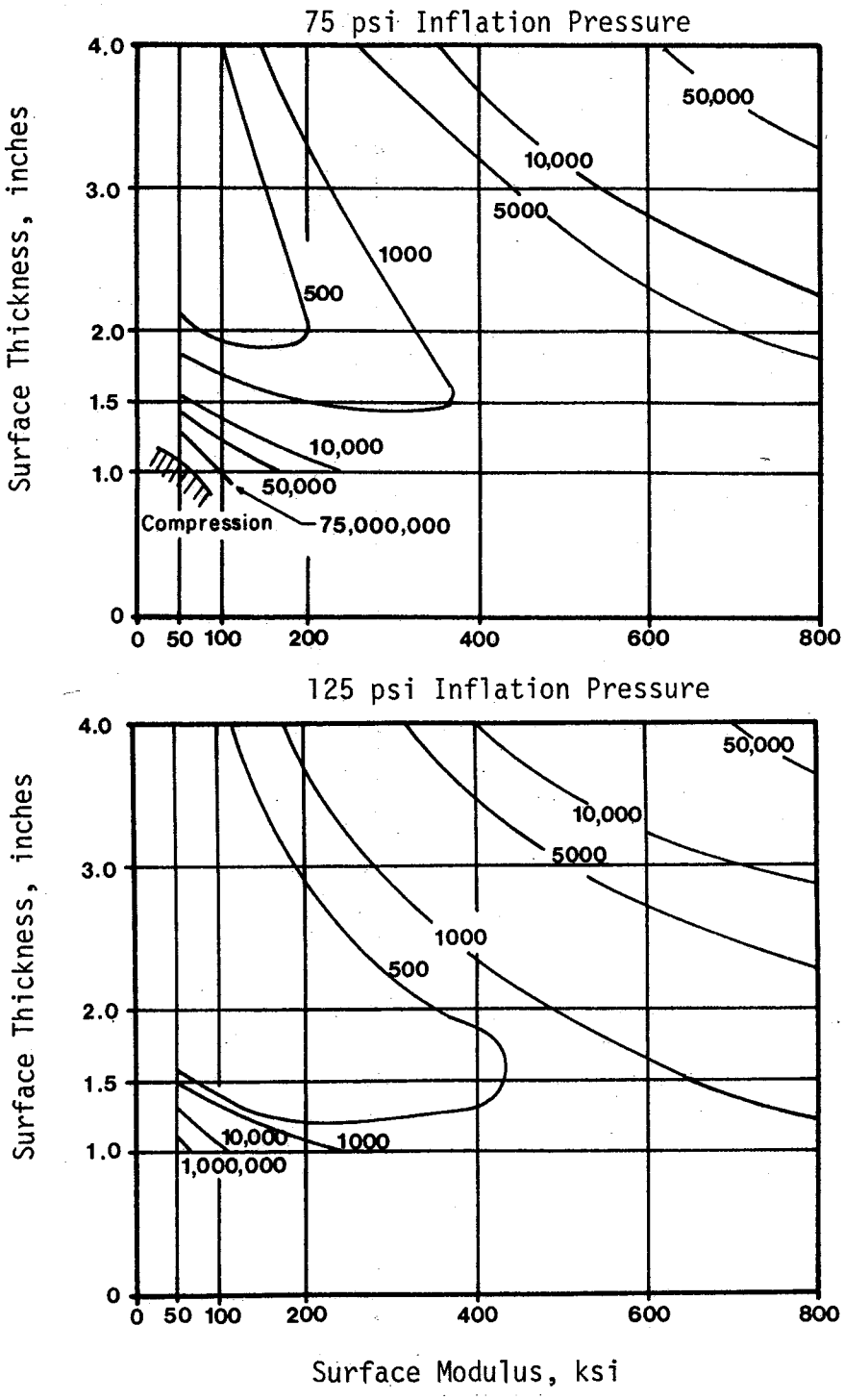


Figure 32. ESAL contours as a function of the tensile strain at the bottom of the surface for a $7000\,\theta^{0.325}$ base modulus and 8-inch base.

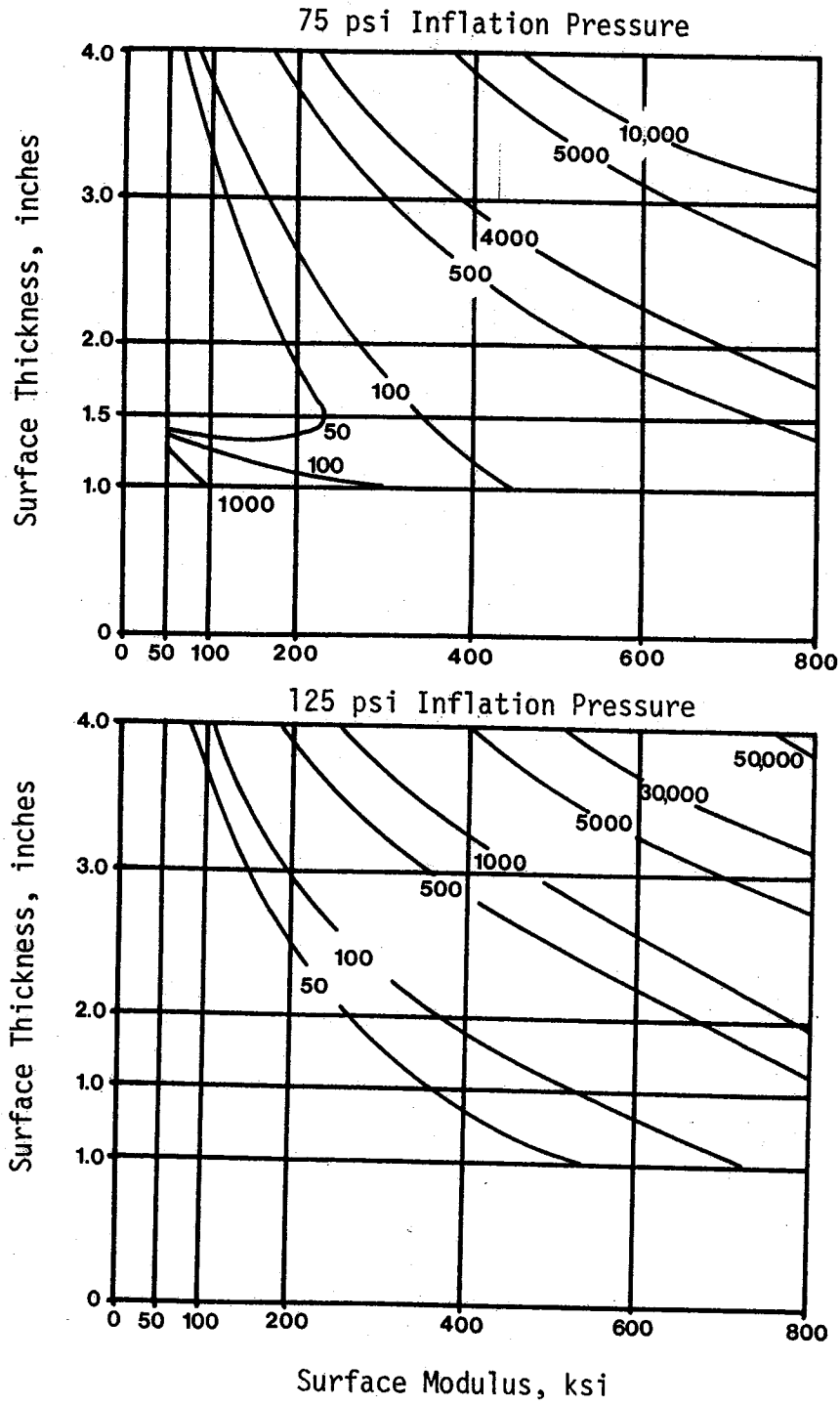


Figure 33. ESAL contours as a function of the tensile strain at the bottom of the surface for a $4886\theta^{0.239}$ base modulus and 8-inch base.

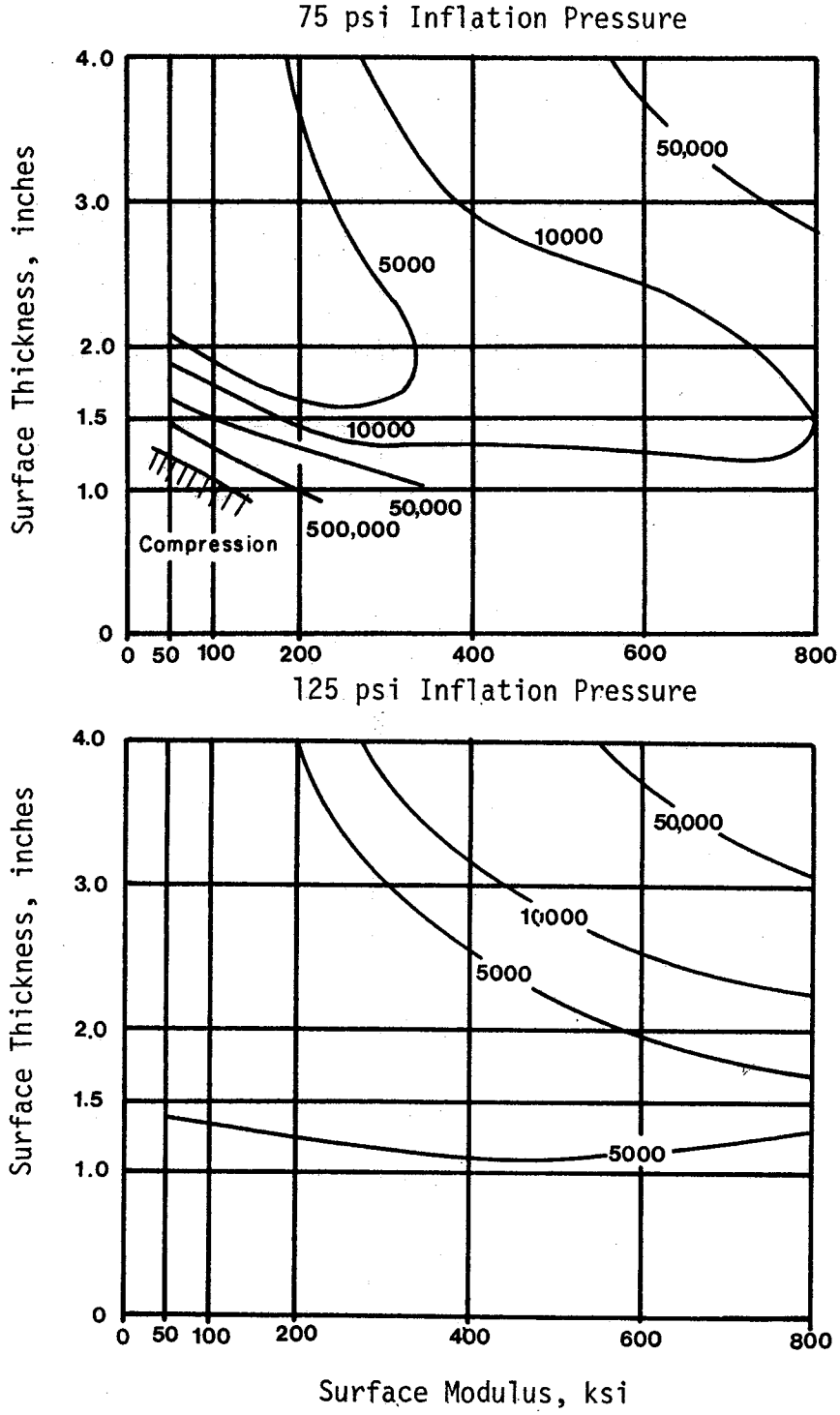


Figure 34. ESAL contours as a function of the tensile strain at the bottom of the surface for a $8787\theta^{0.365}$ base modulus and 14-inch base.

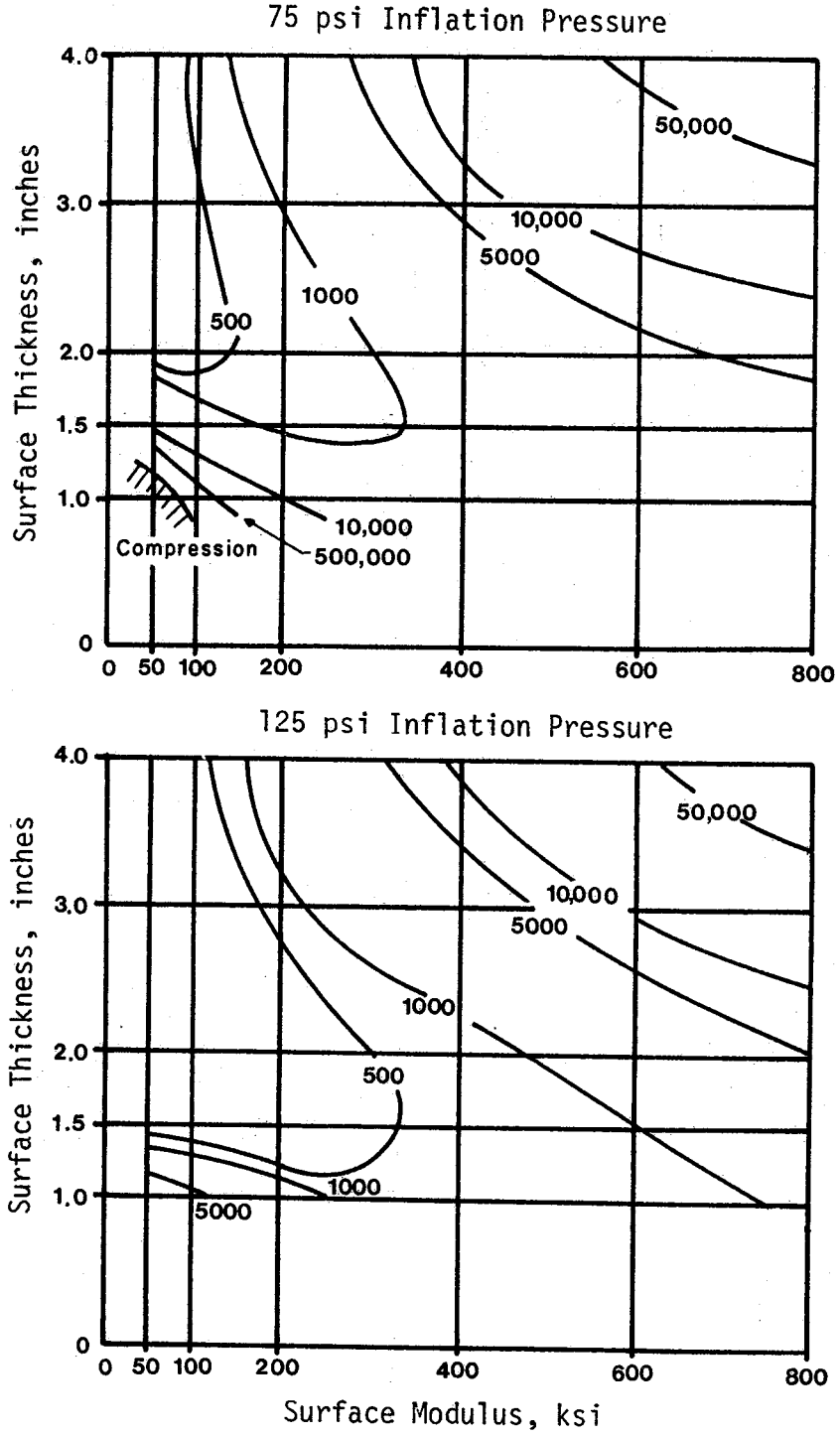


Figure 35. ESAL contours as a function of the tensile strain at the bottom of the surface for a $7000\theta^{0.325}$ base modulus and 14-inch base.

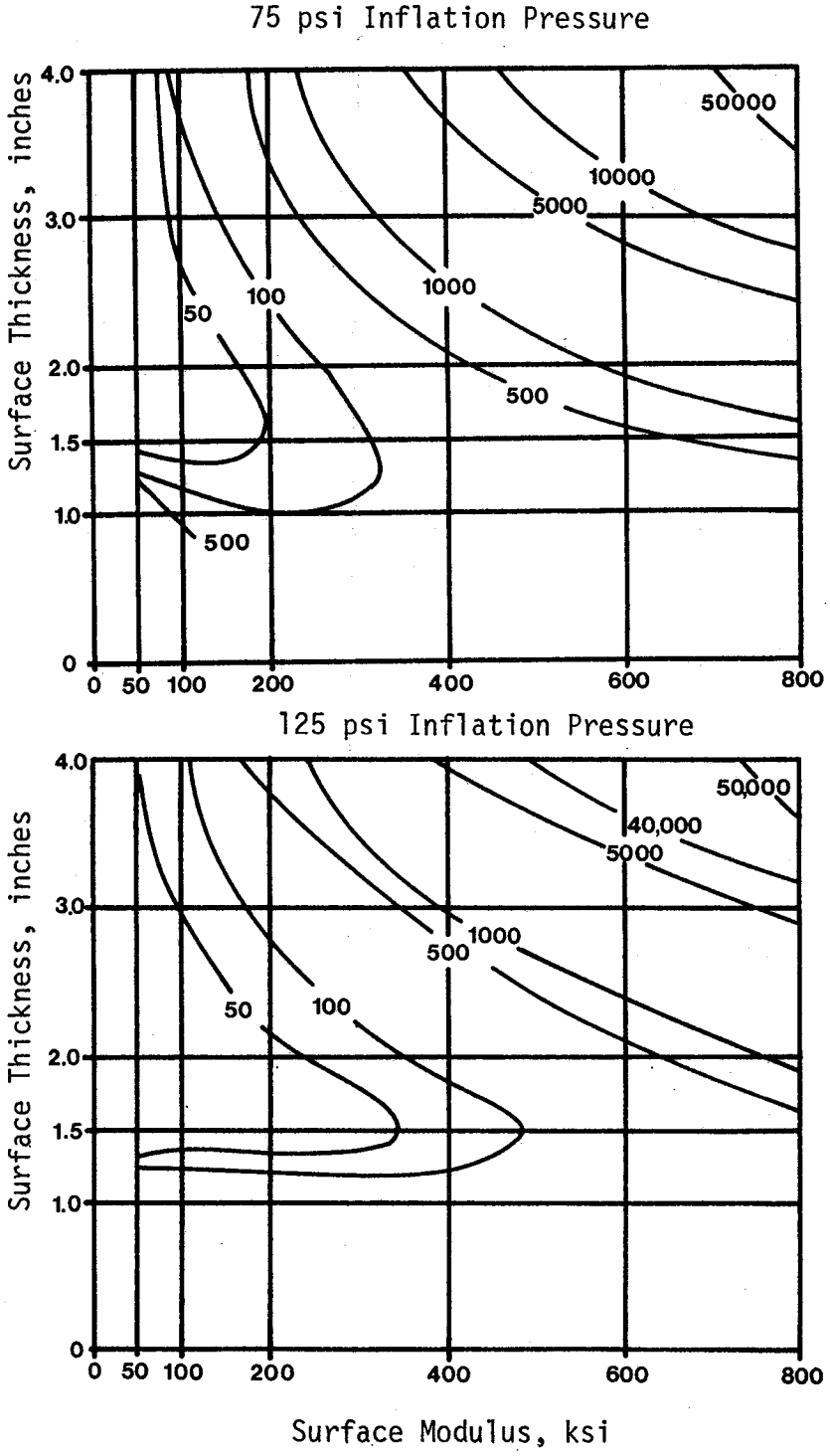


Figure 36. ESAL contours as a function of the tensile strain at the bottom of the surface for a $4886\theta^{0.239}$ base modulus and 14-inch base.

applications until Class 2 cracking is decreased a small amount. Therefore, it is concluded that the base thickness has little effect of the fatigue life of these pavements.

The surface modulus and thickness have a significant effect on the number of ESAL applications. As shown in Figures 31, 33, 34 and 35, the lower strains in the top right and lower left hand corners have ESAL values that are much greater than those in the middle along the diagonal from the upper left to the bottom right hand corner. Therefore, to increase the fatigue life of the pavement, the surfaces should be either kept flexible and stiff or strong and thick.

The tire inflation pressure was a significant effect on the fatigue life, especially for surfaces that are less than or equal to 1.5 inches. Since the ESAL applications decrease dramatically in the lower left hand region, the tire inflation pressure has a significant effect on the fatigue life for these thin surface and weak modulus combinations.

Next to be discussed will be the fatigue effects due to the tensile strains at the top of the surface. As shown in Figure 37 through 42, the base modulus does not effect the ESAL applications as significantly as it did for the tensile strains at the bottom of the surface. However, with the strong base condition the ESAL applications over 1,000,000 cover a larger amount of surface thickness and modulus combinations than for the moderate and weak base conditions. This region of ESAL applications over 1,000,000 occurs in the upper right hand corners of the figures.

Comparisons of Figures 37 and 39 to Figures 40 through 42, indicate that with increased base thickness the number of load application until Class 2 cracking is increased slightly, with the layout increase occurring for the combinations of thin surfaces with low moduli.

The surface modulus and thickness have the greatest effect on the number of ESAL applications when considering the tensile strain at the top of the surface. As shown in Figures 37 through 42, the lower ESAL applications occur in the bottom left hand corner, then begin to increase towards the upper right hand corner. Therefore, to increase the fatigue life of the pavement due to tensile strains at the top of the surface, the surfaces should be kept strong and thick.

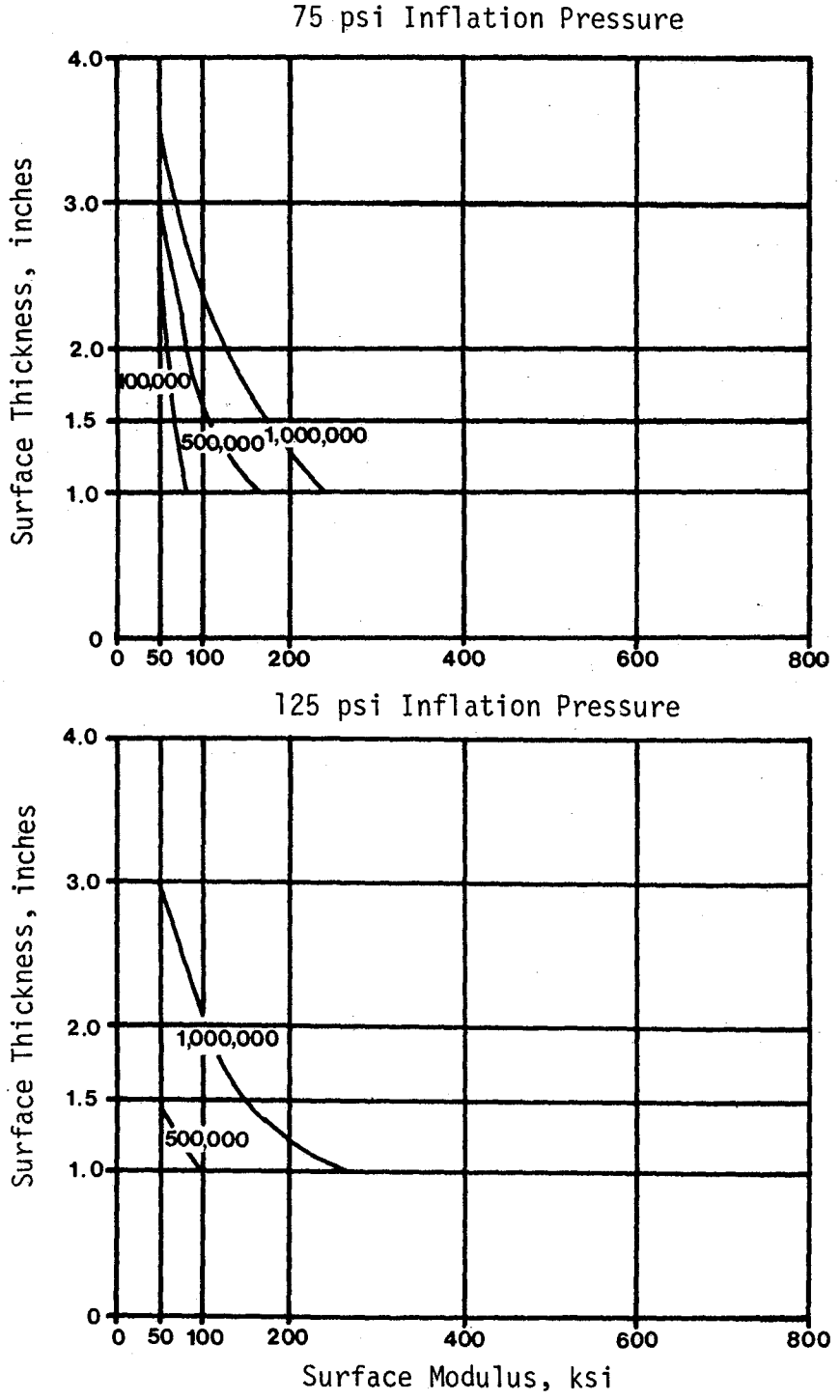


Figure 37. ESAL contours as a function of the tensile strain at the top of the surface for a 8787 $\theta^{0.365}$ base modulus and 8-inch base.

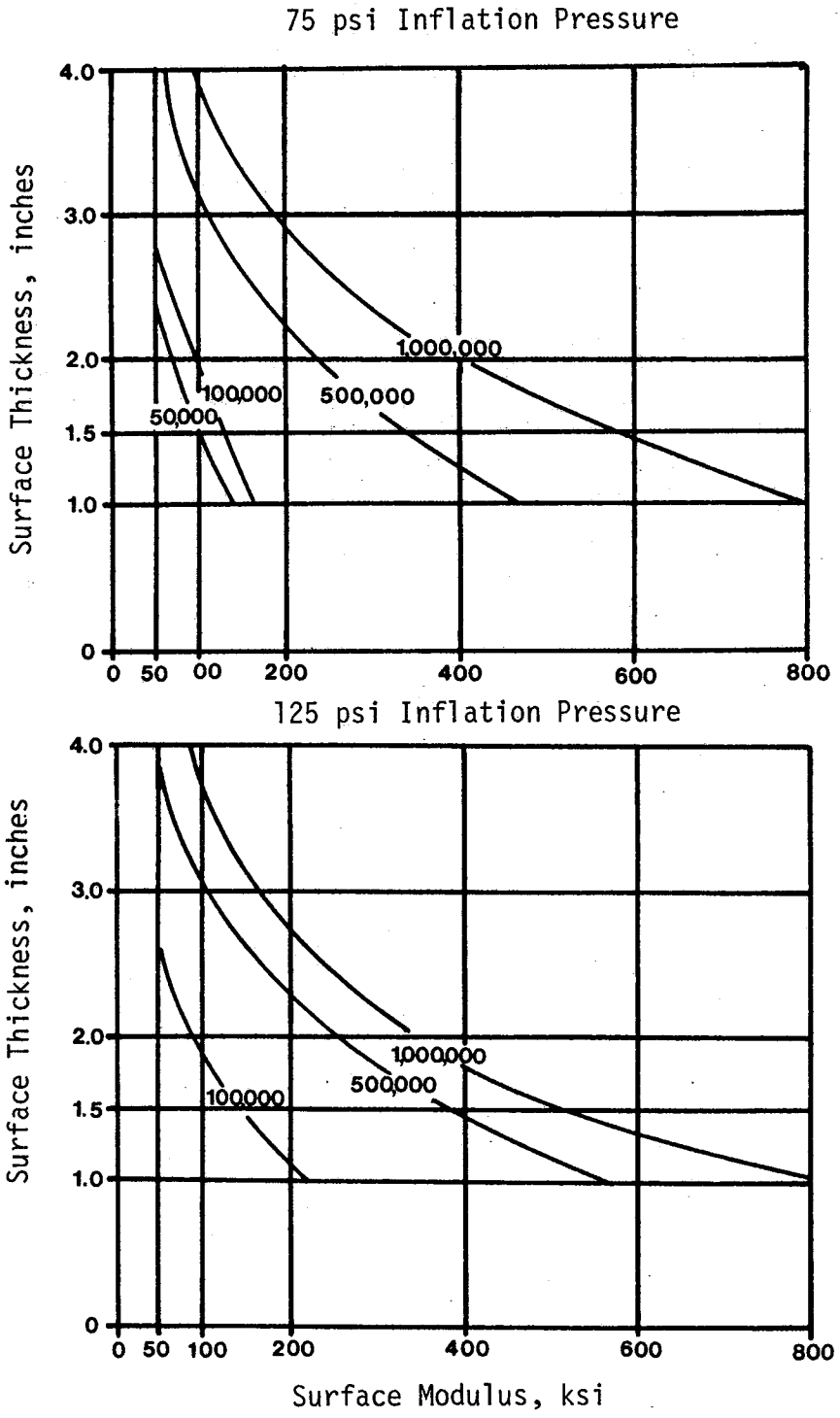


Figure 38 . ESAL contours as a function of the tensile strain at the top of the surface for a 7000 $\theta^{0.325}$ base modulus and 8-inch base.

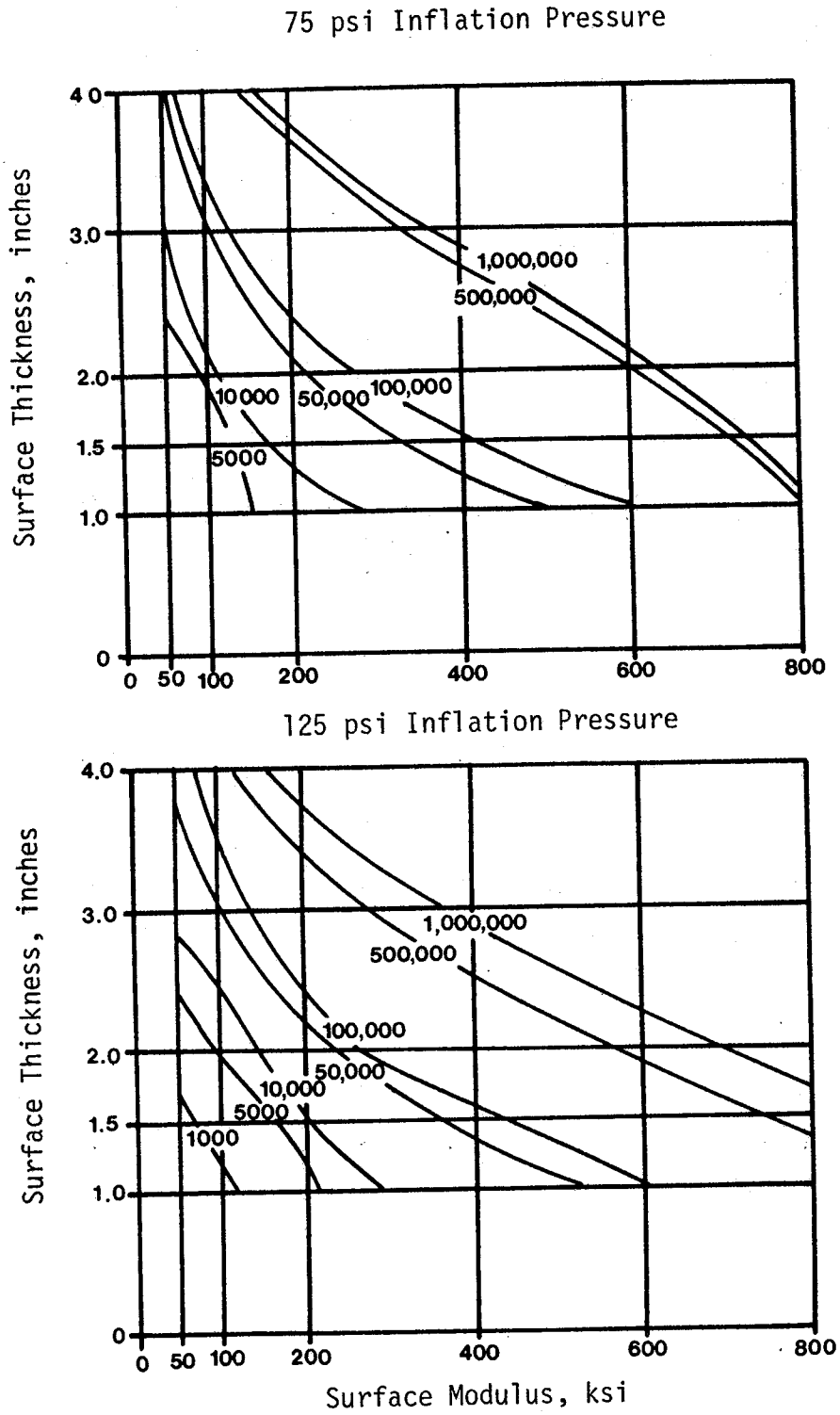


Figure 39 . ESAL contours as a function of the tensile strain at the top of the surface for a 4886 $\theta^{0.239}$ base modulus and 8-inch base.

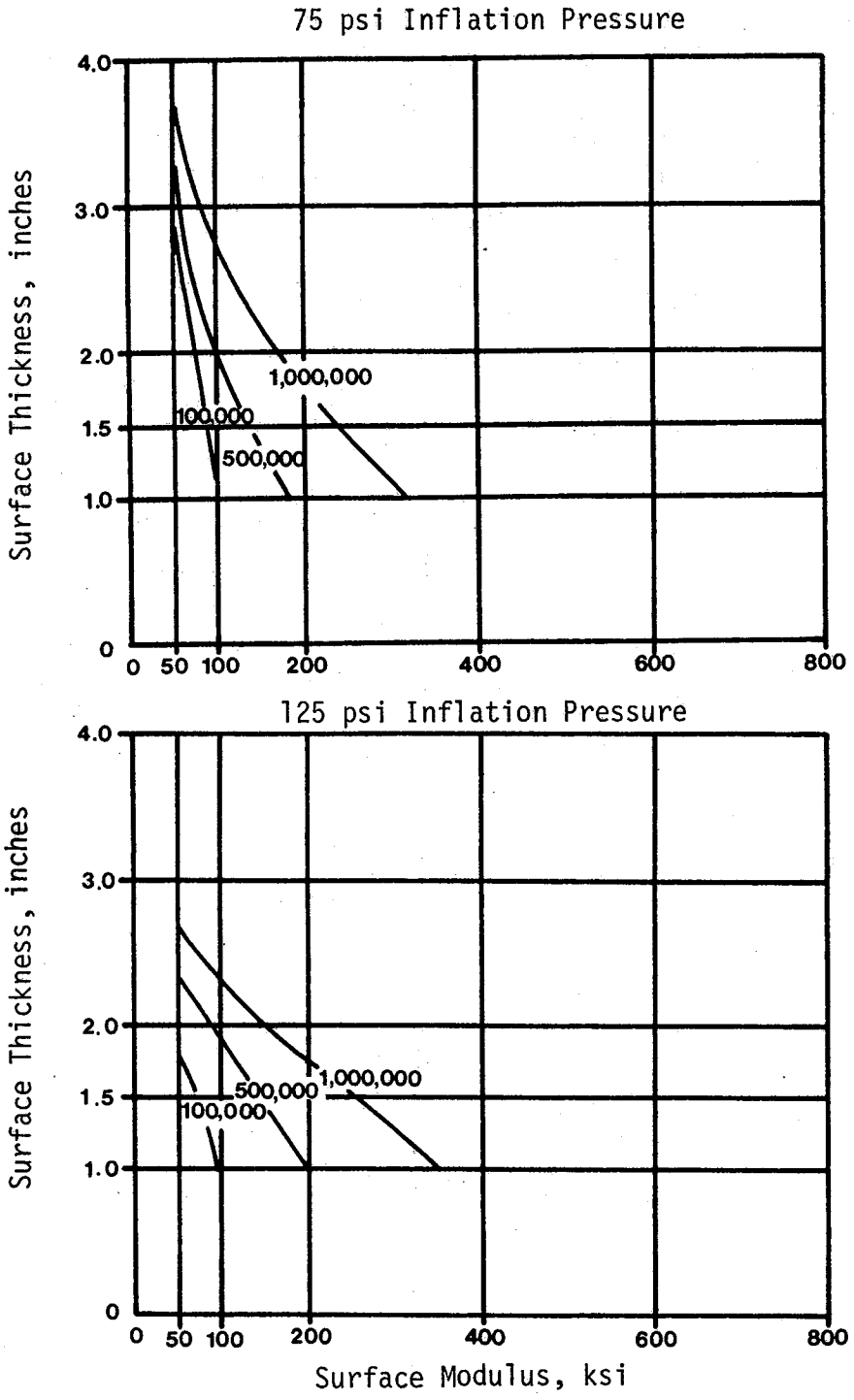


Figure 40 . ESAL contours as a function of the tensile strain at the top of the surface for a 8787 $\theta^{0.365}$ base modulus and 14-inch base.

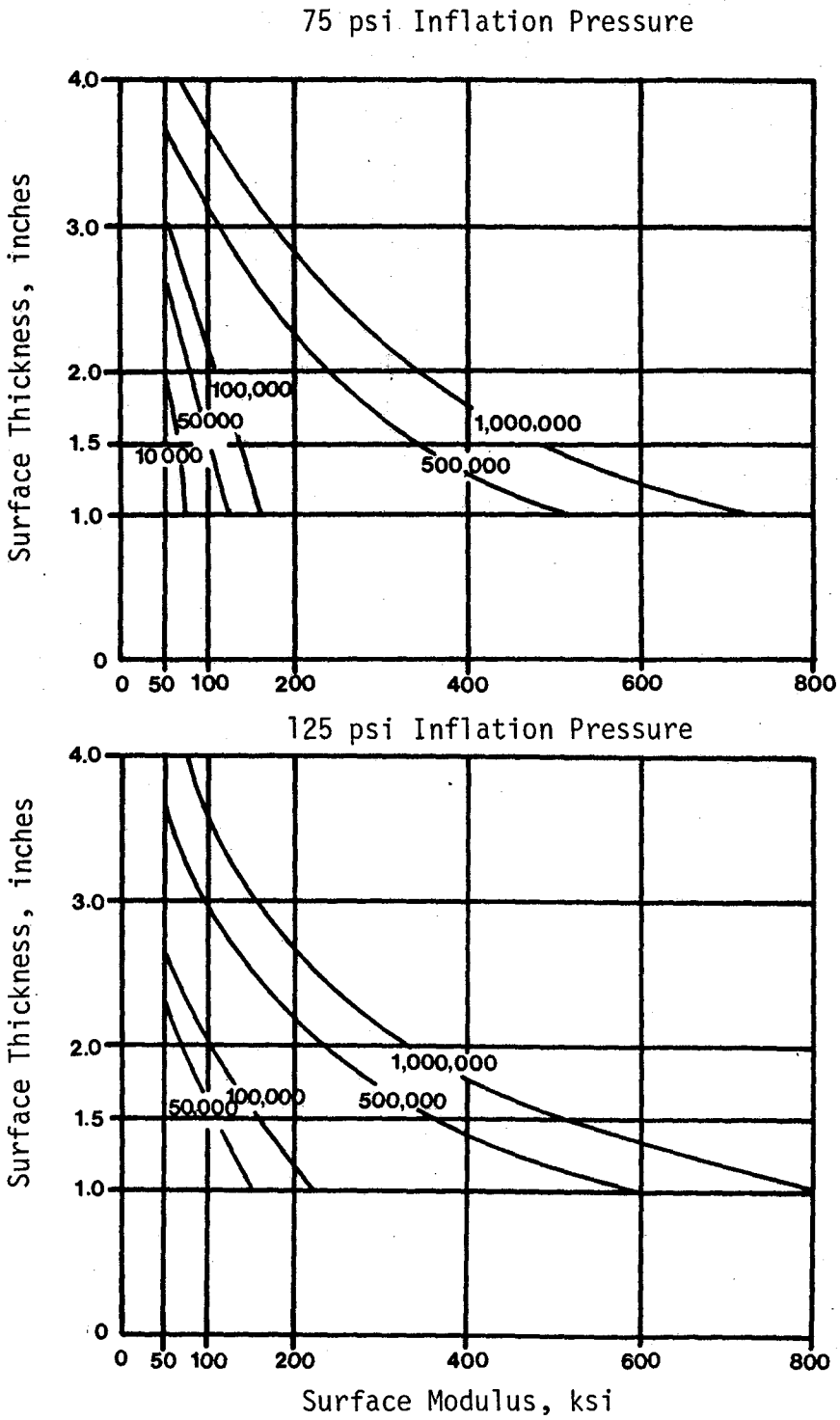


Figure 41 . ESAL contours as a function of the tensile strain at the top of the surface for a 7000 $\theta^{0.325}$ base modulus and 14-inch base.

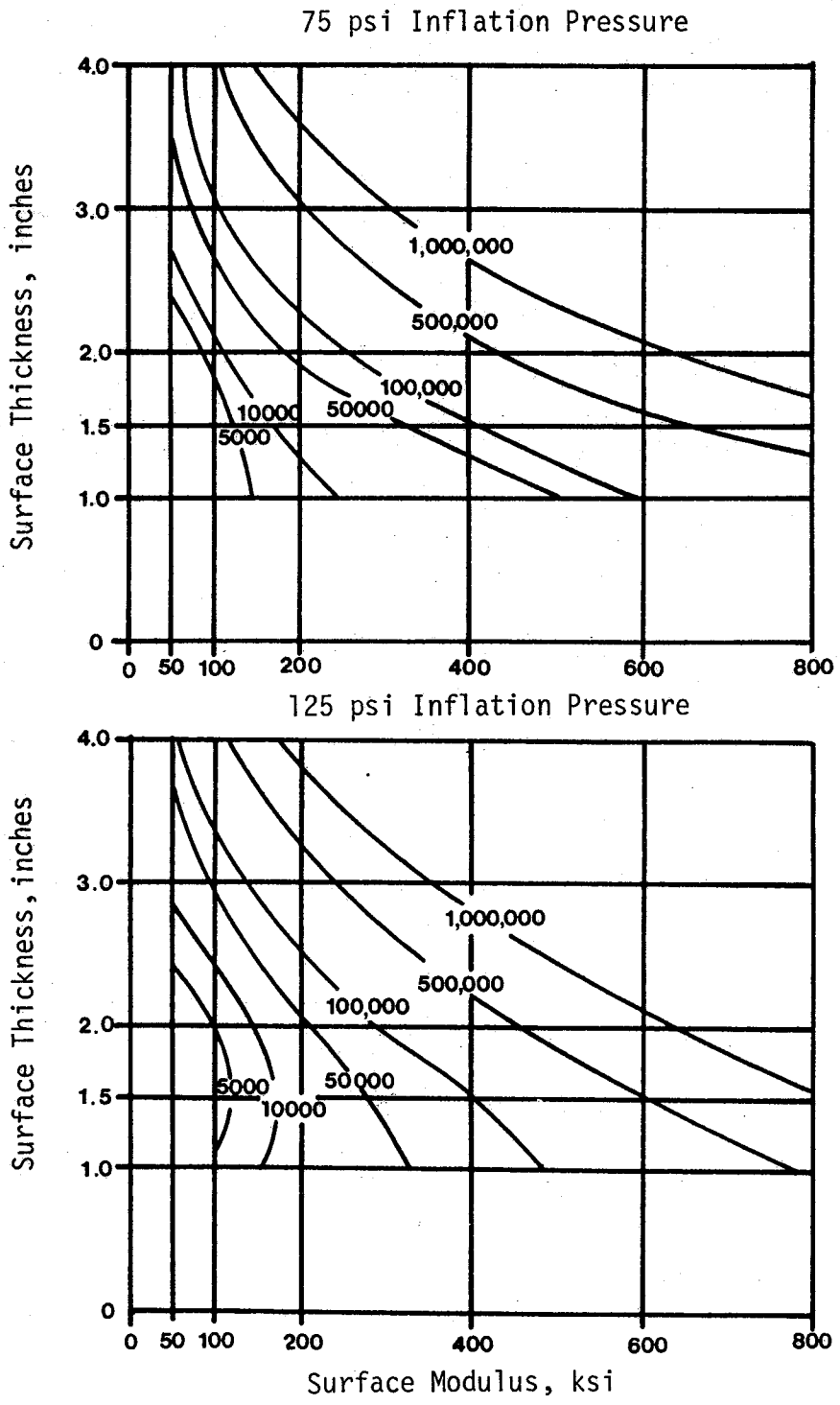


Figure 42 . ESAL contours as a function of the tensile strain at the top of the surface for a 4886 $\theta^{0.239}$ base modulus and 14-inch base.

The tire inflation pressure has a small effect on the fatigue caused by strains at the top of the surface. The ESAL applications are actually increased with increased tire pressure. But this increase is so small it can be attributed to modeling error, because the tensile strains at the top of the surface were calculated at distances away from the centerline of the tire print where maximum strain occurred; this radius increases with increased tire inflation pressure. Therefore, it is expected that the tensile strains further away from the centerline of the tire load are less than those closer to the tire load.

## Rutting Effects

The calculation of the cumulative permanent deformations in pavement structures is a very complicated problem and is still the subject of much research. However, study has shown that protection of the subgrade can occur if the vertical compressive strains are kept below a critical level thereby preventing excessive rutting. The compressive strains at the top of the subgrade have been calculated using ILILPAVE and are used to estimate the number of 18-kip axle load applications until the pavement experiences excessive wheelpath rutting.

Like the fatigue criteria, the vertical compressive strain criteria can be expressed by an equation relating the number of 18-kip load applications to the vertical compressive strain at the top of the subgrade with the coefficients being determined from analysis of in-situ pavements. The coefficients vary substantially depending upon the design methodology from which the compressive strain criteria are determined. Three different compressive strain criteria were reviewed.

To minimize surface rutting Santucci (18) at Chevron developed an equation from analyses of pavements designed by the California (Cal-trans) procedure (19):

$$W_{18} = 1.03 \times 10^{18} \left(\frac{1}{\varepsilon_c}\right)^{4.48}$$

where:

$W_{18}$ = number of weighted 18-kip axle loads prior to excessive rut depth; and

$\varepsilon_c$ = compressive micro-strain at the top of the subgrade.

Also, Brown, Pell, and Stock (20) at the University of Nottingham developed a compressive strain criteria based on analyses using the Great Britain Road Note 29 procedure:

$$W_{18} = 3.00 \times 10^{15} \left(\frac{1}{\varepsilon_c}\right)^{3.57}$$

Shell engineers (21) used results from the AASHO Road Test to develop a compressive strain criteria equation:

$$W_{18} = 6.15 \times 10^{17} \left(\frac{1}{\varepsilon_c}\right)^{4.0}$$

These three curves have been plotted in Figure 43. These curves show that the Chevron and Nottingham curves give more conservative values for the number of weighted 18-kip axle loads for a given compressive strain on the subgrade, than does the Shell curve. For example, using the Chevron and Nottingham curves, a compressive strain of 1000 microinches/inch would limit the number of weighted 18-kip axle loads to approximately 160,000 applications, while the Shell curve would limit the number to 600,000 applications.

Since the tensile strain criteria section used data from the AASHO Road Test, and since it is desirable to have consistency among the different parts of the analysis methodologies, the Shell compressive strain equation was selected for use in this analysis.

The calculated vertical compressive strains at the top of the subgrade for all of the ILLIPAVE runs are listed in Appendix F. For each subgrade compressive strain, the ESAL calculated from the Shell equation is also given. The compressive strain levels corresponding to a range of 18-kip ESAL applications are given in Table 3. Data in this table can be used along with the strains in Figures 24 through 29 to determine the

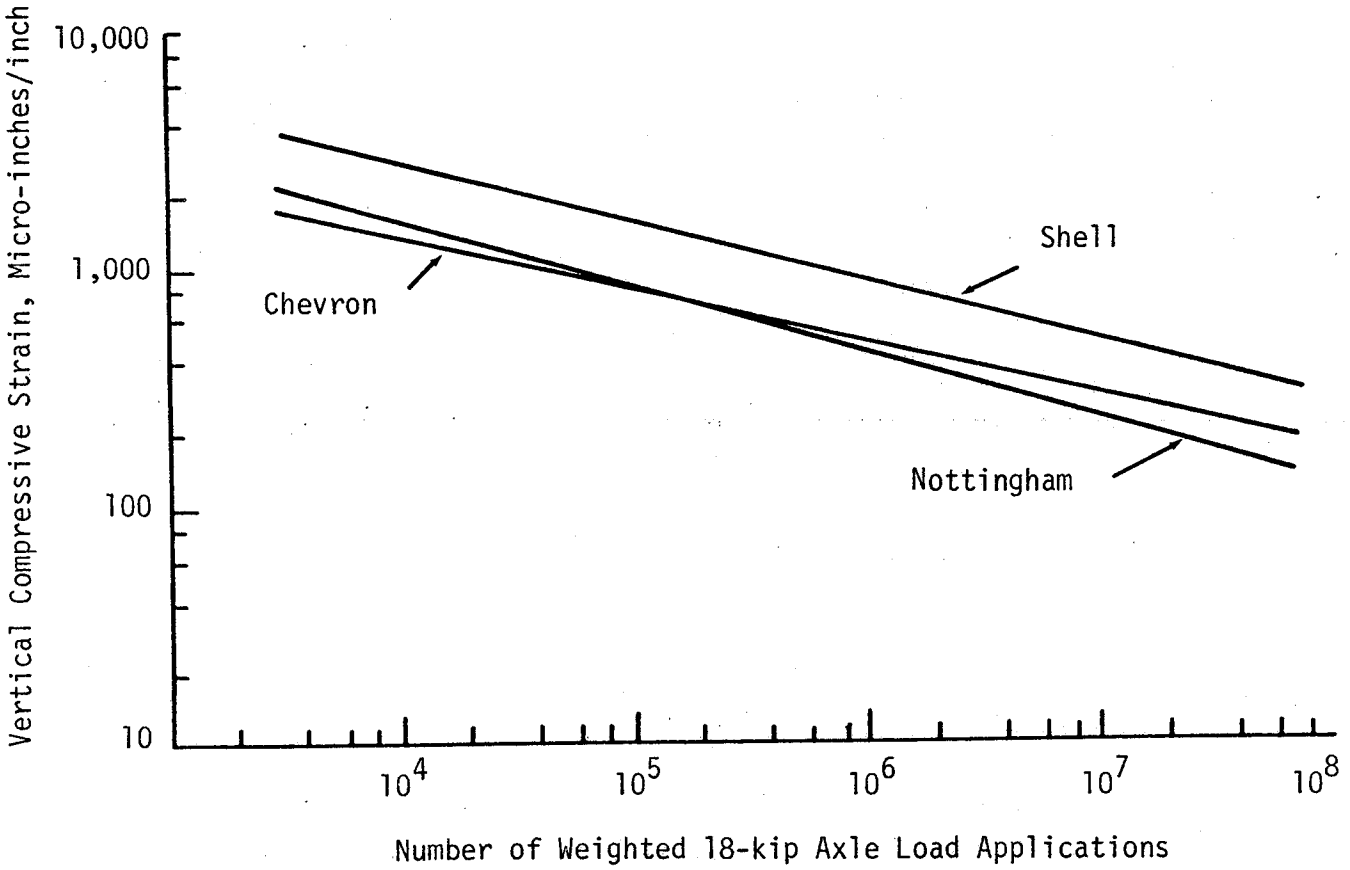


Figure 43. Vertical Compressive Strain versus the number of weighted 18-kip axle load applications for three different rutting equations.

Table 3. Compressive strains at the top of the subgrade for a range of numbers of equivalent standard 18-kip axle loads using $W_{18} = 6.15 \times 10^{17} (\frac{1}{\varepsilon_c})^{4.0}$.

| Vertical Compressive Strain on Subgrade (microinches/inch) | ESAL |
|---|---|
| 592 | 5,000,000 |
| 885 | 1,000,000 |
| 1,053 | 500,000 |
| 1,575 | 100,000 |
| 1,872 | 50,000 |
| 2,800 | 10,000 |
| 3,330 | 5,000 |
| 4,979 | 1,000 |

ESAL for a particular material property and pavement thickness combination.

For the 8-inch base, Figures 24 through 26, the vertical subgrade strain ranges from approximately 400 microinches/inch in the upper right corners to a maximum of 2,500 microinches/inch in Figure 26. Increasing the base thickness to 14 inches, Figure 27 through 29, significantly reduces vertical subgrade strains from approximately 300 microinches/inch in the upper right corners to a maximum of 1,000 microinches/inch in Figure 27. The decrease in compressive strain for all material combinations increases the rutting life of the pavement tremendously. As shown in Figure 24 and 26, the effect of base modulus on the compressive strains in the subgrade is not as significant as the influence of base thickness. For a 1-inch surface and all surface moduli on the weak base, Figure 26, the ESAL ranges from approximately 30,000 to 80,000 applications for the 8-inch base, but for the strong base condition the ESAL ranges from approximately 90,000 to 200,000 applications. The effects of base modulus are most significant for thin surfaces and low modulus combinations and are minimal for surface thicknesses of 2 inches or more. Therefore, it can be concluded that the base thickness is the most important factor in controlling rutting in the subgrade.

As noted previously, the tire inflation pressure has almost no effect on rutting when considering only the subgrade vertical compressive strain; however, rutting in the surface layer due to the higher tire pressures is still under study; and results will be included in a later report.

## Combined Effects

From the previous study of strain effects, conclusions can be made about each condition of strain at the bottom and top of the surface and subgrade. However, the effects of these individual strain conditions must be combined to gain an understanding of the behavior of the whole pavement structure.

Review of the tensile strains at the bottom of the surface, in Figures 12 through 17, indicates that adequately performing thin asphalt concrete pavements should have high modulus flexible bases and either low surface moduli and thicknesses or high surface moduli and thicknesses. The data show only a slight reduction in tensile strain at the bottom of the surface with increasing base thickness. Data in Figure 18 through 23 show that the surface moduli should be kept low for thin surfaces to insure that the tensile strains at the top of the surface will be less than those at the bottom. Tensile strains at the top of the surface are higher than those at the bottom for 1.5 inch and 100 ksi surfaces at 75 psi inflation pressure for both 8- and 14-inch strong and moderately strong bases. The tensile strains at the top increase slightly for low surface thicknesses but do not increase as much as those at the bottom of the surface. For surface thickness greater than 1.5 inches and for all surface and base moduli the tensile strains at the bottom are greater than those at the top.

While increasing base thickness from 8 to 14 inches does not significantly decrease the tensile strains in the surface, it does significantly reduce compressive strains at the top of the subgrade. The compressive strains for 8-inch bases under low surface modulus and thickness combinations are high, these strains are greatly reduced by increasing the base thickness to 14 inches. The changes in inflation pressure have almost no effect on these compressive strains.

Table 4 has been prepared to tie these analyses together so that comparisons and trends can be more easily made. This table shows the relationship of the surface moduli and thickness, and the base moduli and thickness on 18-kip ESAL predictions using tensile strains in the surface and compressive strains at the top of the subgrade. The effects of shear stress in the base is not included because those effects are negligible for the base conditions of this study.

The general classes of performance were chosen to reflect service levels in terms of 18-kip ESALs for each of the 3 limiting criteria: tensile strains at top and bottom of the surface and compressive strains at the top of the subgrade. In Table 4 a highway able to withstand

Table 4. ESAL Applications Based on Different Limiting Criteria.

| BASE PROPERTIES | | | | SURFACE PROPERTIES | | | | | | | | |
|---|---|---|---|---|---|---|---|---|---|---|---|---|
| | | | | 4 inches | | | 2 inches | | | 1 inch | | |
| | | | | 800 | 400 | 50 | 800 | 400 | 50 | 800 | 400 | 50 |
| THIN | WEAK | 1* | | A | L | L | L | L | L | L | L | L |
| | | 2 | | H | H | L | H | A | L | A | L | L |
| | | 3 | | H | H | A | H | A | L | A | L | L |
| | STIFF | 1 | | A | L | L | L | L | L | L | L | C |
| | | 2 | | H | H | H | H | H | L | H | H | L |
| | | 3 | | H | H | H | H | A | A | A | A | A |
| THICK | WEAK | 1 | | A | L | L | L | L | L | L | L | L |
| | | 2 | | H | H | H | H | A | L | A | L | L |
| | | 3 | | H | H | H | H | H | H | H | H | A |
| | STIFF | 1 | | A | L | L | L | L | L | L | L | C |
| | | 2 | | H | H | H | H | H | L | H | H | L |
| | | 3 | | H | H | H | H | H | H | H | H | H |

ESAL Letter Designation

500,000 and up - H
50,000 to 500,000 - A
0 to 50,000 - L
Surface in Compression - C

Tire Inflation Pressure = 75 psi

* Limiting Criteria are based on: (1) Tensile Strain at Bottom of Surface
(2) Tensile Strain at Top of Surface
(3) Compressive Strain at Top of Subgrade

500,000 or more ESALs for a particular limiting criteria is assumed to provide a high (H) level of performance; between 50,000 to 500,000 ESALs the performance is adequate (A); below 50,000 ESALs the performance is low (L); the letter C indicates that the surface is in compression. The adequate level of ESALs was considered to be a typical level of traffic served for low volume roads over a 10 year period. Also, this table is based on the ESAL applications produced at an inflation pressure of 75 psi; however, a change of inflation pressure to 125 psi does not affect the letter designations.

For a roadway to serve adequately, all three limiting criteria must have an A or H for a material combinations. For adequate service, only one material combination works: a 4-inch surface thickness with a modulus of 800 ksi over any base thickness or moduli. However, a second combination will probably work fairly well especially if the effects of cracking that indicate at the surface can be controlled with minor maintenance. This second combination consists of a 1-inch surface with a modulus of 50 ksi on an 8-inch stiff base. Only these 2 combinations offer the material for providing adequate resistance to fatigue cracking and rutting.

The following general trends can be noted for review of Table 5: (1) the tensile strains at the bottom of the surface will almost always control the number of ESAL applications for surfaces other than those which are stiff and thick or weak and thin, (2) the tensile strains at the top of the surface will usually control for surfaces with very low moduli, (3) the compressive strains at the top of the subgrade will usually control the design for a thin, weak surface above a thin, weak base, and (4) surface thicknesses between 1.5 and 3 inches should generally be avoided since no material combination provides adequate service for the limiting criteria assumed in this report.

# CHAPTER VI

# CONCLUSIONS

The study and evaluation of the presented data lead to the following general conclusions:

## TIRE MODEL EFFECTS

1. The differences between stresses and strains calculated using the Tielking tire model and the uniform pressure model are very significant. For the Tielking tire model, the tensile strains at the bottom of the surface are almost 100 percent higher than those for the uniform pressure model for surfaces less than two inches thick; for 1-inch surfaces, the increase in strain is about the same magnitude as that produced by increasing the uniform pressure from 75 to 125 psi.
2. These large increases in strain produced using the Tielking tire model may help to explain why thin pavements crack in service before the strains calculated from the uniform pressure models indicate that fatigue cracking should begin.

Because the Tielking tire model produces tire contact pressure distributions that correspond closely to laboratory measured pressure distributors, that model was used to produce the data included in the remainder of this study. The following conclusions were based on outputs generated using Tielking tire pressure distributions and a set of surface and base combinations typical of Texas farm-to-market pavements:

## TIRE PRESSURE EFFECTS

1. The effects of increased tire pressures on tensile strains at the bottom of the surface are greater for low modulus surfaces less than 1.5 inches on low modulus bases. Generally these tensile strains are

high enough to produce significant fatigue cracking problems especially for pavement surface thicknesses ranging from 1.5 to 3 inches.

2. The effects of increased tire pressures on tensile strains at the top of the surface are minimal, especially for high modulus, thick surfaces on high modulus bases.
3. The effects of increased tire pressures on compressive strains at the top of the subgrade are also minimal, especially for pavements with thick bases.

SURFACE EFFECTS

Surface thicknesses between 1.5 and 3 inches should probably be avoided since no material combinations investigated provided adequate service based on the limiting criteria included in this report.

BASE EFFECTS

1. Thicker base layers having high stiffness produce a stiffer pavement system that exhibits lower strains at the bottom of the surface layer. Changes in the base modulus significantly affect the number of ESAL applications calculated from tensile strains at the bottom of the surface. In fact if thin surfaces are used, the bottom flexible base moduli should be as high as possible.
2. A 14-inch base produces considerably lower compressive strains at the top of the subgrade than those produced by an 8-inch base. This reduction is significant, varying from one-half to one-third the compressive strains for the 8-inch base.

COMBINED EFFECTS

The results of this study indicate that to provide adequate service, the pavement structure should consist of a surface that is either

flexible and thin on a stiff, thick base, or a surface that is stiff and thick on any of the bases investigated.

# CHAPTER VII

## RECOMMENDATIONS

Based on the analyses conducted in this study, the following recommendations are made:

1. A detailed analysis of the permanent deformations in the pavement surface should be conducted to determine the effects of the increased tire pressures on rutting of these pavements.

2. A small set of computer runs should be made using a three-dimensional finite element pavement program to determine if there are significant differences between the stresses and strains obtained using the circular tire print required in ILLIPAVE and the actual tire contact shape and pressures developed with the Tielking tire model.

3. The fatigue and rutting equations used to approximate the number of equivalent standard axle loads should be developed using performance data for thin flexible highways in Texas.

## REFERENCES


1. Harrison, W. J., Wardle, L. J. and Gerrard, C. M., "CRANLAY and PLANE - Computer Programs for Circle and Strip Loads on Layered Anisotropic Media", Commonwealth Scientific and Industrial Research Organizations, Australia, 1972.

2. "ILLIPAVE - A Finite Element Program for the Analysis of Pavements", Construction Engineering Laboratory and the Transportation Facilities Group, Department of Civil Engineering, University of Illinois at Urbana, Illinois, May, 1982.

3. Wilson, E. L., "A Digital Computer Program for the Finite Element Analysis of Solids with Non-Linear Material Properties", University of California at Berkeley, Berkeley, California, 1965.

4. Wilson, E. L., "A Digital Computer Program - A Finite Element Analysis of Axisymmetric Solids with Orthotropic, Non-linear Material Properties", Masters Thesis, University of California at Berkeley, Berkeley, California, July , 1967.

5. Duncan, J. M., Monismith, C. L., and Wilson, E. L., "Finite Element Analysis of Pavements", Highway Research Record 228, Highway Research Board, Washington, D.C., 1968.

6. Love, A. E. H., "The Stress Produced on a Semi-Infinite Body by Pressure on Part of the Boundary", Philosophical Transactions of the Royal Society, Series A, Vol. 228, 1929.

7. Burmister, D. M., "Theory of Stresses and Displacements in Layered Systems", Proceedings, Vol. 23, Highway Research Board, Washington, D.C., pp. 126-148, 1943.

8. Schapery, R. A. and Tielking, J. T., "Investigation of Tire - Pavement Interaction During Maneuvering; Theory and Results", Report No. FHWA-RD-78-72, Federal Highway Administration, Washington, D.C., June, 1977.

9. Tillerson, J. R. and Haisler, W. E., "SAMMSOR II - A Finite Element Program to Determine Stiffness and Mass Matrices of Shells of Revolution", TEES-RPT-70-18, Texas A&M University, College Station, Texas, October, 1970.

10. Haisler, W. E. and Stricklin, J. A., "SNASOR II - A Finite Element Program for the Static Nonlinear Analysis of Shells of Revolution", TEES-RP-70-20, Texas A&M University, College Station, Texas, October, 1970.

11. Tielking, J. T. and Schapery, R. A., "A Method for Shell Contact Analysis", Computer Methods in Applied Mechanics and Engineering, Vol. 26, No. 2, pp. 181-195, May, 1981.

12. Tielking, J. T. and Schapery, R. A., "Calculation of Tire - Pavement Shear Forces", ASME Symposium Proceedings, The General Problem of Rolling Contact, ASME AMD-Vol. 40, pp. 19-39, 1980.

13. May, R. W. and Witczak, M. W., "Effective Granular Modulus to Model Pavement Responses", Transportation Research Record 810, Transportation Research Board, Washington, D. C., 1981.

14. Monismith, C. L., "Fatigue Characteristics of Asphalt Paving Mixtures and Their Use in Pavement Design,", University of New Mexico, Symposium on Fatigue in Asphalt Pavements, January 7, 1981.

15 _____ Triaxial Compression Tests for Disturbed Soils and Base Materials, Test Method Tex-117-E, Manual of Testing Procedures, Volume 1, State Department of Highways and Public Transportation, Austin, Texas, December, 1982.

16. "The AASHO Road Test - Report 5 - Pavement Research", Highway Research Board Special Report 61E, Washington, D.C., 1962.

17. "Asphalt Concrete Overlays of Flexible Pavements, Vol. 1, Development of New Design Criteria", Final Report, Federal Highway Adminstration, Washington, D.C., June, 1975.

18. Santucci, L. E., "Thickness Design Procedure for Asphalt and Emulsified Asphalt Mixes", Proceedings, Vol. 1, Fourth International Conference on the Structural Design of Asphalt Pavements, University of Michigan, Ann Arbor, Michigan, pp. 424-456, 1977.

19. State of California Department of Transportation, Planning Manual, Part 7, Sacramento, California.

20. Brown, S. F., Pell, P. S., and Stock, A. F., "The Application of Simplified, Fundamental Design Procedures for Flexible Pavements", Proceedings, Vol. 1, Fourth International Conference on the Structural Design of Asphalt Pavements, University of Michigan, Ann Arbor, Michigan, pp. 327-341, 1977.

21. Shell International Petroleum Company Limited, Shell Pavement Design Manual, London, 1978.

APPENDIX A. DEVIATION OF THE UZ AND UR NODAL FORCE VALUES.

UZ Nodal Forces:

1. 10.00-20 bias ply truck tire with an inflation pressure of 75 psi. The stresses are obtained from the Tielking (4) tire model program and then plotted. The pressures are taken along the axis perpendicular to the direction of travel at the center of the tire print and are assumed to vary linearly between nodes.

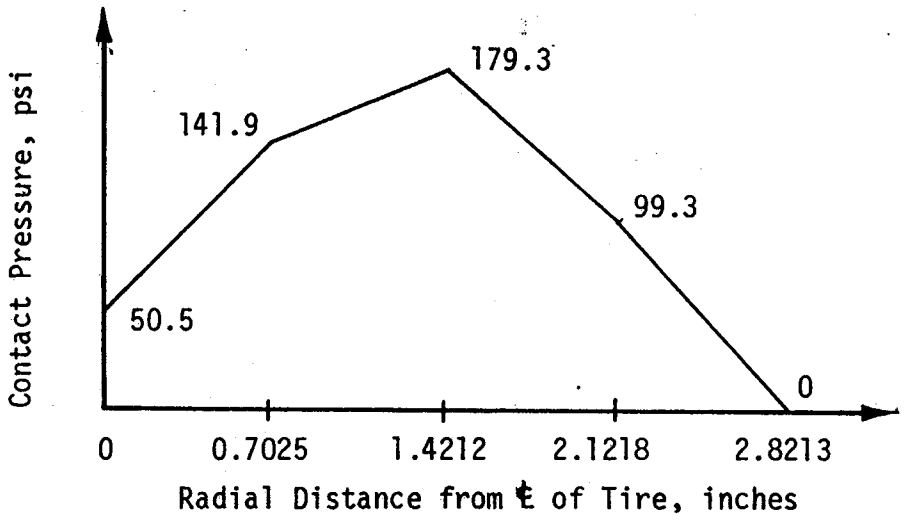


The stresses are then broken down into equal incremental size and uniform pressures within each increment. The pressure at each new equal increment node is calculated using the assumption that the pressure varies linearly between nodes. The average value between the two equal increment nodes is the uniform contact pressure for that increment.

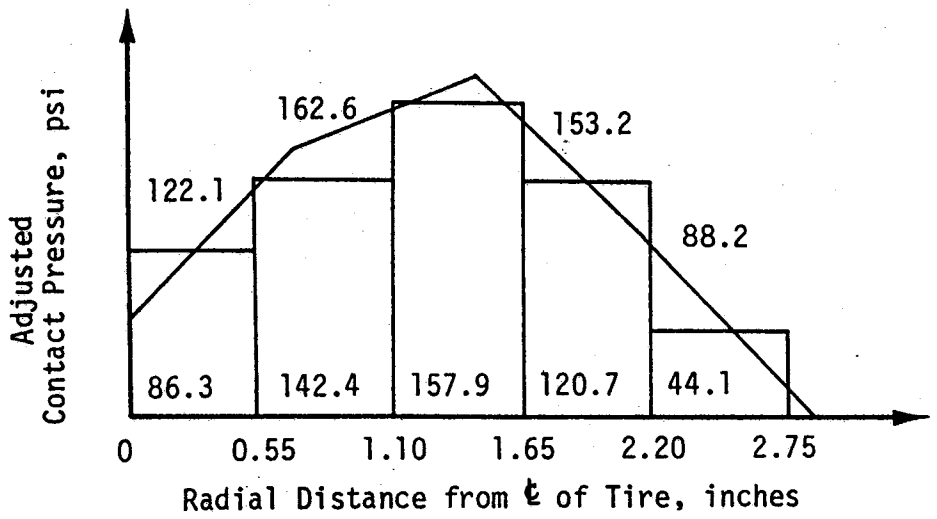


The total radial distance is now adjusted such that the total load from Tielking's elliptical tire print (4) equals to the total tire load of a circular tire print. This is done by a computer program that approximates the radius needed to maintain the desired load, 4500 pounds in this case, with the uniform pressures remaining the same between the nodes. This is explained in greater detail in Appendix B.

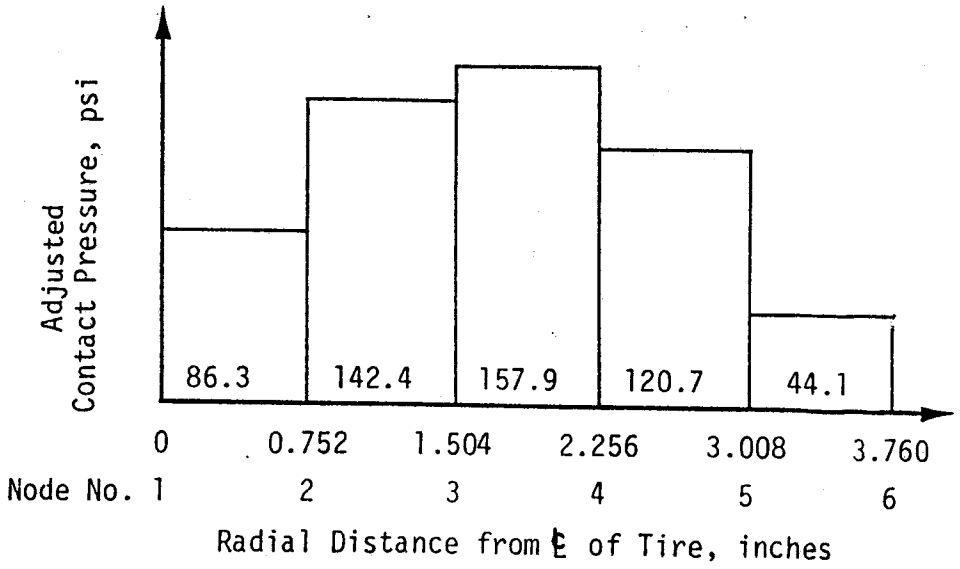

Pappas' Theorem is now utilized do produce the UZ nodal force values. The program ADJRAD computes the UZ values; the actual UZ values calculated below may vary a small amount due to round-off.

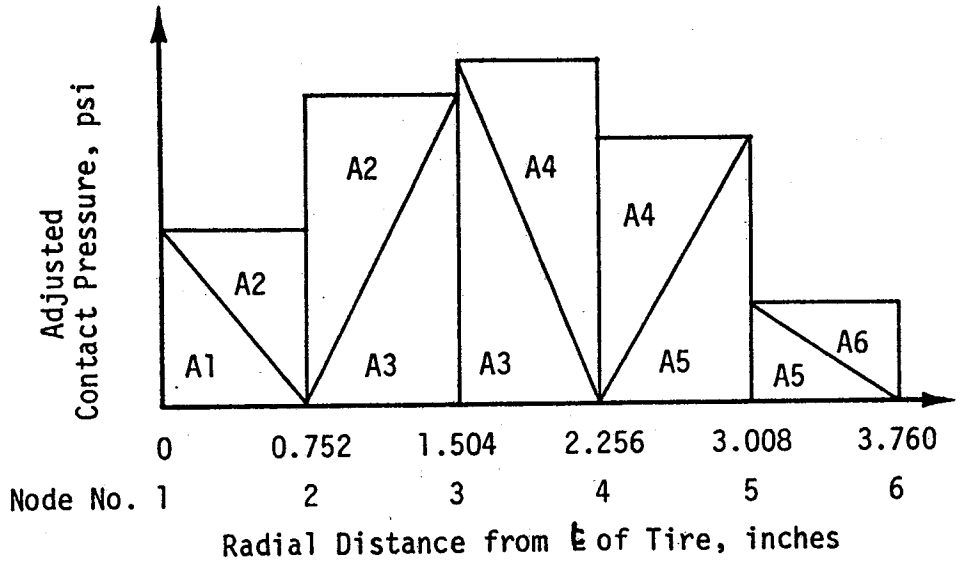


$$UZ(2) = [(1/2)(0.752)(86.3)(2/3)(2/3)(0.752) + (1/2)(0.752)(142.4)[(0.752) + (1/2)(0.752)]] = 70.12$$

$$UZ(3) = [(1/2)(0.752)(142.4)[(2/3)(0.752) + (0.752)] + (1/2)(0.752)(157.9)[(1.504) + (1/3)(0.752)]] = 171.68$$

$$UZ(4) = [(1.2)(0.752)(157.9)[(2/3)(0.752) + (1.504)] + (1.2)(0.752)(120.7)[(2.256) + (1/3)(0.752)]] = 233.36$$

$$UZ(5) = [(1/2)(0.752)(120.7)[(2/3)(0.752) + (2.256)] + (1/2)(0.752)(44.1)[(3.008) + (1/3)(0.752)]] = 179.59$$

$$UZ(6) = [(1/2)(0.752)(44.1)[(2/3)(0.752) + (3.008)]] = 58.33$$

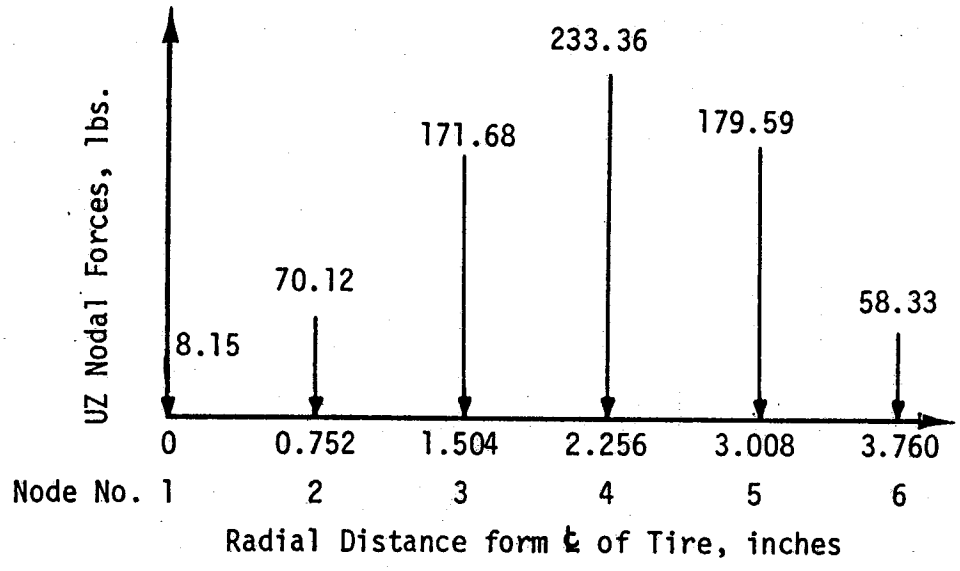


2. 10.0-20 bias ply truck tire with an inflation pressure of 125 psi. The procedure for calculating the UZ nodal force values is exactly the same as for the 10.00-20 bias ply truck tire with an inflation pressure of 75 psi. Therefore, only the graphical and numerical presentation will be shown.

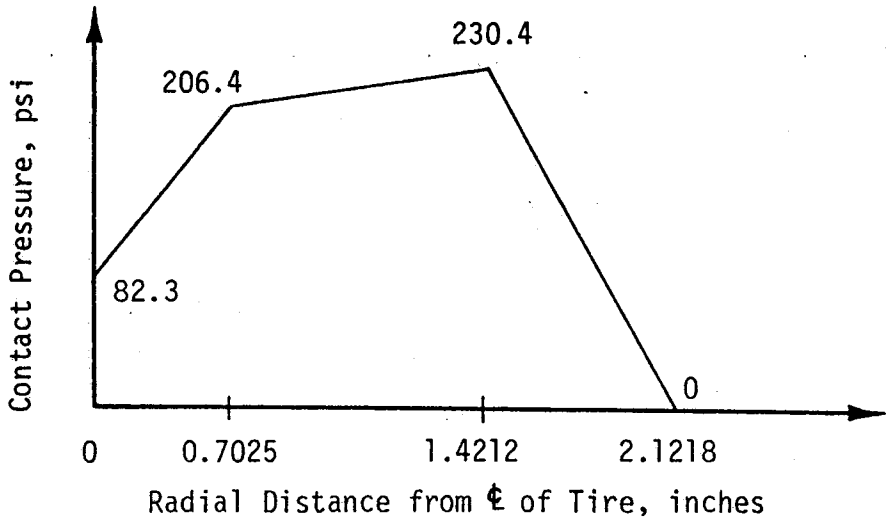

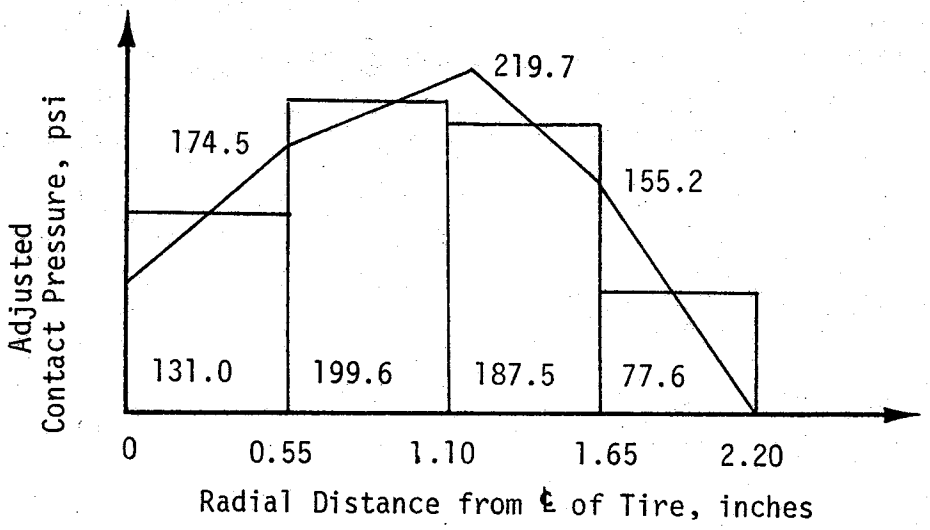
Adjusted
Contact Pressure, psi
219.7
174.5
155.2
131.0
199.6
187.5
77.6
0
0.55
1.10
1.65
2.20
Radial Distance from ℄ of Tire, inches

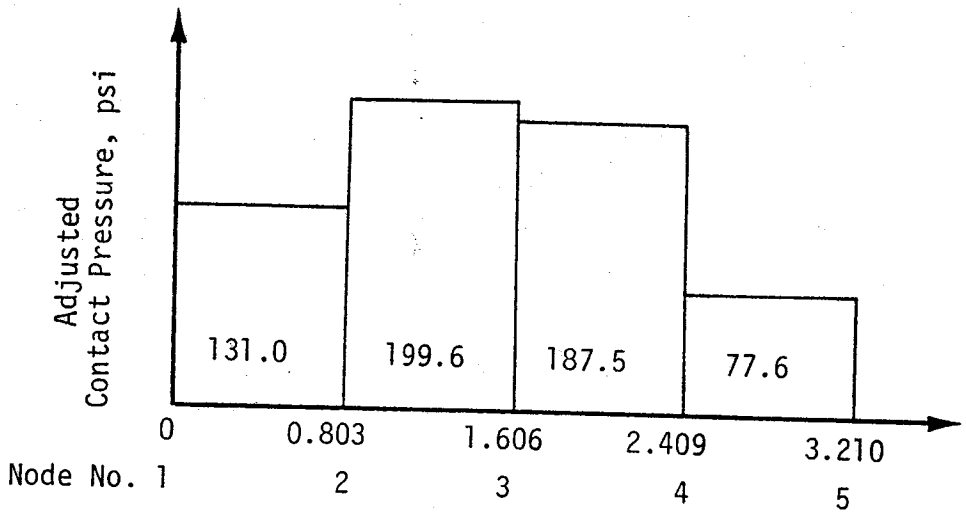
Adjusted
Contact Pressure, psi
131.0
199.6
187.5
77.6
0
0.803
1.606
2.409
3.210
Node No. 1
2
3
4
5
Radial Distance from ℄ of Tire, inches

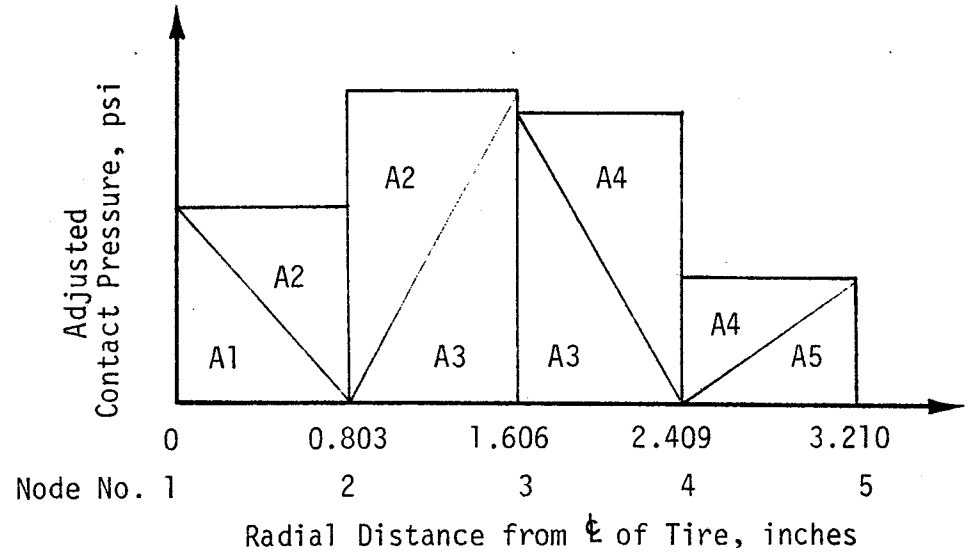
Adjusted
Contact Pressure, psi
A2
A4
A2
A1
A3
A3
A4
A5
0
0.803
1.606
2.409
3.210
Node No. 1
2
3
4
5
Radial Distance from ℄ of Tire, inches

$$UZ(1) = [(1/2)(0.803)(131.0)(1/3)(0.803)] = 14.09$$

$$UZ(2) = [(1/2)(0.803)(131.0)(2/3)(0.803) + (1/2)(0.803)(199.6)[(0.803) + (1.3)(0.803)]] = 114.02$$

$$UZ(3) = [(1/2)(0.803)(199.6)[(2/3)(0.803) + (0.803)] + (1/2)(0.803)(187.5)[(1.606) + (1/3)(0.803)]] = 248.44$$

$$UZ(4) = [(/2)(0.803)(187.5)[(2/3)(0.803) + (1.606)] + (1.2)(0.803)(77.6)[(2.409) + (1/3)(0.803)]] = 244.73$$

$$UZ(5) = [(1/2)(0.803)(77.6)[(2/3)(0.803) + (2.409)]] = 91.79$$

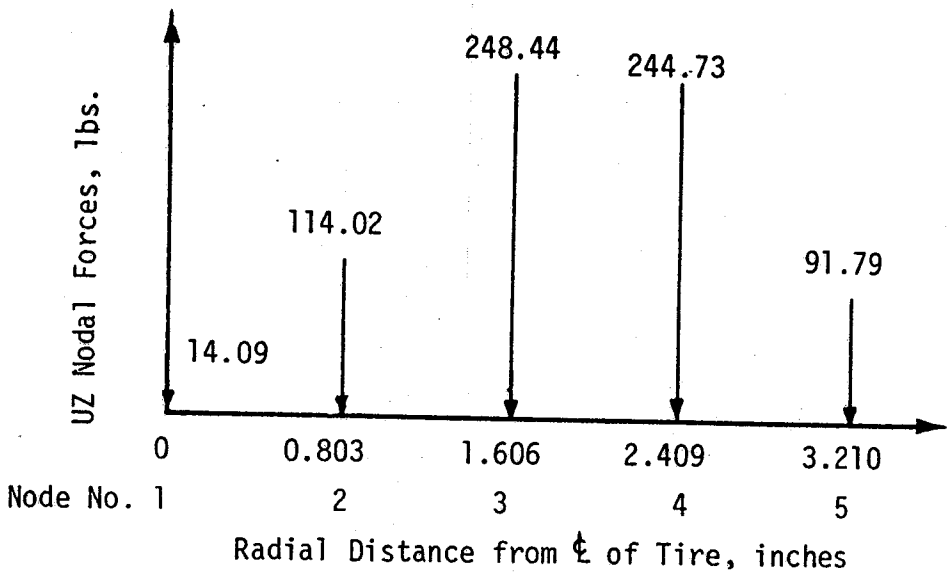

UR Nodal Forces:

1. 10.00-10 bias ply truck tire with an Inflation pressure of 75 psi. From consultation with Dr. J. T. Tielking, it was recommended to model the lateral shear pressure distribution as a sine curve distribution. The sine curve equation is a function of the total radius, R, and a specified maximum lateral shear pressure, c.

$$T_y = c \sin \frac{\pi y}{R}$$

The pressures are calculated at the same nodal distance as those used as the adjusted nodal distances for the 10.00-20 bias ply truck tire with an inflation pressure of 75 psi. The maximum value of lateral shear pressure is 50 psi.

$$T_{0.752} = T_{3.008} = 50 \sin \frac{\pi(0.752)}{3.76} = 29.39$$

$$T_{1.504} = T_{2.256} = 50 \sin \frac{\pi(1.504)}{3.76} = 47.55$$

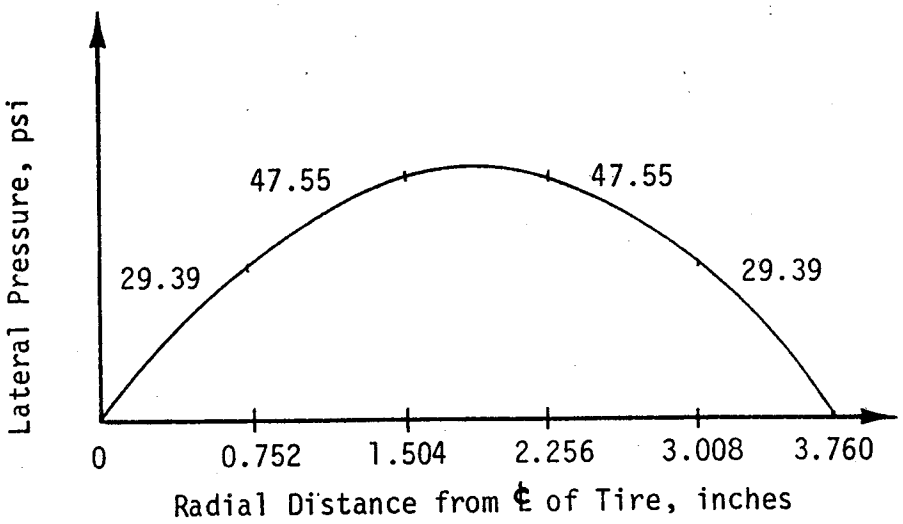

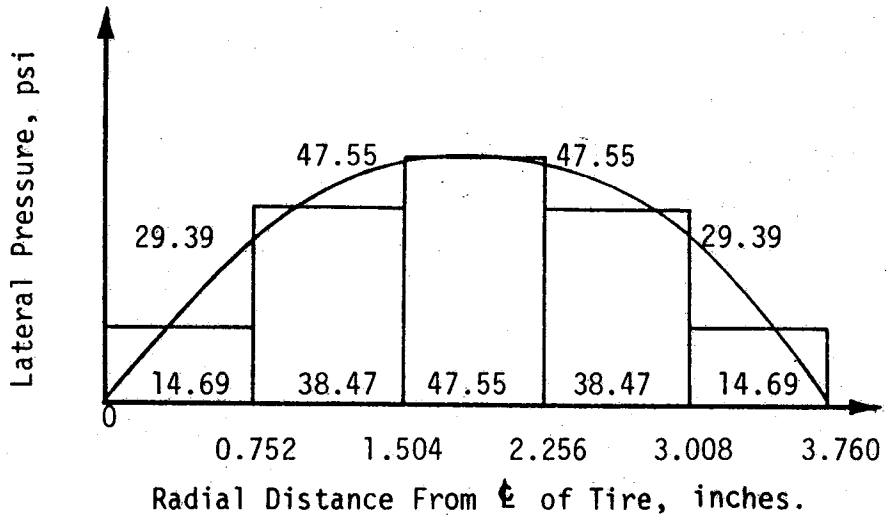


Since the uniform pressures within the increments will not give the same total lateral load as the sine curve distribution, the total amount of lateral load of the sine curve pressure distribution is calculated using Pappa's Theorem. This value is considered to be the true lateral load.

$$\text{True load} = 2\pi\left(\frac{3.76}{2}\right)\int_0^{3.76} 50 \sin \frac{y}{3.76}\, dy$$

$$\text{True load} = 2\pi\left(\frac{3.76}{2}\right)\left[\frac{50(3.76)}{\pi} \cos \frac{\pi y}{3.76}\,\Big|_0^{3.76}\right]$$

$$\text{True load} = 2\pi\left(\frac{3.76}{2}\right)\left[\frac{50(3.76)}{\pi} (\cos \pi - \cos 0)\right]$$

$$\text{True load} = 2\pi\left(\frac{3.76}{2}\right)\left[\frac{50(3.76)(2)}{\pi}\right]$$

True load = 1413.76 lbs.

The total load that is produced by using the uniform pressure is compared with the true load. Since these two total loads are seldom equal, an adjustment is made to the individual pressure within each increment. The adjustment equals to the true load divided by the load produced with uniform pressures. A new and adjusted pressure within each increment is now obtained by multiplying the adjustment value by each uniform pressure. This is explained in greater detail in Appendix C.

Adjustment = 1413.76/1367.22

Adjustment = 1.034

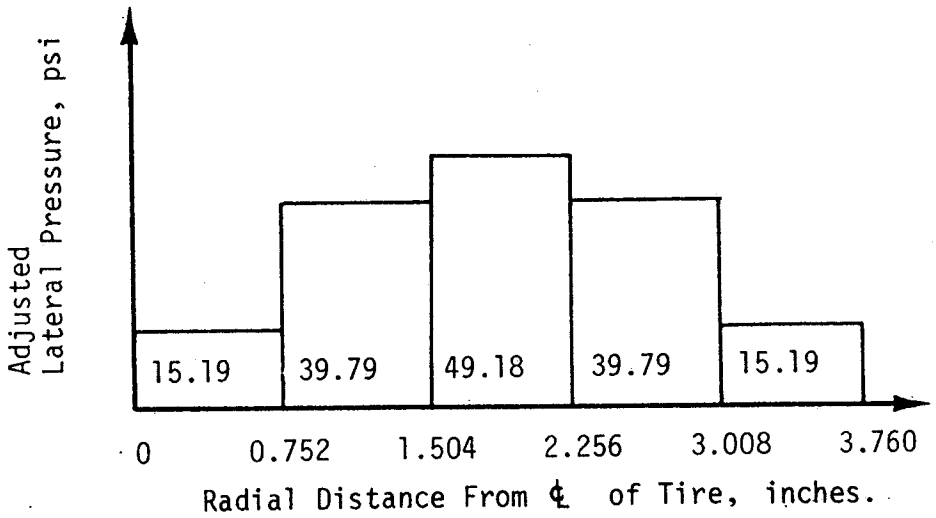


Pappas' Theorem is utilized again to calculate the UR nodal force values from the adjusted uniform pressures. The program PAVELD computes the UR values with more digits, therefore the actual UR values may vary a small amount due to round-off.

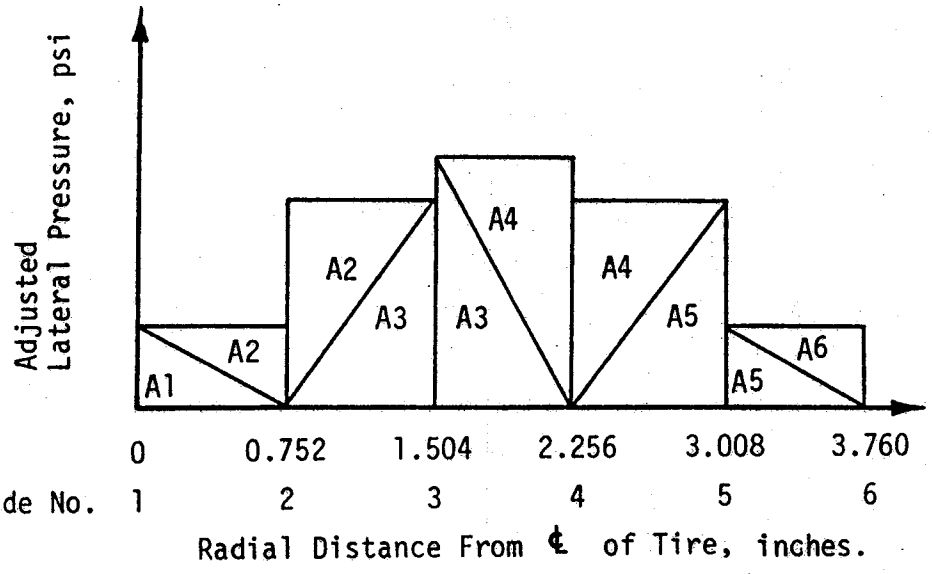


UR(1) is designed as a displacement in ILLIPAVE instead of a force, so since this force is small it will be set equal to zero.

UR(2) = [(1/2)(0.752)(15.19)(2/3)(0.752) +
(1/2)(0.752)(39.79)[(1/3)(0.752) + (0.752)]] = 17.87

UR(3) = [(1/2)(0.752)(39.79) (2/3)().752) +
(1/2)(0.752)(49.18)[(1/3)(0.752) + (1.504)]] = 51.20

UR94) = [(1/2)(0.752)(49.18)[(2/3)(0.752) + 1.504)] +
(1/2)(0.752)(39.79)[(1/3)(0.752) + (2.256)]] = 74.59

UR(5) = [(1/2)(0.752)(39.79)[(2/3)(0.752) + (2.256)] +
(1/2)(0.752)(15.19)[(1/3)(0.752) + (3.008)]] = 59.87

UR(6) = [(1/2)(0.752)(15.19)[(2/3)(0.752) + (3.008)]] = 20.05

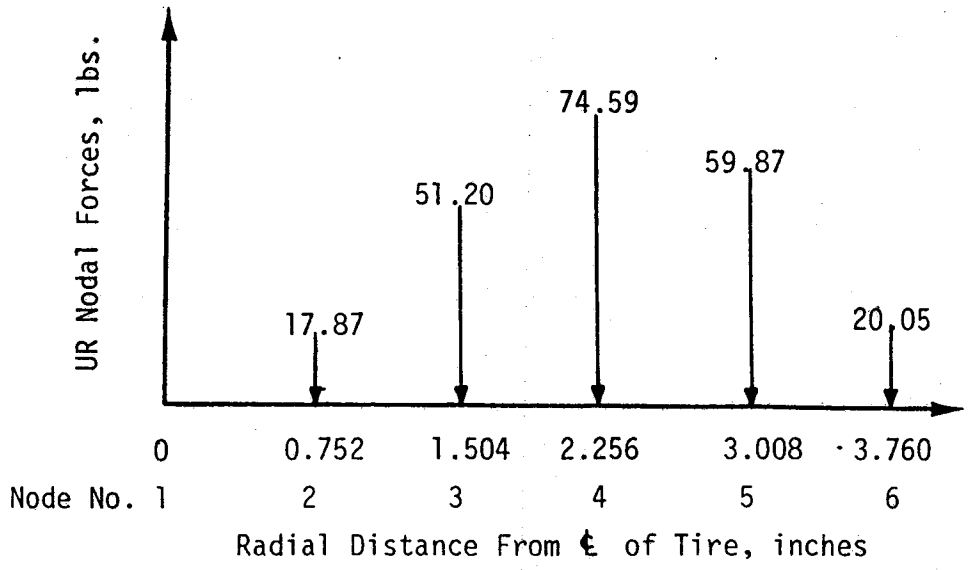

2. 10.00-20 bias ply truck tire with an inflation pressure of 125 psi. The procedure for calculating the UR nodal force values is the same as for the 10.00-20 bias ply truck tire with an inflation pressure of 75 psi. Therefore, only the graphical and numerical presentation will be shown.

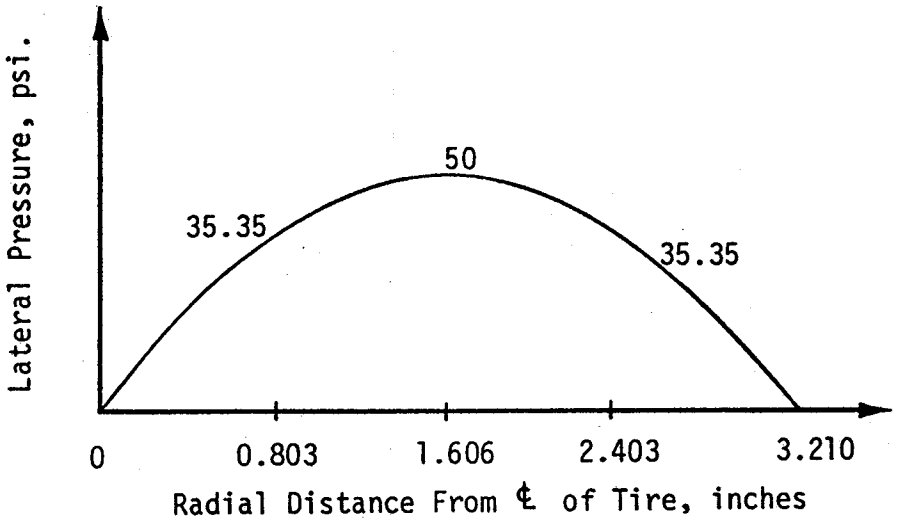


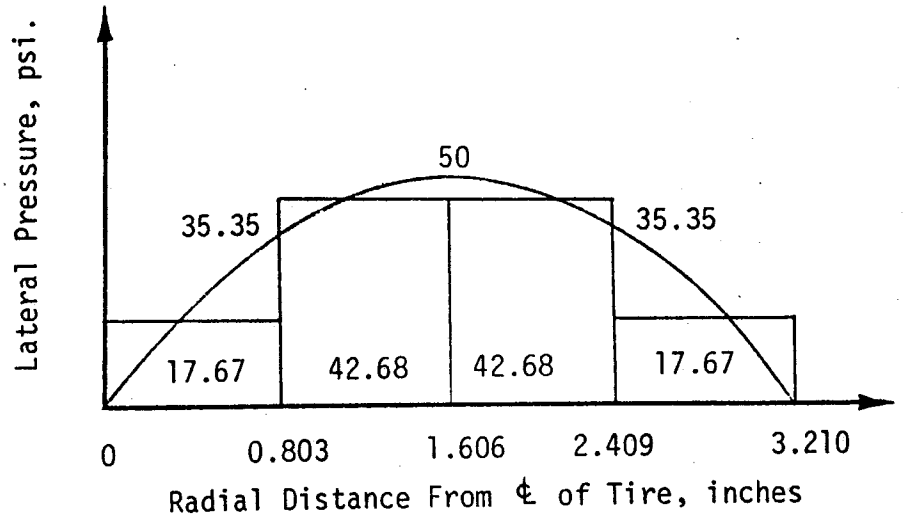

$$\text{True load} = 2\pi\left(\frac{3.21}{2}\right)\int_0^{3.21} 50 \sin\frac{\pi y}{3.21}\, dy$$

$$\text{True load} = 2\pi\left(\frac{3.21}{2}\right)\left[\frac{50(3.21)(2)}{\pi}\right]$$

True load = 1030.41 lbs.

Adjustment = 1030.41/977.62

Adjustment = 1.054

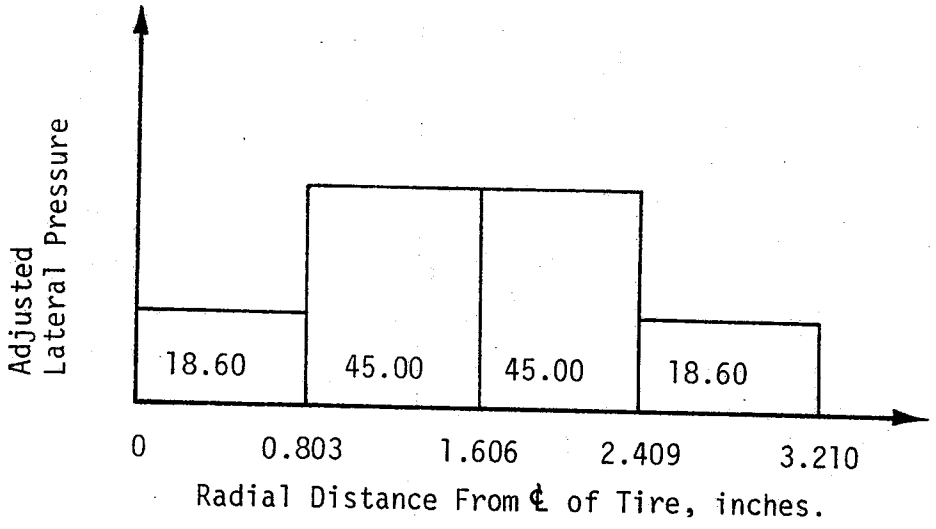


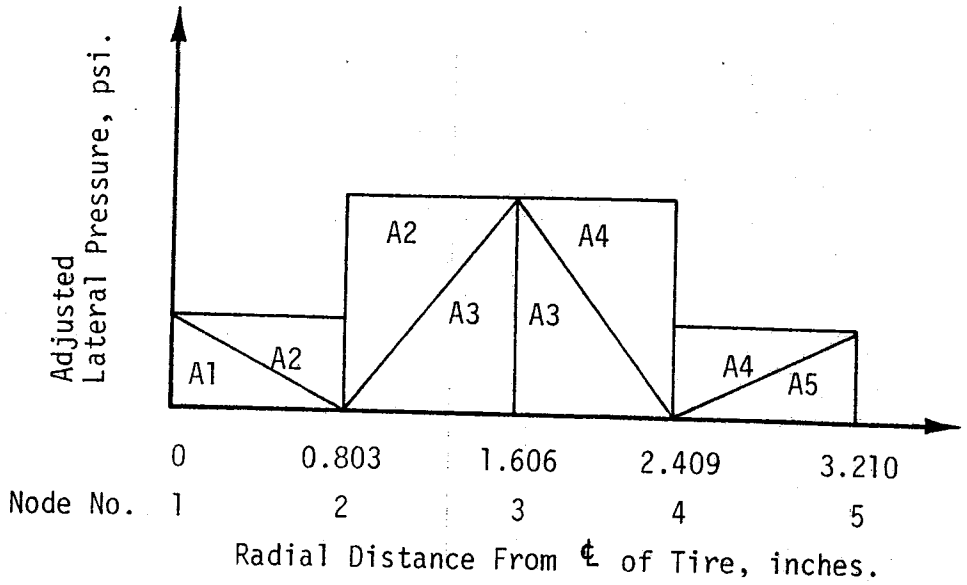

$$UR(1) = 0$$

$$UR(2) = [(1/2)(0.803)(18.60)(2/3)(0.803) + (1/2)(0.803)(45.00)[(1/3)(0.803) + (0.803)]] = 23.33$$

$$UR(3) = [(1/2)(0.803)(45.00)[(2/3)(0.803) + (0.803)] + (1/2)(0.803)(45.00)[(1/3)(0.803) + (1.606)]] = 57.99$$

$$UR(4) = [(1/2)(0.803)(45.00)[(2/3)(0.803) + (0.803)] + (1/2)(0.803)(18.60)[(1/3)(0.803) + (2.409)]] = 58.67$$

$$UR(5) = [(1/2)(0.803)(18.60)[(2/3)(0.803) + (2.409)]] = 22.01$$

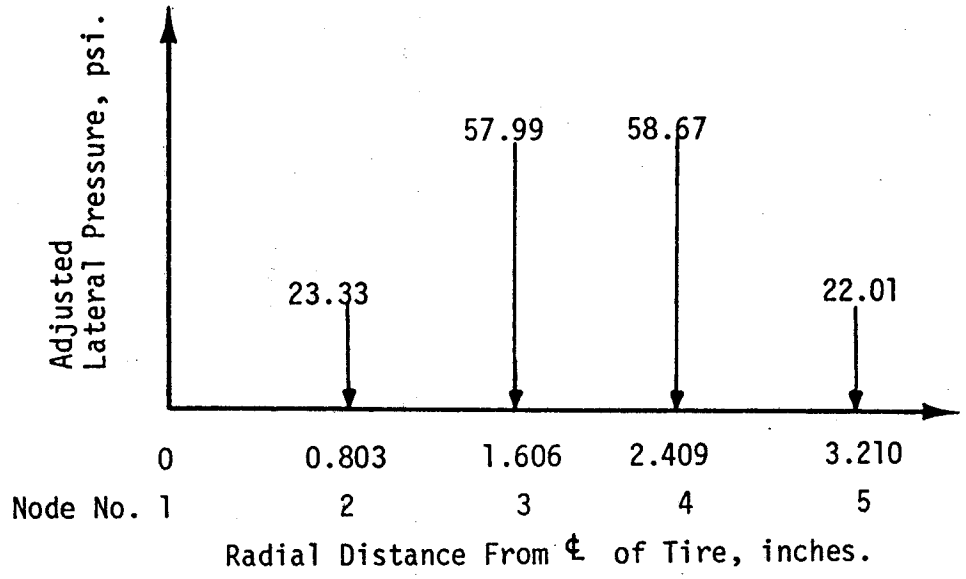

## APPENDIX B. EXPLANATION AND USE OF ADJRAD.

The Tielking (8) tire model gives output for an elliptical tire print. Because ILLIPAVE can only accept a circular tire print, an adjustment will almost always need to be made to insure that the total vertical load remains constant. This can be accomplished in two different ways: the first is to keep the pressures constant within each increment and adjust the increment widths; the second is to adjust the pressures within each increment and keep the increment widths the same. The program ADJRAD uses the first method and the program PAVELD uses the second method.

The values needed for input in ADJRAD are the total radius of the cicular load, the total plate load, the number of strip loads increments, and their corresponding pressure values. The program ADJRAD adjusts the increment widths as follows: the total plate load, TPL, is divided by the plate load, PL. (See line 120 of the program listing for the derivation of PL.). This quotient gives an indication of the adjustment, ADJ, needed in the increment size, DR, to make the total load of the circular tire print equal to the total load of the elliptical tire print. The width of each increment, DR, is adjusted as a function of the adjustment, ADJ, as shown on lines 160 and 170 of the program listing. When the adjustment is between 0.99 and 1.01, the increment width will not change significantly; therefore, at this point, the UZ values are calculated using the new adjusted increment widths. The output consists of a list of the UZ nodal force values at the new nodal radii from the center of the tireprint. Also, the new plate load and adjustment are given as output.

ADJRAD

```
10  DIM Y(30)
20  INPUT"INPUT THE RADIUS";RAD
30  INPUT"INPUT THE TOTAL PLATE LOAD",TPL
40  INPUT"INPUT THE NUMBER OF STRIP LOADS";NLDS
50  DR=RAD/NLDS
60  TRY=0
70  PL=0
80  DR1=0
90  FOR I=1 TO NLDS
100 IF TRY <> 0 THEN GOTO 120
110 PRINT"INPUT Y(";I;")":INPUT Y(I)
120 PL=PL+2*3.14159*Y(I)*(DR1+(DR/2))*DR
130 DR1=DR1+DR
140 NEXT I
150 ADJ=TPL/PL
160 IF ADJ > 1.01 THEN DR=DR+ADJ/10
170 IF ADJ <.99 THEN DR=DR-ADJ/10
180 IF ADJ <= 1.01 AND ADJ => .99 THEN GOTO 240
200 TRY=TRY + 1
210 IF TRY=50 THEN PRINT"START WITH ANOTHER RADIUS.ADJ =";ADJ
220 IF TRY=50 THEN GOTO 440
230 GOTO 70
240 FOR J=1 TO NLDS
250 PRINT"Y(";J;") =";Y(J)
260 NEXT J
270 PRINT
280 DR1=0
290 SUM=0
300 NUZ=NLDS+1
310 FOR K=1 TO NUZ
320 IF K=1 THEN GOTO 370
330 IF K=NUZ THEN GOTO 380
340 UZ(K)=Y(K-1)*(DR/2)*(DR1-(DR/3))
350 UZ(K)=UZ(K)+Y(K)*(DR/2)*(DR1+(DR/3)
360 GOTO 390
370 UZ(K)=Y(K)*(DR/2)*(DR/3)
380 IF K=NUZ THEN UZ(K)=Y(K-1)*(DR/2)*(DR1-(DR/3))
390 DR1=DR1+DR
400 SUM=SUM+2*3.14159*UZ(K)
410 PRINT"X ="'DR1-DR,"UZ(";K;")";UZ(K)
420 NEXT K
430 PRINT:PRINT"THE NEW PLATE LOAD =";SUM,"ADJ =";ADJ
440 END
```

## APPENDIX C. EXPLANATION AND USE OF PAVELD.

As was explained in Appendix B, the Tielking (8) tire model gives output for an elliptical tire print, but ILLPAVE can only accept a circular tire print. These two tire loads are almost always going to be different; therefore, an adjustment must be made in the pressure values or in the total radius. ADJRAD makes adjustments to the total radius by changing the increment widths. PAVELD makes adjustments in the magnitude of the pressure while leaving the increment widths constant.

The values needed for input in PAVELD are the same as ADJRAD: the radius of the circular load; the total plate load; and the number of strip loads with their corresponding pressure values. The program PAVELD adjusts the pressures within the increments as follows: the total plate load, TPL, is divided by the plate load, PL. (See line 100 of the program listing of the derivation of PL.) This quotient is the adjustment, ADJ, that each of the pressure values, Y(I), must be multiplied by to make the total load of the circular tire print equal to the total load of the elliptical tire print. The output consists of a list of the adjusted pressure values, Y(I), and the UR nodal force values at their corresponding radii from the center of the tire print.

```
10  DIM Y(30)
20  INPUT"INPUT THE RADIUS";RAD
30  INPUT"INPUT THE TOTAL PLATE LOAD";TPL
40  INPUT"INPUT THE NUMBER OF STRIP LOADS";NLDS
50  DR=RAD/NLDS
60  PL=0
70  DR1=0
80  FOR I=1 TO NLDS
90  PRINT"INPUT Y(";I;")":INPUT Y(I)
100 PL = PL+2*3.14159*Y(I)*(DR1+(DR/2)*DR
110 DR1=DR1+DR
120 NEXT I
130 ADJ=TPL/PL
140 PRINT"ADJUSTED Y VALUES"
150 FOR J=1 TO NLDS
160 Y(J)=ADJ*(J)
170 PRINT"Y(";J;") = ";Y(J)
180 NEXT J
190 PRINT
200 DR1=0
210 SUM=0
220 NUZ=NLDS+1
230 FOR K=1 TO NUZ
240 IF K=1 THEN GO TO 290
250 IF K=NUZ THEN GOTO 300
260 UR(K)=Y(K-1)*(DR/2)*(DR1-DR/3))
270 UR(K)=UR(K)+Y(K)*(DR/2)*(DR1+(DR/3))
280 UR(K)=Y(K)*(DR/2)*(DR/3)
300 IF K=NUZ THEN UR(K)=Y(K-1)*(DR/2)*(DR1-(DR/3))
310 DR1=DR1+DR
320 SUM=SUM+2*3.14159*UZ(K)
330 PRINT"X =";DR1-DR,"UR(";K;")";UR(K)
340 NEXT K
```

APPENDIX D. TENSILE STRAIN AND ESAL DATA AT THE TOP AND BOTTOM OF THE ASPHALT CONCRETE SURFACE.

The tables presented in this appendix have lines separating the sections of the three base moduli used. The top section uses the base modulus expression $E_B = 8787\,\theta^{0.365}$; the middle section uses the base modulus expression $E_B = 7000\,\theta^{0.325}$; and the bottom section uses the base modulus expression $E_B = 4886\,\theta^{0.239}$.

The 18-kip Equivalent Single Axle Loads (ESAL) are calculated using the expression defined in Chapter V. The ESALs are calculated as a function of the tensile strains in the surface by the equation:

$$W_{18} - 5.0957 \times 10^{-13} \left(\frac{1}{\varepsilon_t}\right)^{4.65644}.$$

The tensile strains at the bottom of the surface are tabulated for strain values at 0.5 inches from the centerline of the tire load. The tensile strains at the top of the surface are tabulated at distances from the centerline of the load where maximum strain occurs; these radii are also presented. The dashed lines indicate that the material is in compression; in these cases, ESAL computations are not applicable.

Surface Thickness = 1 inch
Base Thickness = 8 inches

Tire Inflation Pressure = 75 psi

| Surface Modulus (ksi) | Base Modulus (ksi) | $\varepsilon_T$ Bottom of A.C. ($\times 10^{-6}$ in/in) | $ESAL_{B.S.}$ | Rad. at Max. $\varepsilon_{Top}$ (inches) | $\varepsilon_T$ Top of A.C. ($\times 10^{-6}$ in/in) | $ESAL_{T.S.}$ |
|---|---|---|---|---|---|---|
| 50 | 73.0 | - | - | 3.38 | 326.6 | 8,699 |
| 100 | 69.5 | - | - | 4.45 | 145.9 | 370,724 |
| 200 | 65.7 | 88.3 | 3,842,329 | 5.82 | 119.4 | 942,753 |
| 400 | 61.9 | 245.4 | 32,926 | 5.82 | 98.1 | 2,353,730 |
| 800 | 57.7 | 286.9 | 15,906 | 5.82 | 76.6 | 7,448,102 |
| 50 | 44.8 | - | - | 3.38 | 387.2 | 3,938 |
| 100 | 42.8 | 46.7 | 74,605,347 | 4.45 | 229.5 | 44,978 |
| 200 | 40.7 | 285.4 | 16,299 | 5.82 | 184.6 | 123,927 |
| 400 | 38.5 | 406.7 | 3,133 | 5.82 | 146.4 | 364,865 |
| 800 | 36.0 | 422.3 | 2,629 | 5.82 | 107.1 | 1,564,051 |
| 50 | 18.4 | 258.6 | 25,798 | 3.38 | 649.2 | 355 |
| 100 | 17.7 | 679.6 | 287 | 4.45 | 464.7 | 1,684 |
| 200 | 17.0 | 861.9 | 95 | 5.82 | 353.8 | 5,994 |
| 400 | 16.3 | 840.6 | 107 | 5.82 | 255.9 | 27,090 |
| 800 | 15.3 | 700.2 | 250 | 7.19 | 171.9 | 172,749 |

Surface Thickness = 1.5 inches
Base Thickness = 8 inches

Tire Inflation Pressure = 75 psi

| Surface Modulus (ksi) | Base Modulus (ksi) | $\varepsilon_T$ Bottom of A.C. ($x10^{-6}$in/in) | $ESAL_{B.S.}$ | Rad. at Max. $\varepsilon_{Top}$ (inches) | $\varepsilon_T$ Top of A.C. ($x10^{-6}$in/in) | $ESAL_{T.S.}$ |
|---|---|---|---|---|---|---|
| 50 | 66.0 | 45.6 | 83,363,000 | 3.38 | 280.2 | 17,756 |
| 100 | 61.9 | 220.4 | 54,302 | 5.82 | 135.2 | 528,541 |
| 200 | 57.8 | 333.0 | 7,948 | 7.19 | 112.8 | 1,228,541 |
| 400 | 54.3 | 365.5 | 5,151 | 7.19 | 91.9 | 3,189,943 |
| 800 | 49.5 | 333.1 | 7,936 | 8.57 | 68.4 | 12,618,717 |
| 50 | 40.7 | 265.3 | 22,901 | 3.38 | 320.6 | 9,483 |
| 100 | 38.4 | 456.9 | 1,822 | 5.82 | 218.4 | 56,657 |
| 200 | 36.2 | 538.8 | 846 | 5.82 | 168.8 | 188,026 |
| 400 | 33.8 | 512.8 | 1,064 | 7.19 | 126.9 | 709,906 |
| 800 | 30.7 | 422.8 | 2,615 | 8.57 | 88.2 | 3,862,657 |
| 50 | 17.0 | 1021.0 | 43 | 5.82 | 555.1 | 736 |
| 100 | 16.2 | 1112.2 | 29 | 5.82 | 420.5 | 2,682 |
| 200 | 15.4 | 1015.8 | 44 | 5.82 | 290.0 | 15,130 |
| 400 | 14.4 | 805.2 | 130 | 7.19 | 197.4 | 90,719 |
| 800 | 13.4 | 575.4 | 623 | 5.82 | 87.8 | 3,945,284 |

Surface Thickness = 2 inches
Base Thickness = 8 inches

Tire Inflation Pressure = 75 psi

| Surface Modulus (ksi) | Base Modulus (ksi) | $\varepsilon_T$ Bottom of A.C. ($\times 10^{-6}$ in/in) | $ESAL_{B.S.}$ | Rad. at Max. $\varepsilon_{Top}$ (inches) | $\varepsilon_T$ Top of A.C. ($\times 10^{-6}$ in/in) | $ESAL_{T.S.}$ |
|---|---|---|---|---|---|---|
| 50 | 59.6 | 322.6 | 9,213 | 3.38 | 232.2 | 42,594 |
| 100 | 56.7 | 400.0 | 3,385 | 7.19 | 126.5 | 720,419 |
| 200 | 53.1 | 426.0 | 2,524 | 8.57 | 103.6 | 1,825,753 |
| 400 | 48.4 | 388.1 | 3,896 | 8.57 | 78.7 | 6,566,762 |
| 800 | 42.8 | 309.7 | 11,141 | 11.31 | 56.4 | 30,982,594 |
| 50 | 37.4 | 580.8 | 596 | 5.82 | 240.0 | 36,520 |
| 100 | 35.6 | 630.8 | 406 | 7.19 | 189.5 | 109,722 |
| 200 | 33.2 | 598.7 | 518 | 7.19 | 144.5 | 387,747 |
| 400 | 30.2 | 494.8 | 1,257 | 8.57 | 102.3 | 1,936,326 |
| 800 | 26.8 | 365.1 | 5,178 | 11.31 | 68.6 | 12,448,321 |
| 50 | 16.1 | 1311.1 | 13 | 5.82 | 475.0 | 1,520 |
| 100 | 15.3 | 1185.8 | 21 | 7.19 | 337.1 | 7,507 |
| 200 | 14.3 | 948.0 | 61 | 7.19 | 228.3 | 46,090 |
| 400 | 13.1 | 681.5 | 283 | 8.57 | 145.8 | 371,909 |
| 800 | 12.0 | 452.0 | 1916 | 11.31 | 90.0 | 3,515,854 |

Surface Thickness = 4 inches
Base Thickness = 8 inches

Tire Inflation Pressure = 75 psi

| Surface Modulus (ksi) | Base Modulus (ksi) | $\varepsilon_T$ Bottom of A.C. ($x10^{-6}$in/in) | $ESAL_{B.S.}$ | Rad. at Max. $\varepsilon_{Top}$ (inches) | $\varepsilon_T$ Top of A.C. ($x10^{-6}$in/in) | $ESAL_{T.S.}$ |
|---|---|---|---|---|---|---|
| 50 | 46.7 | 588.7 | 560 | 11.31 | 106.3 | 1,619,621 |
| 100 | 42.6 | 480.6 | 1,440 | 11.31 | 83.7 | 4,929,333 |
| 200 | 37.6 | 370.2 | 4,854 | 21.75 | 66.3 | 14,590,675 |
| 400 | 32.1 | 258.5 | 25,844 | 21.75 | 55.2 | 34,245,937 |
| 800 | 26.5 | 164.9 | 209,647 | 21.75 | 41.1 | 135,234,107 |
| 50 | 29.8 | 762.9 | 167 | 9.94 | 141.5 | 427,539 |
| 100 | 27.1 | 596.7 | 526 | 11.31 | 106.6 | 1,598,505 |
| 200 | 24.0 | 431.0 | 2,391 | 15.25 | 72.0 | 9,937,715 |
| 400 | 20.7 | 287.7 | 15,701 | 21.75 | 61.0 | 21,506,146 |
| 800 | 17.5 | 175.2 | 158,111 | 21.75 | 43.5 | 103,828,585 |
| 50 | 13.3 | 1136.9 | 26 | 9.94 | 226.6 | 47,722 |
| 100 | 12.2 | 805.1 | 130 | 11.31 | 151.5 | 311,088 |
| 200 | 11.0 | 528.9 | 922 | 15.25 | 89.7 | 3,570,944 |
| 400 | 9.9 | 323.4 | 9,107 | 21.75 | 68.3 | 12,704,978 |
| 800 | 8.8 | 188.5 | 112,459 | 23.92 | 47.9 | 66,292,188 |

Surface Thickness = 1 inch
Base Thickness = 8 inch

Tire Inflation Pressure = 125 psi

| Surface Modulus (ksi) | Base Modulus (ksi) | $\varepsilon_T$ Bottom of A.C. ($x10^{-6}$ in/in) | $ESAL_{B.S.}$ | Rad. at Max. $\varepsilon_{Top}$ (inches) | $\varepsilon_T$ Top of A.C. ($x10^{-6}$ in/in) | $ESAL_{T.S.}$ |
|---|---|---|---|---|---|---|
| 50 | 75.5 | - | - | 3.84 | 160.8 | 232,725 |
| 100 | 72.1 | - | - | 5.09 | 135.2 | 528,541 |
| 200 | 68.2 | 240.7 | 36,028 | 5.09 | 122.7 | 830,356 |
| 400 | 64.0 | 349.6 | 6,337 | 5.09 | 103.1 | 1,867,350 |
| 800 | 60.0 | 376.0 | 4,515 | 6.35 | 81.3 | 5,644,453 |
| 50 | 46.2 | - | - | 3.84 | 275.8 | 19,114 |
| 100 | 44.2 | 295.6 | 13,841 | 5.09 | 235.6 | 39,806 |
| 200 | 42.0 | 488.9 | 1,329 | 5.09 | 198.9 | 87,577 |
| 400 | 39.5 | 561.1 | 700 | 5.09 | 156.4 | 268,233 |
| 800 | 37.0 | 528.9 | 922 | 6.35 | 115.5 | 1,100,410 |
| 50 | 18.8 | 797.6 | 136 | 3.84 | 638.5 | 384 |
| 100 | 18.1 | 1103.7 | 30 | 5.09 | 514.8 | 1,045 |
| 200 | 17.4 | 1183.8 | 22 | 5.09 | 394.3 | 3,618 |
| 400 | 16.5 | 1058.9 | 36 | 5.09 | 273.9 | 19,740 |
| 800 | 15.5 | 836.6 | 109 | 6.35 | 185.9 | 119,972 |

Surface Thickness = 1.5 inches
Base Thickness .= 8 inches

Tire Inflation Pressure = 125 psi

| Surface Modulus (ksi) | Base Modulus (ksi) | $\varepsilon_T$ Bottom of A.C. ($x10^{-6}$in/in) | $ESAL_{B.S.}$ | Rad. at Max. $\varepsilon_{Top}$ (inches) | $\varepsilon_T$ Top of A.C. ($x10^{-6}$in/in) | $ESAL_{T.S.}$ |
|---|---|---|---|---|---|---|
| 50 | 67.6 | 270.7 | 20,850 | 3.84 | 134.4 | 543,351 |
| 100 | 63.6 | 390.0 | 3,808 | 6.35 | 126.7 | 715,139 |
| 200 | 60.7 | 457.7 | 1,807 | 6.35 | 113.6 | 1,188,770 |
| 400 | 56.5 | 454.6 | 1,865 | 6.35 | 92.3 | 3,126,080 |
| 800 | 51.1 | 392.8 | 3,683 | 7.60 | 69.4 | 11,794,077 |
| 50 | 41.6 | 556.3 | 728 | 5.09 | 251.7 | 29,260 |
| 100 | 39.8 | 672.3 | 302 | 5.09 | 213.0 | 63,663 |
| 200 | 37.7 | 690.8 | 266 | 6.35 | 174.0 | 163,253 |
| 400 | 34.9 | 618.2 | 446 | 7.60 | 127.7 | 689,433 |
| 800 | 31.5 | 488.8 | 1,331 | 7.60 | 90.1 | 3,497,721 |
| 50 | 17.4 | 1478.8 | 8 | 5.09 | 579.1 | 604 |
| 100 | 16.7 | 1433.9 | 9 | 5.09 | 431.2 | 2,386 |
| 200 | 15.8 | 1231.0 | 18 | 6.35 | 308.2 | 11,396 |
| 400 | 14.7 | 938.8 | 64 | 7.60 | 202.4 | 80,745 |
| 800 | 13.5 | 653.6 | 344 | 8.86 | 125.1 | 758,737 |

Surface Thickness = 2 inches
Base Thickness = 8 inches

Tire Inflation Pressure = 125 psi

| Surface Modulus (ksi) | Base Modulus (ksi) | $\varepsilon_T$ Bottom of A.C. ($\times 10^{-6}$ in/in) | $ESAL_{B.S.}$ | Rad. at Max. $\varepsilon_{Top}$ (inches) | $\varepsilon_T$ Top of A.C. ($\times 10^{-6}$ in/in) | $ESAL_{T.S.}$ |
|---|---|---|---|---|---|---|
| 50 | 61.9 | 526.9 | 938 | 10.12 | 133.3 | 564,547 |
| 100 | 59.2 | 540.9 | 830 | 7.60 | 120.9 | 889,510 |
| 200 | 55.1 | 523.6 | 966 | 7.60 | 102.8 | 1,892,860 |
| 400 | 49.9 | 452.0 | 1,916 | 8.86 | 79.2 | 6,375,936 |
| 800 | 43.7 | 347.7 | 6,500 | 10.12 | 57.1 | 29,253,189 |
| 50 | 38.9 | 822.9 | 118 | 6.35 | 220.5 | 54,188 |
| 100 | 36.9 | 800.4 | 134 | 6.35 | 187.2 | 116,142 |
| 200 | 34.2 | 712.2 | 231 | 7.60 | 145.0 | 381,561 |
| 400 | 30.8 | 566.7 | 668 | 8.86 | 103.0 | 1,850,574 |
| 800 | 27.2 | 406.7 | 3,132 | 10.12 | 69.8 | 11,482,639 |
| 50 | 16.4 | 1662.2 | 4 | 6.35 | 465.2 | 1,675 |
| 100 | 15.6 | 1414.1 | 9 | 6.35 | 344.6 | 6,776 |
| 200 | 14.5 | 1090.8 | 32 | 7.60 | 232.7 | 42,170 |
| 400 | 13.3 | 764.5 | 166 | 8.86 | 149.0 | 336,149 |
| 800 | 12.1 | 496.7 | 1,235 | 11.37 | 91.4 | 3,272,017 |

Surface Thickness = 4 inches
Base Thickness = 8 inches

Tire Inflation Pressure = 125 psi

| Surface Modulus (ksi) | Base Modulus (ksi) | $\varepsilon_T$ Bottom of A.C. ($x10^{-6}$in/in) | $ESAL_{B.S.}$ | Rad. at Max. $\varepsilon_{Top}$ (inches) | $\varepsilon_T$ Top of A.C. ($x10^{-6}$in/in) | $ESAL_{T.S.}$ |
|---|---|---|---|---|---|---|
| 50 | 47.5 | 668.5 | 310 | 11.37 | 101.7 | 1,990,097 |
| 100 | 43.3 | 528.6 | 924 | 11.37 | 81.6 | 5,548,471 |
| 200 | 38.1 | 397.8 | 3,473 | 11.37 | 59.0 | 25,117,575 |
| 400 | 32.3 | 274.6 | 19,507 | 21.75 | 54.5 | 36,342,745 |
| 800 | 26.6 | 174.0 | 163,253 | 21.75 | 40.6 | 143,165,669 |
| 50 | 30.2 | 851.3 | 100 | 11.37 | 136.0 | 514,219 |
| 100 | 27.4 | 648.9 | 356 | 11.37 | 104.3 | 1,769,392 |
| 200 | 24.2 | 460.2 | 1,762 | 11.37 | 71.2 | 10,468,439 |
| 400 | 20.8 | 303.5 | 12,241 | 21.75 | 59.0 | 25,117,575 |
| 800 | 17.5 | 182.6 | 130,407 | 21.75 | 43.0 | 109,571,094 |
| 50 | 13.4 | 1241.0 | 17 | 10.12 | 220.3 | 54,417 |
| 100 | 12.3 | 860.7 | 95 | 11.37 | 149.0 | 336,149 |
| 200 | 11.1 | 559.4 | 710 | 11.37 | 90.9 | 3,356,670 |
| 400 | 10.0 | 340.6 | 7,155 | 21.75 | 67.3 | 13,608,222 |
| 800 | 8.8 | 195.8 | 94,223 | 21.75 | 47.4 | 69,611,750 |

Surface Thickness = 1 inch
Base Thickness = 14 inches

Tire Inflation Pressure = 75 psi

| Surface Modulus (ksi) | Base Modulus (ksi) | $\varepsilon_T$ Bottom of A.C. ($\times 10^{-6}$ in/in) | $ESAL_{B.S.}$ | Rad. at Max. $\varepsilon_{Top}$ (inches) | $\varepsilon_T$ Top of A.C. ($\times 10^{-6}$ in/in) | $ESAL_{T.S.}$ |
|---|---|---|---|---|---|---|
| 50 | 67.9 | - | - | 3.38 | 404.2 | 3,224 |
| 100 | 65.7 | - | - | 3.38 | 188.2 | 113,296 |
| 200 | 63.0 | 133.8 | 554,790 | 4.45 | 126.2 | 728,429 |
| 400 | 59.7 | 234.9 | 40,362 | 5.82 | 103.8 | 1,809,430 |
| 800 | 56.0 | 275.5 | 19,212 | 5.82 | 81.0 | 5,742,459 |
| 50 | 42.5 | - | - | 3.38 | 457.8 | 1,805 |
| 100 | 41.0 | 128.9 | 660,051 | 4.45 | 250.0 | 30,198 |
| 200 | 39.3 | 309.5 | 11,175 | 5.82 | 186.0 | 119,672 |
| 400 | 37.2 | 399.7 | 3,396 | 5.82 | 148.4 | 342,525 |
| 800 | 35.0 | 403.8 | 3,239 | 5.82 | 108.6 | 1,465,968 |
| 50 | 17.8 | 358.9 | 5,607 | 3.38 | 673.0 | 300 |
| 100 | 17.3 | 708.1 | 237 | 4.45 | 465.0 | 1,679 |
| 200 | 16.6 | 855.9 | 98 | 5.82 | 347.0 | 6,561 |
| 400 | 15.8 | 826.4 | 115 | 5.82 | 251.2 | 29,532 |
| 800 | 15.0 | 686.6 | 273 | 7.19 | 165.4 | 206,712 |

Surface Thickness = 1.5 inches
Base Thickness = 14 inches

Tire Inflation Pressure = 75 psi

| Surface Modulus (ksi) | Base Modulus (ksi) | $\varepsilon_T$ Bottom of A.C. ($\times 10^{-6}$ in/in) | $ESAL_{B.S.}$ | Rad. at Max. $\varepsilon_{Top}$ (inches) | $\varepsilon_T$ Top of A.C. ($\times 10^{-6}$ in/in) | $ESAL_{T.S.}$ |
|---|---|---|---|---|---|---|
| 50 | 62.1 | 148.4 | 342,525 | 3.38 | 369.8 | 4,878 |
| 100 | 59.1 | 265.4 | 22,861 | 4.45 | 156.0 | 271,451 |
| 200 | 56.3 | 336.4 | 7,580 | 5.82 | 122.0 | 852,775 |
| 400 | 53.0 | 352.2 | 6,122 | 5.82 | 91.0 | 3,339,528 |
| 800 | 48.6 | 315.4 | 10,234 | 7.19 | 66.0 | 14,902,073 |
| 50 | 38.9 | 346.4 | 6,614 | 3.38 | 394.6 | 3,606 |
| 100 | 37.1 | 475.4 | 1,515 | 5.82 | 225.0 | 49,323 |
| 200 | 35.4 | 527.9 | 530 | 5.82 | 174.0 | 163,253 |
| 400 | 33.1 | 494.0 | 1,267 | 7.19 | 123.6 | 802,575 |
| 800 | 30.3 | 405.8 | 3,165 | 7.19 | 84.3 | 4,768,077 |
| 50 | 16.5 | 1039.0 | 40 | 4.45 | 562.2 | 694 |
| 100 | 15.9 | 1104.2 | 30 | 5.82 | 415.0 | 2,851 |
| 200 | 15.2 | 996.3 | 48 | 5.82 | 287.0 | 15,881 |
| 400 | 14.2 | 793.0 | 140 | 7.19 | 192.0 | 103,226 |
| 800 | 13.2 | 571.6 | 642 | 8.57 | 120.6 | 899,860 |

Surface Thickness = 2 inches
Base Thickness = 14 inches

Tire Inflation Pressure = 75 psi

| Surface Modulus (ksi) | Base Modulus (ksi) | $\varepsilon_T$ Bottom of A.C. ($\times 10^{-6}$ in/in) | $ESAL_{B.S.}$ | Rad. at Max. $\varepsilon_{Top}$ (inches) | $\varepsilon_T$ Top of A.C. ($\times 10^{-6}$ in/in) | $ESAL_{T.S.}$ |
|---|---|---|---|---|---|---|
| 50 | 57.4 | 379.8 | 4,308 | 3.38 | 313.8 | 10,479 |
| 100 | 55.2 | 411.7 | 2,959 | 5.82 | 133.0 | 570,501 |
| 200 | 51.9 | 414.7 | 2,861 | 7.19 | 103.0 | 1,875,807 |
| 400 | 47.5 | 371.8 | 4,757 | 7.19 | 74.6 | 8,424,572 |
| 800 | 42.3 | 294.6 | 14,061 | 9.94 | 51.7 | 46,459,865 |
| 50 | 36.4 | 607.9 | 482 | 3.38 | 311.4 | 10,861 |
| 100 | 34.8 | 626.3 | 420 | 5.82 | 193.3 | 100,033 |
| 200 | 32.5 | 580.4 | 598 | 7.19 | 142.6 | 412,397 |
| 400 | 29.7 | 477.5 | 1,484 | 8.57 | 97.4 | 2,433,539 |
| 800 | 26.5 | 353.7 | 6,002 | 9.94 | 64.9 | 16,115,180 |
| 50 | 15.7 | 1295.9 | 14 | 5.82 | 471.4 | 1,575 |
| 100 | 15.0 | 1166.0 | 23 | 7.19 | 326.8 | 8,674 |
| 200 | 14.0 | 932.7 | 66 | 7.19 | 222.3 | 52,175 |
| 400 | 13.0 | 589.9 | 554 | 8.57 | 141.1 | 433,212 |
| 800 | 11.8 | 451.8 | 1,920 | 11.31 | 87.9 | 3,924,427 |

Surface Thickness = 4 inches
Base Thickness = 14 inches

Tire Inflation Pressure = 75 psi

| Surface Modulus (ksi) | Base Modulus (ksi) | $\varepsilon_T$ Bottom of A.C. ($x10^{-6}$in/in) | $ESAL_{B.S.}$ | Rad. at Max. $\varepsilon_{Top}$ (inches) | $\varepsilon_T$ Top of A.C. ($x10^{-6}$in/in) | $ESAL_{T.S.}$ |
|---|---|---|---|---|---|---|
| 50 | 45.7 | 585.4 | 575 | 3.38 | 117.8 | 1,003,876 |
| 100 | 42.0 | 466.7 | 1,651 | 11.31 | 75.1 | 8,166,557 |
| 200 | 37.2 | 357.4 | 5,718 | 11.31 | 56.0 | 32,026,627 |
| 400 | 31.9 | 250.5 | 29,918 | 21.75 | 50.6 | 51,353,402 |
| 800 | 26.3 | 161.9 | 228,359 | 21.75 | 38.8 | 176,825,238 |
| 50 | 29.2 | 751.1 | 180 | 9.94 | 131.3 | 605,719 |
| 100 | 26.6 | 582.8 | 587 | 11.31 | 99.4 | 2,213,778 |
| 200 | 23.7 | 423.2 | 2,603 | 11.31 | 69.1 | 12,034,407 |
| 400 | 20.5 | 283.2 | 16,897 | 21.75 | 57.8 | 27,639,653 |
| 800 | 17.2 | 163.9 | 215,670 | 21.75 | 42.8 | 111,975,711 |
| 50 | 13.0 | 1122.6 | 28 | 9.94 | 209.7 | 68,464 |
| 100 | 12.0 | 801.3 | 133 | 11.31 | 146.7 | 361,403 |
| 200 | 10.9 | 528.2 | 927 | 11.31 | 90.3 | 3,461,794 |
| 400 | 9.8 | 326.7 | 8,687 | 21.75 | 71.5 | 10,265,474 |
| 800 | 8.6 | 189.8 | 108,917 | 21.75 | 49.7 | 55,829,291 |

Surface Thickness = 1 inch
Base Thickness = 14 inches

Tire Inflation Pressure = 125 psi

| Surface Modulus (ksi) | Base Modulus (ksi) | $\varepsilon_T$ Bottom of A.C. ($x10^{-6}$in/in) | $ESAL_{B.S.}$ | Rad. at Max. $\varepsilon_{Top}$ (inches) | $\varepsilon_T$ Top of A.C. ($x10^{-6}$in/in) | $ESAL_{T.S.}$ |
|---|---|---|---|---|---|---|
| 50 | 70.2 | 12.6 | - | 2.81 | 262.6 | 24,018 |
| 100 | 67.9 | 156.9 | 264,276 | 3.84 | 154.3 | 285,660 |
| 200 | 65.0 | 280.6 | 17,639 | 5.09 | 136.3 | 508,970 |
| 400 | 61.5 | 350.3 | 6,278 | 5.09 | 114.5 | 1,145,881 |
| 800 | 58.1 | 361.1 | 5,450 | 5.09 | 86.9 | 4,139,183 |
| 50 | 43.7 | 169.9 | 182,424 | 3.84 | 323.8 | 9,055 |
| 100 | 42.2 | 370.4 | 4,841 | 5.09 | 246.2 | 32,431 |
| 200 | 40.2 | 507.1 | 1,121 | 5.09 | 208.7 | 70,005 |
| 400 | 38.3 | 548.9 | 775 | 5.09 | 163.9 | 215,670 |
| 800 | 35.9 | 508.1 | 1,111 | 5.09 | 115.5 | 1,100,410 |
| 50 | 29.9 | 422.4 | 2,626 | 3.84 | 424.7 | 2,560 |
| 100 | 28.8 | 661.0 | 326 | 5.09 | 343.2 | 6,906 |
| 200 | 27.4 | 779.0 | 152 | 5.09 | 278.9 | 18,145 |
| 400 | 25.9 | 769.5 | 161 | 5.09 | 206.8 | 73,050 |
| 800 | 24.1 | 662.6 | 323 | 6.35 | 144.1 | 392,785 |

Surface Thickness = 1.5 inches
Base Thickness = 14 inches

Tire Inflation Pressure = 125 psi

| Surface Modulus (ksi) | Base Modulus (ksi) | $\varepsilon_T$ Bottom of A.C. ($x10^{-6}$in/in) | $ESAL_{B.S.}$ | Rad. at Max. $\varepsilon_{Top}$ (inches) | $\varepsilon_T$ Top of A.C. ($x10^{-6}$in/in) | $ESAL_{T.S.}$ |
|---|---|---|---|---|---|---|
| 50 | 63.3 | 359.2 | 5,586 | 2.81 | 226.4 | 47,918 |
| 100 | 61.5 | 422.2 | 2,632 | 5.09 | 147.7 | 350,150 |
| 200 | 58.7 | 456.0 | 1,839 | 5.09 | 122.5 | 836,688 |
| 400 | 54.8 | 438.9 | 2,197 | 6.35 | 95.9 | 2,615,920 |
| 800 | 49.9 | 372.3 | 4,728 | 6.35 | 67.2 | 13,702,773 |
| 50 | 39.9 | 615.3 | 456 | 3.84 | 283.3 | 16,870 |
| 100 | 38.5 | 680.5 | 285 | 5.09 | 231.1 | 43,546 |
| 200 | 36.6 | 680.6 | 285 | 5.09 | 175.9 | 155,202 |
| 400 | 34.0 | 598.4 | 519 | 6.35 | 130.7 | 618,776 |
| 800 | 30.9 | 471.2 | 1,578 | 7.60 | 87.4 | 4,030,068 |
| 50 | 16.9 | 1466.8 | 8 | 5.09 | 581.6 | 592 |
| 100 | 16.3 | 1415.9 | 9 | 5.09 | 432.4 | 2,355 |
| 200 | 15.4 | 1208.9 | 20 | 6.35 | 302.7 | 12,392 |
| 400 | 14.4 | 924.4 | 68 | 6.35 | 196.5 | 92,670 |
| 800 | 13.3 | 648.2 | 358 | 8.86 | 124.1 | 787,628 |

Surface Thickness = 2 inches
Base Thickness = 14 inches

Tire Inflation Pressure = 125 psi

| Surface Modulus (ksi) | Base Modulus (ksi) | $\varepsilon_T$ Bottom of A.C. ($x10^{-6}$in/in) | $ESAL_{B.S.}$ | Rad. at Max. $\varepsilon_{Top}$ (inches) | $\varepsilon_T$ Top of A.C. ($x10^{-6}$in/in) | $ESAL_{T.S.}$ |
|---|---|---|---|---|---|---|
| 50 | 59.8 | 431.4 | 2,381 | 2.81 | 175.6 | 156,441 |
| 100 | 57.2 | 544.0 | 809 | 6.35 | 131.6 | 599,316 |
| 200 | 53.5 | 507.8 | 1,114 | 6.35 | 103.0 | 1,875,807 |
| 400 | 48.7 | 431.3 | 2,383 | 7.60 | 75.8 | 7,821,265 |
| 800 | 43.1 | 332.6 | 7,992 | 10.12 | 52.3 | 44,029,510 |
| 50 | 37.7 | 835.6 | 110 | 5.09 | 237.3 | 38,496 |
| 100 | 35.8 | 788.6 | 143 | 6.35 | 190.7 | 106,544 |
| 200 | 33.3 | 689.8 | 268 | 6.35 | 143.3 | 403,100 |
| 400 | 30.2 | 547.4 | 785 | 7.60 | 98.9 | 2,266,376 |
| 800 | 26.8 | 394.4 | 3,614 | 10.12 | 65.8 | 15,114,162 |
| 50 | 16.1 | 1633.7 | 5 | 5.09 | 457.5 | 1,811 |
| 100 | 15.2 | 1390.0 | 10 | 6.35 | 339.1 | 7,303 |
| 200 | 14.2 | 848.8 | 102 | 7.60 | 226.2 | 48,116 |
| 400 | 13.1 | 758.3 | 172 | 8.86 | 143.6 | 399,194 |
| 800 | 11.9 | 497.3 | 1,228 | 11.37 | 89.3 | 3,646,037 |

Surface Thickness = 4 inches
Base Thickness = 14 inches

Tire Inflation Pressure = 125 inches

| Surface Modulus (ksi) | Base Modulus (ksi) | $\varepsilon_T$ Bottom of A.C. ($\times 10^{-6}$ in/in) | $ESAL_{B.S.}$ | Rad. at Max. $\varepsilon_{Top}$ (inches) | $\varepsilon_T$ Top of A.C. ($\times 10^{-6}$ in/in) | $ESAL_{T.S.}$ |
|---|---|---|---|---|---|---|
| 50 | 46.4 | 622.4 | 432 | 10.12 | 85.7 | 4,416,057 |
| 100 | 42.5 | 513.4 | 1,059 | 11.37 | 73.0 | 9,319,503 |
| 200 | 37.6 | 384.6 | 4,064 | 11.37 | 55.2 | 34,245,937 |
| 400 | 32.1 | 266.8 | 22,308 | 21.75 | 49.8 | 55,309,184 |
| 800 | 26.3 | 169.4 | 184,945 | 21.75 | 38.3 | 187,833,803 |
| 50 | 29.5 | 836.9 | 109 | 10.12 | 124.9 | 764,410 |
| 100 | 26.9 | 633.4 | 398 | 11.37 | 97.2 | 2,456,943 |
| 200 | 23.8 | 451.1 | 1,934 | 11.37 | 68.3 | 12,704,978 |
| 400 | 20.5 | 298.0 | 13,329 | 21.75 | 57.0 | 29,492,931 |
| 800 | 17.2 | 182.2 | 131,746 | 21.75 | 42.1 | 120,912,647 |
| 50 | 13.1 | 958.2 | 58 | 10.12 | 211.3 | 66,083 |
| 100 | 12.1 | 863.2 | 94 | 11.37 | 144.5 | 387,747 |
| 200 | 10.9 | 559.9 | 707 | 11.37 | 89.8 | 3,552,465 |
| 400 | 9.8 | 344.5 | 6,785 | 21.75 | 70.5 | 10,961,301 |
| 800 | 8.6 | 197.7 | 90,080 | 21.75 | 49.1 | 59,077,805 |

## APPENDIX E. SHEAR STRESS DATA AT THE TOP OF THE BASE.

The tables presented in this appendix have lines separating the sections of the three base moduli used. The top section uses the base modulus expression $E_B = 8787\theta^{0.365}$; the middle section uses the base modulus expression $E_B = 7000\theta^{0.325}$; and the bottom section uses the base modulus expression $E_B = 4886\theta^{0.239}$.

The shear stresses at the top of the base are tabulated at the distance from the center of the tire load where maximum shear stress occurs. This distance increased slightly with increased surface thickness, but generally occurred at the edge of the tire print. The vertical compresive stresses are tabulated at the location where maximum shear stress occurred.

Surface Thickness = 1.0 inch

Tire Pressure = 75 psi

| Surface Modulus, ksi | Stress at Top of 8-inch Base, psi | | Stress at Top of 14-inch Base, psi | |
|---|---|---|---|---|
| | Vertical Compressive | Maximum Shear | Vertical Compressive | Maximum Shear |
| 50 | 83.7 | 33.3 | 78.1 | 31.2 |
| 100 | 77.7 | 33.2 | 74.7 | 30.8 |
| 200 | 73.2 | 32.8 | 71.2 | 29.6 |
| 400 | 68.1 | 30.6 | 66.3 | 27.1 |
| 800 | 61.4 | 26.4 | 60.4 | 23.2 |
| 50 | 81.1 | 32.6 | 76.2 | 30.9 |
| 100 | 75.7 | 32.2 | 72.6 | 30.0 |
| 200 | 70.9 | 30.6 | 68.5 | 27.9 |
| 400 | 64.9 | 27.1 | 63.0 | 24.5 |
| 800 | 57.2 | 22.1 | 56.1 | 20.0 |
| 50 | 76.3 | 30.7 | 72.2 | 29.6 |
| 100 | 71.2 | 28.7 | 68.0 | 27.2 |
| 200 | 65.0 | 25.0 | 62.5 | 23.6 |
| 400 | 57.6 | 20.2 | 55.3 | 18.9 |
| 800 | 48.5 | 14.9 | 47.2 | 14.2 |

Surface Thickness = 1.5 inch

Tire Pressure = 75 psi

| Surface Modulus, ksi | Stress at Top of 8-inch Base, psi | | Stress at Top of 14-inch Base, psi | |
|---|---|---|---|---|
| | Vertical Compressive | Maximum Shear | Vertical Compressive | Maximum Shear |
| 50 | 74.8 | 33.3 | 72.2 | 30.5 |
| 100 | 70.3 | 32.6 | 68.0 | 29.1 |
| 200 | 64.1 | 30.1 | 62.6 | 26.3 |
| 400 | 56.4 | 25.3 | 55.7 | 22.0 |
| 800 | 47.2 | 19.2 | 47.3 | 16.7 |
| 50 | 72.9 | 32.3 | 69.8 | 29.6 |
| 100 | 67.4 | 30.4 | 65.0 | 27.3 |
| 200 | 60.5 | 26.5 | 58.8 | 23.5 |
| 400 | 52.0 | 20.9 | 51.1 | 18.5 |
| 800 | 42.1 | 14.8 | 41.9 | 13.2 |
| 50 | 67.8 | 28.6 | 64.5 | 26.6 |
| 100 | 61.0 | 24.4 | 58.3 | 22.6 |
| 200 | 52.6 | 19.0 | 50.6 | 17.6 |
| 400 | 43.0 | 13.4 | 41.6 | 12.5 |
| 800 | 26.7 | 8.9 | 26.6 | 8.5 |

Surface Thickness = 2.0 inch

Tire Pressure = 75 psi

| Surface Modulus, ksi | Stress at Top of 8-inch Base, psi | | Stress at Top of 14-inch Base, psi | |
|---|---|---|---|---|
| | Vertical Compressive | Maximum Shear | Vertical Compressive | Maximum Shear |
| 50 | 68.3 | 31.7 | 65.8 | 28.2 |
| 100 | 62.0 | 29.7 | 60.4 | 25.9 |
| 200 | 54.3 | 25.4 | 53.6 | 21.9 |
| 400 | 45.2 | 19.4 | 45.2 | 16.8 |
| 800 | 35.1 | 13.1 | 35.7 | 11.5 |
| 50 | 65.3 | 29.9 | 62.8 | 26.7 |
| 100 | 58.4 | 26.5 | 56.7 | 23.4 |
| 200 | 50.0 | 21.1 | 49.0 | 18.7 |
| 400 | 40.3 | 15.1 | 40.1 | 13.4 |
| 800 | 24.2 | 9.7 | 24.8 | 8.8 |
| 50 | 59.1 | 24.8 | 56.2 | 22.5 |
| 100 | 50.8 | 19.6 | 48.7 | 17.8 |
| 200 | 41.4 | 13.9 | 31.5 | 12.8 |
| 400 | 25.7 | 9.1 | 25.4 | 8.5 |
| 800 | 19.4 | 5.5 | 19.1 | 5.3 |

Surface Thickness = 4.0 inch

Tire Pressure = 75 psi

| Surface Modulus, ksi | Stress at Top of 8-inch Base, psi | | Stress at Top of 14-inch Base, psi | |
|---|---|---|---|---|
| | Vertical Compressive | Maximum Shear | Vertical Compressive | Maximum Shear |
| 50 | 32.5 | 19.0 | 32.9 | 16.4 |
| 100 | 27.2 | 15.2 | 28.0 | 13.2 |
| 200 | 21.4 | 10.6 | 22.2 | 9.4 |
| 400 | 15.4 | 6.4 | 16.1 | 5.8 |
| 800 | 10.1 | 3.4 | 8.6 | 3.2 |
| 50 | 30.5 | 16.6 | 30.6 | 14.5 |
| 100 | 25.0 | 12.4 | 25.3 | 10.9 |
| 200 | 19.1 | 8.1 | 19.4 | 7.2 |
| 400 | 13.4 | 4.6 | 13.6 | 4.2 |
| 800 | 7.3 | 2.4 | 7.3 | 2.3 |
| 50 | 26.6 | 11.8 | 25.9 | 10.7 |
| 100 | 20.8 | 7.8 | 20.2 | 7.2 |
| 200 | 15.2 | 4.6 | 12.0 | 4.3 |
| 400 | 9.0 | 2.6 | 8.4 | 2.4 |
| 800 | 6.0 | 1.4 | 5.6 | 1.3 |

Surface Thickness = 1.0 inch

Tire Pressure = 125 psi

| Surface Modulus, ksi | Stress at Top of 8-inch Base, psi | | Stress at Top of 14-inch Base, psi | |
|---|---|---|---|---|
| | Vertical Compressive | Maximum Shear | Vertical Compressive | Maximum Shear |
| 50 | 126.0 | 39.8 | 114.0 | 37.1 |
| 100 | 117.0 | 39.8 | 109.0 | 36.6 |
| 200 | 108.0 | 39.0 | 102.0 | 35.0 |
| 400 | 98.9 | 35.9 | 93.6 | 31.6 |
| 800 | 86.5 | 30.2 | 82.8 | 26.4 |
| 50 | 121.0 | 39.3 | 110.0 | 36.7 |
| 100 | 112.0 | 38.5 | 104.0 | 35.5 |
| 200 | 103.0 | 36.2 | 96.7 | 32.7 |
| 400 | 91.9 | 31.4 | 86.9 | 28.1 |
| 800 | 78.1 | 24.7 | 74.7 | 22.1 |
| 50 | 111.0 | 36.8 | 108.0 | 36.1 |
| 100 | 102.0 | 33.8 | 101.0 | 34.1 |
| 200 | 90.2 | 28.7 | 92.1 | 30.3 |
| 400 | 76.9 | 22.3 | 81.0 | 24.9 |
| 800 | 46.2 | 16.6 | 49.1 | 18.9 |

Surface Thickness = 1.5 inch

Tire Pressure = 125 psi

| Surface Modulus, ksi | Stress at Top of 8-inch Base, psi | | Stress at Top of 14-inch Base, psi | |
|---|---|---|---|---|
| | Vertical Compressive | Maximum Shear | Vertical Compressive | Maximum Shear |
| 50 | 109.0 | 39.0 | 102.0 | 35.3 |
| 100 | 101.0 | 37.9 | 94.8 | 33.4 |
| 200 | 90.2 | 34.2 | 85.4 | 29.7 |
| 400 | 76.9 | 28.0 | 51.2 | 24.2 |
| 800 | 43.6 | 20.9 | 44.4 | 18.2 |
| 50 | 105.0 | 37.7 | 97.3 | 34.0 |
| 100 | 95.0 | 34.9 | 88.9 | 30.9 |
| 200 | 82.8 | 29.6 | 53.8 | 26.1 |
| 400 | 47.9 | 22.9 | 47.8 | 20.4 |
| 800 | 39.6 | 16.1 | 39.8 | 14.5 |
| 50 | 94.0 | 32.7 | 58.2 | 29.9 |
| 100 | 55.6 | 27.3 | 53.9 | 25.2 |
| 200 | 49.1 | 21.1 | 47.8 | 19.5 |
| 400 | 40.8 | 14.7 | 39.8 | 13.7 |
| 800 | 31.7 | 9.5 | 31.1 | 8.9 |

Surface Thickness = 2.0 inch

Tire Pressure = 125 psi

| Surface Modulus, ksi | Stress at Top of 8-inch Base, psi | | Stress at Top of 14-inch Base, psi | |
|---|---|---|---|---|
| | Vertical Compressive | Maximum Shear | Vertical Compressive | Maximum Shear |
| 50 | 95.6 | 35.9 | 89.5 | 31.5 |
| 100 | 85.5 | 33.0 | 54.4 | 28.5 |
| 200 | 49.0 | 27.8 | 49.2 | 24.0 |
| 400 | 41.6 | 21.1 | 42.3 | 18.2 |
| 800 | 32.9 | 14.1 | 33.9 | 12.4 |
| 50 | 90.1 | 33.6 | 56.4 | 29.7 |
| 100 | 52.5 | 29.2 | 51.9 | 25.7 |
| 200 | 46.0 | 23.2 | 45.7 | 20.4 |
| 400 | 37.8 | 16.4 | 38.0 | 14.5 |
| 800 | 28.8 | 10.4 | 29.2 | 9.3 |
| 50 | 53.7 | 27.5 | 51.9 | 24.9 |
| 100 | 47.3 | 21.5 | 45.8 | 19.5 |
| 200 | 39.2 | 15.2 | 38.1 | 13.9 |
| 400 | 30.3 | 9.7 | 29.6 | 9.0 |
| 800 | 22.0 | 5.7 | 17.2 | 5.4 |

Surface Thickness = 4.0 inch

Tire Pressure = 125 psi

| Surface Modulus, ksi | Stress at Top of 8-inch Base, psi | | Stress at Top of 14-inch Base, psi | |
|---|---|---|---|---|
| | Vertical Compressive | Maximum Shear | Vertical Compressive | Maximum Shear |
| 50 | 40.6 | 20.3 | 40.3 | 17.4 |
| 100 | 33.3 | 16.0 | 33.5 | 13.8 |
| 200 | 25.3 | 11.0 | 25.8 | 9.5 |
| 400 | 13.6 | 6.5 | 14.2 | 5.9 |
| 800 | 9.1 | 3.5 | 9.5 | 3.2 |
| 50 | 37.5 | 17.6 | 36.8 | 15.2 |
| 100 | 29.8 | 12.9 | 29.6 | 11.2 |
| 200 | 22.0 | 8.2 | 17.0 | 7.4 |
| 400 | 12.1 | 4.8 | 12.2 | 4.4 |
| 800 | 8.0 | 2.5 | 7.9 | 2.3 |
| 50 | 31.3 | 12.2 | 30.1 | 10.9 |
| 100 | 18.4 | 8.0 | 17.9 | 7.3 |
| 200 | 13.8 | 4.8 | 13.4 | 4.5 |
| 400 | 9.6 | 2.6 | 9.1 | 2.5 |
| 800 | 6.4 | 1.4 | 5.2 | 1.3 |

## APPENIDX F. COMPRESSIVE STRAIN AND ESAL DATA AT THE TOP OF THE SUBGRADE.

The tables presented in this appendix have lines separating the sections of the three base moduli used. The top section uses the base modulus expression $E_B = 8787\,\theta^{0.365}$; the middle section uses the base modulus expression $E_B = 7000\,\theta^{0.239}$; and the bottom section uses the base modulus expression $E_B = 4886\,\theta^{0.239}$.

The Equivalent Standard Axle Loads (ESAL) are calculated using the expression defined in Chapter V. The ESALs are calculated as a function of the vertical compressive strains at the top of the subgrade by the equations:

$$W_{18} = 6.15 \times 10^{17} \left(\frac{1}{\varepsilon_c}\right)^{4.0}$$

The compressive strains at the top of the subgrade are tabulated for strain values at 0.5 inches from the centerline of the tire load.

Surface Thickness = 1.0 inch

Tire Pressure = 75 psi

| Surface Modulus (ksi) | 8-inch Base Thickness | | 14-inch Base Thickness | |
|---|---|---|---|---|
| | ε Top of Subgrade ($\times 10^{-6}$ in/in) | ESAL | ε Top of Subgrade ($\times 10^{-6}$ in/in) | ESAL |
| 50 | 1690 | 75,900 | 750 | 1,886,900 |
| 100 | 1620 | 90,300 | 730 | 2,125,000 |
| 200 | 1550 | 105,900 | 710 | 2,429,400 |
| 400 | 1480 | 129,500 | 680 | 2,824,000 |
| 800 | 1360 | 177,600 | 650 | 3,445,000 |
| 50 | 1980 | 40,100 | 880 | 1,036,700 |
| 100 | 1890 | 48,100 | 850 | 1,190,400 |
| 200 | 1800 | 58,600 | 820 | 1,377,800 |
| 400 | 1690 | 75,900 | 780 | 1,642,500 |
| 800 | 1550 | 105,400 | 740 | 2,088,700 |
| 50 | 2580 | 13,900 | 1100 | 424,000 |
| 100 | 2430 | 17,600 | 1060 | 482,700 |
| 200 | 2270 | 23,100 | 1010 | 583,700 |
| 400 | 2080 | 32,500 | 950 | 752,800 |
| 800 | 1820 | 55,800 | 870 | 1,065,300 |

Surface Thickness = 1.5 inches

Tire Pressure = 75 psi

| Surface Modulus (ksi) | 8-inch Base Thickness | | 14-inch Base Thickness | |
|---|---|---|---|---|
| | ε Top of Subgrade ($\times 10^{-6}$ in/in) | ESAL | ε Top of Subgrade ($\times 10^{-6}$ in/in) | ESAL |
| 50 | 1560 | 104,600 | 710 | 2,376,700 |
| 100 | 1470 | 131,600 | 680 | 2,794,100 |
| 200 | 1370 | 175,100 | 660 | 3,306,600 |
| 400 | 1260 | 245,800 | 610 | 4,325,700 |
| 800 | 1130 | 381,500 | 570 | 6,031,600 |
| 50 | 1790 | 59,500 | 820 | 1,361,100 |
| 100 | 1700 | 74,100 | 780 | 1,637,400 |
| 200 | 1560 | 102,900 | 740 | 2,040,400 |
| 400 | 1400 | 150,400 | 690 | 2,704,900 |
| 800 | 1230 | 266,400 | 620 | 4,082,700 |
| 50 | 2280 | 22,900 | 1010 | 587,500 |
| 100 | 2100 | 31,900 | 950 | 744,400 |
| 200 | 1880 | 49,700 | 890 | 997,900 |
| 400 | 1630 | 88,200 | 800 | 1,501,100 |
| 800 | 1340 | 191,200 | 690 | 2,710,500 |

Surface Thickness = 2.0 inches

Tire Pressure = 75 psi

| Surface Modulus (ksi) | 8-inch Base Thickness | | 14-inch Base Thickness | |
|---|---|---|---|---|
| | ε Top of Subgrade ($\times 10^{-6}$ in/in) | ESAL | ε Top of Subgrade ($\times 10^{-6}$ in/in) | ESAL |
| 50 | 1430 | 146,900 | 670 | 3,031,600 |
| 100 | 1300 | 195,900 | 640 | 3,769,000 |
| 200 | 1200 | 291,600 | 600 | 4,902,000 |
| 400 | 1070 | 465,400 | 550 | 6,921,500 |
| 800 | 870 | 1,052,100 | 480 | 11,497,000 |
| 50 | 1630 | 86,600 | 760 | 1,810,400 |
| 100 | 1500 | 120,000 | 720 | 2,304,900 |
| 200 | 1350 | 185,200 | 670 | 3,133,100 |
| 400 | 1170 | 330,500 | 600 | 4,709,500 |
| 800 | 940 | 795,600 | 520 | 8,742,000 |
| 50 | 2000 | 38,000 | 920 | 855,700 |
| 100 | 1780 | 60,900 | 850 | 1,164,800 |
| 200 | 1550 | 107,000 | 770 | 1,760,600 |
| 400 | 1270 | 234,000 | 660 | 3,171,800 |
| 800 | 970 | 700,400 | 540 | 7,457,100 |

Surface Thickness = 4.0 inches

Tire Pressure = 75 psi

| Surface Modulus (ksi) | 8-inch Base Thickness | | 14-inch Base Thickness | |
|---|---|---|---|---|
| | $\varepsilon$ Top of Subgrade ($\times 10^{-6}$ in/in) | ESAL | $\varepsilon$ Top of Subgrade ($\times 10^{-6}$ in/in) | ESAL |
| 50 | 990 | 636,600 | 520 | 8,545,900 |
| 100 | 830 | 1,273,600 | 460 | 13,370,200 |
| 200 | 670 | 3,005,700 | 400 | 24,842,800 |
| 400 | 500 | 9,638,000 | 320 | 60,588,800 |
| 800 | 340 | 44,515,300 | 240 | 201,104,200 |
| 50 | 1100 | 418,300 | 570 | 5,848,200 |
| 100 | 910 | 909,300 | 500 | 9,855,800 |
| 200 | 700 | 2,490,500 | 420 | 20,305,900 |
| 400 | 510 | 9,450,800 | 320 | 56,481,200 |
| 800 | 330 | 51,222,200 | 230 | 225,872,100 |
| 50 | 1230 | 266,400 | 630 | 3,795,200 |
| 100 | 970 | 686,200 | 530 | 7,554,200 |
| 200 | 700 | 2,532,900 | 420 | 19,760,400 |
| 400 | 470 | 12,624,800 | 300 | 73,117,600 |
| 800 | 300 | 80,374,300 | 210 | 328,060,400 |

Surface Thickness = 1.0 inch

Tire Pressure = 125 psi

| Surface Modulus (ksi) | 8-inch Base Thickness | | 14-inch Base Thickness | |
|---|---|---|---|---|
| | $\varepsilon$ Top of Subgrade ($\times 10^{-6}$ in/in) | ESAL | $\varepsilon$ Top of Subgrade ($\times 10^{-6}$ in/in) | ESAL |
| 50 | 1700 | 72,800 | 750 | 1,905,000 |
| 100 | 1640 | 85,800 | 730 | 2,115,800 |
| 200 | 1580 | 98,200 | 710 | 2,407,800 |
| 400 | 1492 | 124,000 | 690 | 2,777,800 |
| 800 | 1390 | 164,200 | 650 | 3,389,800 |
| 50 | 2000 | 38,600 | 870 | 1,050,800 |
| 100 | 1900 | 46,500 | 850 | 1,183,500 |
| 200 | 1820 | 55,700 | 820 | 1,362,800 |
| 400 | 1720 | 69,900 | 790 | 1,619,100 |
| 800 | 1570 | 101,600 | 740 | 2,053,900 |
| 50 | 2360 | 12,900 | 1050 | 505,600 |
| 100 | 2480 | 16,300 | 1010 | 584,100 |
| 200 | 2330 | 21,000 | 970 | 696,000 |
| 400 | 2120 | 30,300 | 920 | 872,400 |
| 800 | 1850 | 53,100 | 850 | 1,185,100 |

Surface Thickness = 1.5 inches

Tire Pressure = 125 psi

| Surface Modulus (ksi) | 8-inch Base Thickness | | 14-inch Base Thickness | |
|---|---|---|---|---|
| | ε Top of Subgrade ($\times 10^{-6}$ in/in) | ESAL | ε Top of Subgrade ($\times 10^{-6}$ in/in) | ESAL |
| 50 | 1570 | 100,400 | 710 | 2,412,000 |
| 100 | 1490 | 126,200 | 680 | 2,829,000 |
| 200 | 1380 | 167,600 | 650 | 3,402,300 |
| 400 | 1270 | 234,700 | 610 | 4,314,200 |
| 800 | 1130 | 378,400 | 560 | 6,054,300 |
| 50 | 1810 | 57,200 | 820 | 1,378,600 |
| 100 | 1710 | 71,100 | 780 | 1,648,000 |
| 200 | 1580 | 99,600 | 740 | 2,051,000 |
| 400 | 1430 | 146,900 | 690 | 2,717,300 |
| 800 | 1230 | 268,700 | 620 | 4,123,100 |
| 50 | 2300 | 22,000 | 1010 | 597,800 |
| 100 | 2120 | 30,500 | 950 | 753,500 |
| 200 | 1900 | 47,700 | 890 | 1,001,200 |
| 400 | 1650 | 83,900 | 800 | 1,504,500 |
| 800 | 1340 | 189,500 | 690 | 2,741,200 |

Surface Thickness = 2.0 inches

Tire Pressure = 125 psi

| Surface Modulus (ksi) | 8-inch Base Thickness | | 14-inch Base Thickness | |
|---|---|---|---|---|
| | ε Top of Subgrade ($\times 10^{-6}$ in/in) | ESAL | ε Top of Subgrade ($\times 10^{-6}$ in/in) | ESAL |
| 50 | 1430 | 146,600 | 670 | 3,100,700 |
| 100 | 1330 | 195,700 | 630 | 3,839,000 |
| 200 | 1220 | 277,200 | 590 | 4,955,000 |
| 400 | 1080 | 460,000 | 540 | 7,026,900 |
| 800 | 870 | 1,052,500 | 480 | 11,686,300 |
| 50 | 1650 | 83,300 | 760 | 1,852,000 |
| 100 | 1500 | 119,300 | 710 | 2,355,000 |
| 200 | 1350 | 183,800 | 660 | 3,182,100 |
| 400 | 1170 | 330,800 | 600 | 4,817,900 |
| 800 | 940 | 789,100 | 510 | 8,850,100 |
| 50 | 2010 | 37,700 | 910 | 879,000 |
| 100 | 1800 | 58,300 | 850 | 1,188,800 |
| 200 | 1550 | 106,700 | 960 | 1,807,200 |
| 400 | 1270 | 233,000 | 660 | 3,274,000 |
| 800 | 960 | 718,900 | 530 | 7,708,900 |

Surface Thickness = 4.0 inches

Tire Pressure = 125 psi

| Surface Modulus (ksi) | 8-inch Base Thickness | | 14-inch Base Thickness | |
|---|---|---|---|---|
| | ε Top of Subgrade ($\times 10^{-6}$ in/in) | ESAL | ε Top of Subgrade ($\times 10^{-6}$ in/in) | ESAL |
| 50 | 990 | 654,200 | 510 | 8,907,600 |
| 100 | 830 | 1,299,900 | 460 | 13,929,500 |
| 200 | 670 | 3,078,500 | 390 | 25,870,700 |
| 400 | 500 | 9,900,800 | 310 | 62,504,100 |
| 800 | 340 | 46,407,800 | 230 | 206,247,600 |
| 50 | 1100 | 418,600 | 560 | 6,081,000 |
| 100 | 900 | 931,800 | 490 | 10,256,100 |
| 200 | 700 | 2,547,400 | 410 | 21,014,100 |
| 400 | 500 | 9,707,300 | 320 | 58,790,500 |
| 800 | 340 | 46,407,800 | 230 | 232,026,300 |
| 50 | 1220 | 276,800 | 630 | 3,960,300 |
| 100 | 960 | 713,800 | 530 | 7,873,500 |
| 200 | 700 | 2,626,900 | 410 | 20,758,000 |
| 400 | 470 | 12,908,100 | 300 | 75,532,400 |
| 800 | 290 | 84,098,300 | 210 | 340,519,300 |